

# Chemical Implication of Local Features of the Electron Density Distribution

E. Kraka and D. Cremer

Theoretical Chemistry, University of Göteborg, Kemigården 3, S-41296 Göteborg, Sweden

Investigation of the electron density distribution  $\rho(\mathbf{r})$ , its associated Laplace field  $\nabla^2\rho(\mathbf{r})$ , and the energy density distribution  $H(\mathbf{r})$  leads to a unique definition and description of atoms in molecules, chemical bonds, molecular structure, and structural changes. From the local features of  $\rho(\mathbf{r})$ ,  $\nabla^2\rho(\mathbf{r})$ , and  $H(\mathbf{r})$  valuable insight into the bonding mechanism and the reactive behavior of a molecule is gained, in particular into distortions of the valence shell of an atom upon bond formation; the order,  $\pi$ -character, polarity, and bent character of a bond; the degree of electron delocalization and bond equalization in a conjugated  $\pi$ -system; the extent of through-bond and through-space interactions; the sites that are prone to electrophilic or nucleophilic attack; and the bonds that can easily be broken in a molecule. Important chemical concepts or models such as  $\pi$ - and  $\sigma$ -aromaticity, homoaromaticity, ring strain, the frontier orbital model or the HSAB concept can be reevaluated on the basis of the density analysis. This is demonstrated for a number of examples ranging from  $\pi$ -delocalization in polyenes and cyclopolyenes, the peculiar stability of three-membered rings, the basicity of N containing aromatic molecules to the bonding in  $\pi$ -complexes. Furthermore, the analysis of  $\rho(\mathbf{r})$ ,  $\nabla^2\rho(\mathbf{r})$ , and  $H(\mathbf{r})$  opens fascinating avenues into new areas such as the chemistry of helium organic compounds.

1	Introduction . . . . .	457
2	Analysis of the Electron Density Distribution $\rho(\mathbf{r})$ . . . . .	459
2.1	Definition of an Atom in a Molecule . . . . .	461
2.2	From Atoms to Chemical Bonds . . . . .	463
2.3	Distinction Between Covalent Bonds and Closed Shell Interactions . . . . .	465
2.4	Description of the Covalent Bond . . . . .	466
2.5	Definition of Molecular Structure and Structural Changes . . . . .	468
3	The Laplace Field of the Electron Density Distribution $\rho(\mathbf{r})$ . . . . .	471
3.1	Mathematical Meaning of the Laplace Field of a Scalar Function . . . . .	472
3.2	Physical Meaning of the Laplace Field of $\rho(\mathbf{r})$ . . . . .	473
3.3	Chemical Meaning of the Laplace Field of $\rho(\mathbf{r})$ . . . . .	475
3.4	The Laplace Field of a Molecule . . . . .	479
4	Description of $\pi$ -Conjugation . . . . .	482
4.1	Conjugation in Polyenes . . . . .	483
4.2	Conjugation in Cyclic Systems — Aromaticity and Antiaromaticity . . . . .	487
4.3	Hyperconjugation and Anomeric Effects . . . . .	490
5	Description of Homoconjugation . . . . .	491
5.1	$\pi$ -Character of Three-membered Rings . . . . .	491
5.2	Homoconjugation . . . . .	493
5.3	Homoaromaticity . . . . .	495

5.4	Do Neutral Homoaromatic Compounds Exist? . . . . .	497
5.5	Homoantiaromaticity — Fact or Fiction? . . . . .	500
5.6	Distinction Between Homoconjugation and Through-Space Interactions . . . . .	501
6	Description of Strain . . . . .	505
6.1	Baeyer Strain — Description of Bent Bonds . . . . .	506
6.2	From Three-membered Rings to $\pi$ -Complexes — Limits of the Concept of Strain . . . . .	507
6.3	Pitzer Strain and Dunitz-Schomaker Strain . . . . .	509
6.4	Energetic Consequences of Strain . . . . .	511
7	$\sigma$ -Conjugation — Models of $\sigma$ -Electron Delocalization . . . . .	512
7.1	$\sigma$ -Conjugation . . . . .	512
7.2	Ribbon, Surface, and Volume Delocalization of $\sigma$ -Electrons . . . . .	513
7.3	Surface Delocalization and Bonding in Cyclopropane . . . . .	517
7.4	Pro and Cons of $\sigma$ -Aromaticity . . . . .	519
8	Chemical Reactivity . . . . .	521
8.1	Chemical Reactivity as Reflected by Properties of $\varrho(\mathbf{r})$ . . . . .	522
8.2	The Structure Diagram . . . . .	524
8.3	Chemical Reactivity as Reflected by the Laplace Field $\nabla^2\varrho(\mathbf{r})$ . . . . .	527
9	Concluding Remarks and Outlook . . . . .	534
10	References . . . . .	537

## Index of Symbol

A, B	denote atoms
A	degree of bond equalization based on bond orders n
C	Configuration space
D	degree of $\pi$ -delocalization based on $\pi$ -character $\eta$
a, b	constants in bond order — electron density relationship
d	deviation of bond path from internuclear connection line
d $\mathbf{r}$	volume element in three-dimensional space
d $\omega$	volume element in n-dimensional space
d $\sigma$	surface element
E	molecular electronic energy
F( $\mathbf{r}$ )	force density
G( $\mathbf{r}$ )	kinetic energy density
H( $\mathbf{r}$ )	electronic energy density
H <sub>b</sub>	electronic energy density at the bond critical point $\mathbf{r}_b$
K	number of bonds
K <sub><math>\sigma</math></sub> , K <sub><math>\pi</math></sub>	number of $\sigma$ and $\pi$ bonds
L( $\mathbf{r}$ )	one-particle Lagrange density
l <sub>A</sub> <sup>AB</sup>	value of $-\nabla^2\varrho(\mathbf{r})$ in the valence shell of atom A at position $\mathbf{r}_A^{AB}$ in direction of bond AB
l <sub>A</sub> <sup>n</sup>	value of $-\nabla^2\varrho(\mathbf{r})$ in the lone pair region of atom A
l <sub>A</sub> <sup>h</sup>	value of $-\nabla^2\varrho(\mathbf{r})$ at a concentration hole in the valence shell of atom A
N	number of $\pi$ electrons
n	bond order

$n_a$	number of maxima $\mathbf{r}_a$ of $\varrho(\mathbf{r})$
$n_b$	number of bond critical points $\mathbf{r}_b$ of $\varrho(\mathbf{r})$
$n_r$	number of ring critical points $\mathbf{r}_r$ of $\varrho(\mathbf{r})$
$n_c$	number of cage critical points $\mathbf{r}_c$ of $\varrho(\mathbf{r})$
$\mathbf{n}(\mathbf{r})$	unit vector normal to surface $S(\mathbf{r})$
$M_A^i$	$i$ th order moment of atom $A$
$\hat{O}(\mathbf{r})$	one-electron operator
$O(\Omega_A)$	atomic property, represented by the operator $\hat{O}(\mathbf{r})$
$p$	distance of a point on the valence shell from the nucleus
$Q$	degree of $\pi$ -delocalization
$R_b$	bond path length
$R_e$	equilibrium distance between two atoms
$\mathbf{R}$	nuclear configuration (geometry)
$R_c$	catastrophe point
$r$	rank of the Hessian matrix (matrix of second derivatives) of $\varrho(\mathbf{r})$
$\mathbf{r}$	position vector in molecular space
$\mathbf{r}_A$	position vector of a critical point of $\nabla^2\varrho(\mathbf{r})$ in the valence shell of atom $A$
$\mathbf{r}_a$	position vector of a maximum of $\varrho(\mathbf{r})$
$\mathbf{r}_b$	position vector of a bond critical point of $\varrho(\mathbf{r})$
$\mathbf{r}_c$	position vector of a cage critical point of $\varrho(\mathbf{r})$
$\mathbf{r}_r$	position vector of a ring critical point of $\varrho(\mathbf{r})$
$S(\mathbf{r})$	zero-flux surface
$S(A, B)$	zero-flux surface between atoms $A$ and $B$
$s$	signature of the Hessian matrix of $\varrho(\mathbf{r})$
$T$	kinetic energy
$V$	potential energy
$V(\mathbf{r})$	potential energy density
$\mathbf{W}$	control space in catastrophe diagram
$\mathbf{v}_1, \mathbf{v}_2, \mathbf{v}_3$	eigenvectors of the Hessian matrix of $\varrho(\mathbf{r})$ , direction of the principal curvatures
$\mathbf{u}_i$	normalized eigenvector of the Hessian matrix
$u, v, w$	control parameters of catastrophe diagram
$x, y, z$	cartesian coordinates
$\alpha$	geometrical angle
$\beta$	interpath angle
$\gamma$	angle between the lines connecting two valence shell critical points with the enclosed nucleus
$\Gamma^1$	first order density matrix
$\varepsilon_b, \varepsilon_r$	ellipticity at bond, ring critical point
$\varepsilon'$	effective ellipticity
$\eta$	$\pi$ -character of a bond
$\lambda_1, \lambda_2, \lambda_3$	eigenvalues of the Hessian matrix of $\varrho(\mathbf{r})$ , (principal curvatures)
$\lambda_1(A - B)$	curvature of single bond $AB$
$\xi$	ratio $(\varrho_r/\varrho_b) \cdot 100$
$\varrho(\mathbf{r})$	spinfree one-particle electron density distribution
$\varrho_b$	electron density at the bond critical point

$\varrho_c$	electron density at the cage critical point
$\varrho_r$	electron density at the ring critical point
$\nabla\varrho(\mathbf{r})$	gradient vector (field) of $\varrho(\mathbf{r})$
$\nabla^2\varrho(\mathbf{r})$	Laplace field of $\varrho(\mathbf{r})$
$\sigma$	standard deviation
$\sigma$	stress tensor
$\tau$	dihedral angle
$\Psi$	molecular wavefunction
$\chi$	electronegativity
$\Omega, \Omega_A$	subspace, atomic subspace of atom A

## 1 Introduction

The molecular wave function of a molecule embodies all the information about structure, stability and reactivity of the molecule. However, the wave function  $\Psi$  contains this information in such a complex form that is difficult to translate into heuristic concepts and ad hoc models familiar to chemists. One way to decode chemically useful information from  $\Psi$  is based on a representation of the wave function by antisymmetrized products of molecular orbitals (MO) [1]. The MOs themselves are formed by a linear combination of atomic orbitals (LCAO) [2], which are the smallest building blocks of the wave function. Hence, it is possible to discuss molecular properties in terms of atomic properties by determining the contribution of individual AOs to the MOs that form the wave function.

The MO approach has been successfully applied to reveal the important role of the valence shell electrons for chemical bonding [3], to distinguish between  $\sigma$ - and  $\pi$ -electrons [4], to describe individual bonds of molecules by hybrid orbitals [5], to draw a connection between Lewis' electron pair model and localized MOs [6], to predict the shape of simple molecules by analyzing MO diagrams [7], to assess the properties of atoms in molecules and chemical bonds in terms of orbital and overlap populations [8], to break up complicated molecules into simpler entities and to describe the union of these entities by perturbational MO (PMO) theory [9], to rationalize the reactivity of molecules by analyzing orbital symmetry [10], to stress the role of the frontier orbitals (FO) in chemical reactions [11], etc. This list of accomplishments achieved by applying MO theory could be easily extended and, therefore, it is not astonishing that most chemists prefer to rationalize the physical and chemical properties of atoms and molecules in terms of the properties of the MOs.

The use of MOs, however, implies some disadvantages that have to do with the fact that MOs (as well as AOs) are nonobservable. Also, MOs can be transformed in many ways (using appropriate unitary transformations) without changing energy, geometry or other molecular properties. A chemical observation that is easy to rationalize with one set of MOs may be difficult to understand when described with a transformed set of MOs. For example, canonical MOs are always delocalized and, therefore, they are not helpful when comparing bond localization in a cycloalkane and in a conjugated cyclopolyene. However, the corresponding localized MOs immediately reveal bond localization in the former and bond delocalization in the latter compound.

Also, many orbital models attribute importance to particular MOs while ignoring the effects of all other MOs. Although this simplified approach is helpful in many cases, its justification is doubtful and application is only possible with advances knowledge of the actual chemical situation. Failures of the approach are corrected by considering the properties of additional MOs. For example, within the FO-model [11], molecular reactivity is considered to be dominated by the properties of HOMO and LUMO. In those cases, where predictions on reactive behavior elucidated from HOMO and LUMO are not in line with experimental observations, the second (third, etc.) HOMO (LUMO) are included into the analysis [12].

Models and concepts based on MO-theory are often easy to understand but

difficult to put on a quantitative basis. For example, homoaromaticity is a result of 1,3 overlap between orbitals thus closing a cyclic conjugated system with  $(4q + 2)$   $\pi$ -electrons [13]. If the topology and the geometry of a cyclic system is known potential homoaromaticity can easily be predicted by counting electrons and analyzing MOs in a qualitative way. However, the question how much orbital overlap is necessary to turn on homoaromatic interactions can not be answered in an unambiguous way.

Considering these disadvantages of MO descriptions of molecules it becomes highly desirable to base a better description on a molecular quantity that is

1. a function of the total wave function,
2. invariant under unitary transformations of the MOs,
3. an observable molecular property,
4. directly related to the molecular energy (stability), geometry (structure), and other molecular properties,
5. dissectable into atomic and bond contributions,
6. indicative of the distribution of negative and positive charge in the molecule,
7. a continuous function of a position vector  $\mathbf{r}$  to allow a distinction between different (reactive) sites in the molecule.

The only quantity that fulfills all these requirements is the total one electron density distribution  $\rho(\mathbf{r})$ . It is a direct function of  $\Psi$ , invariant with regard to unitary transformations of the MOs, and an observable molecular property that can be determined by a combination of X-ray and neutron diffraction experiments [14, 15]. Also it is easy to calculate  $\rho(\mathbf{r})$  once the MOs and the wave function  $\Psi$  of a molecule have been determined [16].

The fundamental role of the one electron density  $\rho(\mathbf{r})$  was pointed out first by Hohenberg and Kohn [17]. They showed that the energy of a nondegenerate (electronic) ground state of a molecule is an unique functional of  $\rho(\mathbf{r})$ . Therefore, physical and chemical properties of a molecule can be related to  $\rho(\mathbf{r})$ .

Bader and co-workers have shown that properties of the electron density distribution  $\rho(\mathbf{r})$  can be used to derive a partitioning of the molecular space into subspaces that are associated with the atoms in a molecule [18–20]. This method has been called “virial partitioning” because the virial theorem remains valid in the subspaces thus obtained. Also, chemical bonds can be described by the properties of  $\rho(\mathbf{r})$  [21–23] and reactive sites in a molecule can be identified by analyzing the properties of  $\rho(\mathbf{r})$  [24–28]. In conclusion, investigation of  $\rho(\mathbf{r})$  provides an improved description of a molecule as compared to the analysis of particular MOs. This does not mean that the analysis of the MOs should be discarded in favour of the analysis of  $\rho(\mathbf{r})$ . On the contrary, information from both MOs and  $\rho(\mathbf{r})$  should be combined in such a way that the most complete and useful description of the molecule emerges. MOs are still to be used for qualitative arguments while the analysis of  $\rho(\mathbf{r})$  proves the basis for

1. defining atoms in molecules and chemical bonds,
2. defining molecular structure and structural changes,
3. quantitatively assessing the properties of atoms in molecules and chemical bonds,
4. specifying chemical models and concepts,
5. relating changes in molecular structure (chemical reactivity) to the local properties of the molecular charge distribution.

We will demonstrate this by briefly reviewing the essential features of the analysis of the electron density distribution  $\rho(\mathbf{r})$ , its gradient vector field  $\nabla\rho(\mathbf{r})$ , and its Laplace field  $\nabla^2\rho(\mathbf{r})$  in Sects. 2 and 3. Then, based on the local properties of  $\rho(\mathbf{r})$  we will describe  $\pi$ -conjugation (Sect. 4), homoconjugation (Sect. 5), and  $\sigma$ -conjugation (Sect. 7). Selected examples will be given to demonstrate both the feasibility and the usefulness of the analysis of  $\rho(\mathbf{r})$  [29–33]. Special emphasis will be laid on a re-consideration of well-known chemical concepts such as aromaticity and antiaromaticity [29] (Sect. 4), homoaromaticity [34–37] (Sect. 5), and  $\sigma$ -aromaticity [38–41] (Sect. 7). A quantitative assessment of the latter requires a deeper understanding of the notion of ring strain, of the relationship of three-membered rings and  $\pi$ -complexes, and of the chemical bonding in cyclopropane [38–44] (Sect. 6). Section 8 will be devoted to the description of chemical reactivity as assessed from the properties of  $\rho(\mathbf{r})$  [45–47]. Sections 2 through 9 establish the scenario of carrying out the analysis of  $\rho(\mathbf{r})$  in such a way that allows reevaluation and improvement of chemical concepts, that leads to new insights into molecular properties, and that lays the basis for discovery of novel compounds. The latter point has been demonstrated in a number of investigations which, e.g. dealt with unknown carbon, beryllium compounds [48], the peculiar structure of dications [49], and the question of the existence of helium compounds [50–51]. Since these studies will be reviewed in another article [52], we will only sketch some highlights of this work in the final chapter of this article which contains concluding remarks and an outlook.

## 2 Analysis of the Electron Density Distribution $\rho(\mathbf{r})$

Figure 1 shows a perspective drawing of the calculated electron density distribution  $\rho(\mathbf{r})$  of the methyl cation,  $\text{CH}_3^+$ , with regard to the plane containing the four nuclei. At the positions of the nuclei,  $\rho(\mathbf{r})$  attains maximal values [53]. In off-nucleus

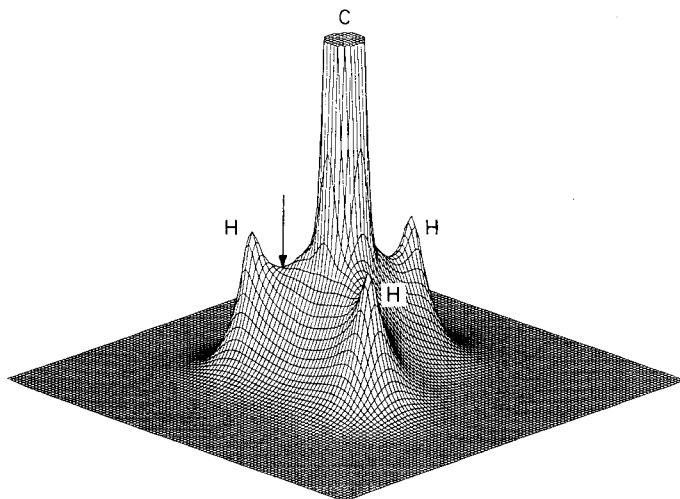


**Fig. 1.** Perspective drawing of the calculated electron density distribution  $\rho(\mathbf{r})$  of the methyl cation,  $\text{CH}_3^+$ , with regard to the plane containing the four nuclei. The position of one of the three saddle points between the C and the H atoms is marked by an arrow. For a better representation values above a threshold are cut off. (HF/6-31G(*p*, *d*) calculations)

direction,  $\rho(\mathbf{r})$  decreases exponentially and quickly approaches zero for large distances from the nuclei. The same pattern is found for all molecules. It seems that  $\rho(\mathbf{r})$  of a molecule is dominated by the electron density distribution of the various atoms constituting the molecule. In so far, one cannot expect much useful information about molecules when analyzing  $\rho(\mathbf{r})$ .

However, a closer look at Fig. 1 reveals that in the bonding region  $\rho(\mathbf{r})$  adopts a distinct behavior that cannot be explained by just superimposing the electron densities of the corresponding atoms. For example, the distribution  $\rho(\mathbf{r})$  possesses relatively large values in the CH bond region. The C and H nuclei are connected by a ridge of maximum electron density like the summits of a mountain range. Any lateral displacement from the path leading along the ridge means a decrease in  $\rho(\mathbf{r})$ . Therefore, we speak of a path of maximum electron density (MED path) linking bonded atoms. As can be seen in Fig. 1, there are just three MED paths between the C atom and the three H atoms, which is in line with the fact that  $\text{CH}_3^+$  contains three CH bonds.

Also, shown in Fig. 1 is the position  $\mathbf{r}_b$  (marked by an arrow) of the minimum of  $\rho(\mathbf{r})$  along the MED path. It corresponds to a maximum of  $\rho(\mathbf{r})$  in all directions perpendicular to the MED path, i.e. it is a saddle point of  $\rho(\mathbf{r})$  in three dimensions. The position  $\mathbf{r}_b$  is uniquely defined by the first and second derivatives of  $\rho(\mathbf{r})$ , collected in the gradient vector  $\nabla\rho(\mathbf{r})$  and the Laplacian  $\nabla^2\rho(\mathbf{r})$ . The value of  $\nabla\rho(\mathbf{r})$  equals zero at  $\mathbf{r}_b$ . Two of the three eigenvalues of the Hessian matrix of  $\rho(\mathbf{r})$  (matrix of the second derivatives),  $\lambda_1$  and  $\lambda_2$  are negative, while the third eigenvalue,  $\lambda_3$ , is positive at  $\mathbf{r}_b$ . The eigenvalue  $\lambda_3$  defines the curvature along the MED path,  $\lambda_1$  and  $\lambda_2$  the curvatures along the principle axes spanning the plane perpendicular to the MED path. The saddle point  $\mathbf{r}_b$  of  $\rho(\mathbf{r})$  can be specified by rank and signature of the Hessian matrix [54]. For  $\lambda_i \neq 0$  ( $i = 1, 2, 3$ ), the rank  $r$  is 3 and the signature  $s$  is given by

$$s = \sum_i \lambda_i / |\lambda_i| \quad (1)$$

Since  $\lambda_1, \lambda_2 < 0$  and  $\lambda_3 > 0$  for  $\mathbf{r}_b$ , the saddle point of  $\rho(\mathbf{r})$  between two bonded atoms is a  $(3, -1)$  stationary (critical) point.

The critical point  $\mathbf{r}_b$  is an important point, not only from a topological point of view but also with regard to the quantum mechanics of an atom in a molecule [18–20]. It is located on a surface  $S(\mathbf{r})$  that partitions molecular space in atomic subspaces. This can be seen when analyzing not only  $\rho(\mathbf{r})$  but also  $\nabla\rho(\mathbf{r})$ . The gradient vector  $\nabla\rho(\mathbf{r})$  always points into the direction of maximum increase of  $\rho(\mathbf{r})$ . If one evaluates the gradient vector of  $\rho(\mathbf{r})$  at a continuous successions of points  $\mathbf{r}$  in molecular space, then a gradient path of  $\nabla\rho(\mathbf{r})$  will result. This is the path traced out by the gradient vector of  $\rho(\mathbf{r})$ . Since it is perpendicular to the contourlines of  $\rho(\mathbf{r})$  at all points in molecular space, it is an orthogonal trajectory of  $\rho(\mathbf{r})$ . The collection of all gradient paths defines the gradient vector field of  $\rho(\mathbf{r})$ .

Figure 2 shows the gradient vector field of the electron density distribution  $\rho(\mathbf{r})$  of  $\text{CH}_3^+$  with regard to the reference plane containing the nuclei. Inspection of the gradient vector field reveals that one can distinguish three different types of trajectories. First, there are those trajectories which terminate at one of the nuclei (type I trajectories). Secondly, there are trajectories that spring at one of the saddle points  $\mathbf{r}_b$  between C and the H nuclei and terminate at one of the nuclei next to  $\mathbf{r}_b$



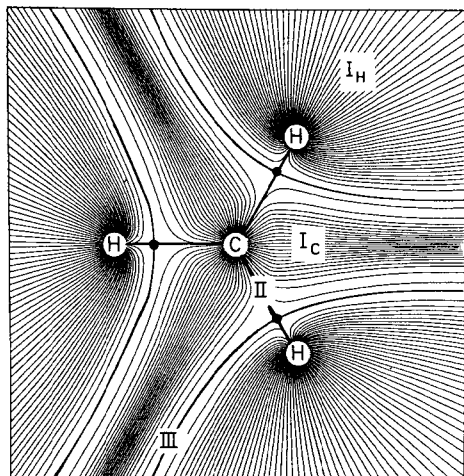


**Fig. 2.** Gradient vector field  $\nabla\rho(\mathbf{r})$  of the electron density distribution of the methyl cation,  $\text{CH}_3^+$ , shown for the plane containing the four nuclei. Saddle points  $\mathbf{r}_b$  are denoted by dots. There are three different types of trajectories. Type  $\text{I}_H(\text{I}_C)$  trajectories start at infinity and end at a H(C) nucleus. Type II trajectories (heavy lines) define the MED paths linking the carbon atom to the hydrogen atoms. Type III trajectories form the three zero-flux surfaces  $S(\mathbf{r})$  between the C and H atoms. In the two dimensional display only their traces can be seen. Type III trajectories spring at infinity and terminate at the saddle points. (HF/6-31G(*p*, *d*) calculations)

(type II trajectories). For each saddle point  $\mathbf{r}_b$  just two type II trajectories exist which define the MED path linking bonded atoms (heavy lines). Finally, there are trajectories that originate at infinity and terminate at the saddle point  $\mathbf{r}_b$  (type III trajectories). In three dimensions, these trajectories define the limiting surface  $S(\mathbf{r})$  separating bonded atoms. In the two-dimensional display of Fig. 2, only traces of the three surfaces  $S(\mathbf{r})$  that separate C and H atoms can be seen. There are no trajectories passing through  $S(\mathbf{r})$  (Fig. 2), i.e. the flux of  $\nabla\rho(\mathbf{r})$  vanishes for all surface points:

$$\nabla\rho(\mathbf{r}) \cdot \mathbf{n}(\mathbf{r}) = 0 \quad \mathbf{r} \in S(\mathbf{r}), \quad (2)$$

where  $\mathbf{n}(\mathbf{r})$  is the unit vector normal to the surface  $S(\mathbf{r})$ . The surface  $S(\mathbf{r})$  is called zero-flux surface [18–20].

## 2.1 Definition of an Atom in a Molecule

As discussed for  $\text{CH}_3^+$  (Fig. 2), the zero-flux surfaces  $S(\mathbf{r})$  partition molecular space into subspaces, each of which contains exactly one and only one atomic nucleus [55]. Since this observation has been made for many molecules [21–23], it is reasonable to consider the subspaces defined by the zero-flux surfaces as *atomic subspaces*. All type I trajectories terminating at a given nucleus form the basin  $\Omega$ . As was first proposed by Bader and co-workers [18–20], the union of a nucleus and its associated basin defines the *atom in a molecule*.

The subspaces given by Eq. (2) are unique since quantum mechanical laws such as the virial theorem are valid in a subspace  $\Omega$  [19]. If one associates  $\Omega$  with an atom one can speak of a “virial atom”. The dissection of the molecules space into atomic subspaces is called the “virial partitioning” method [19]. With the definition of an atom in a molecule, it is possible to determine the properties of atoms in a molecule. For example, the space  $\Omega_A$  that is filled by the gradient paths terminating at one atomic nucleus is the volume of the corresponding atom A.

If  $\varrho(\mathbf{r})$  is integrated over  $\Omega_A$ , the atomic monopole moment  $M_A^0$  will be obtained. The difference between the atomic number  $Z_A$  and  $M_A^0$  yields the atomic charge. If  $\mathbf{r}^n \varrho(\mathbf{r})$  is integrated over  $\Omega_A$  for  $n = 1, 2, \dots$  atomic dipole, quadrupole, ... moments will result. Any atomic property  $O(\Omega_A)$  that can be represented by an one-electron operator  $\hat{O}$  is given by:

$$O(\Omega_A) = \int_{\Omega} \hat{O}(\mathbf{r}) \varrho(\mathbf{r}) \, d\mathbf{r}. \quad (3)$$

The definition of atoms in molecules leads to a detailed and quantitative description of their properties (see, Table 1). In addition, it provides the basis for a definition of the chemical bond.

**Table 1.** Description of atoms in molecules, chemical bonds, and molecular structure in terms of the properties of  $\varrho(\mathbf{r})$

Terms used in Density Analysis	Comment	Chemical Term
<b>1. General definitions</b>		
Nucleus + Basin	Basin $\Omega_A$ is formed by all gradient paths that terminate at the nucleus of atom A.	Atom A
Zero-flux Surface	Surface S (AB) is formed by all gradient paths that terminate at the saddle point $\mathbf{r}_b$ between atoms A and B.	Interatomic surface between atoms A and B
Bond path	<i>Necessary condition:</i> Existence of a maximum electron density (MED) path linking bonded atoms A and B. <i>Sufficient condition:</i> Negative energy density $H(\mathbf{r}_b)$ at the minimum of the MED path.	Covalent bond AB
Molecular graph	Network of MED (bond) paths for a given geometry $\mathbf{R}$ .	Molecule
Molecular structure	Class of all equivalent molecular graphs.	Molecular structure
<b>2. Properties of an atom in a molecule</b>		
$\int_{\Omega} d\mathbf{r} = V$	Volume V of basin $\Omega$ .	Atomic volume
$\int_{\Omega} \mathbf{r}^n \varrho(\mathbf{r}) \, d\mathbf{r} = M^n$	Moments $M^n$ of basin $\Omega$	$n = 0$ : Atomic monopole moment $n = 1$ : Atomic dipole moment $n = 2$ : Atomic quadrupole moment
$O(\Omega) = \int_{\Omega} \hat{O}(\mathbf{r}) \varrho \, d\mathbf{r}$	Any atomic property $O(\Omega)$ which can be represented by a one-electron operator $\hat{O}(\mathbf{r})$ can be obtained by integrating $\hat{O}(\mathbf{r}) \varrho(\mathbf{r})$ over the atomic volume $\Omega$ .	Atomic property O
<b>3. Bond properties of covalent bonds</b>		
Bond path length $R_b$	$R_b \geq R_e$ ; $R_b$ is larger than the geometrical distance $R_e$ for bent bonds.	Bond length
Interpath angle $\beta$	$\beta$ is (normally) larger (or smaller) than the geometrical angle $\alpha$ in strained rings.	Bond angle
Bond order n	Evaluated from $\varrho_b$ according to Eq. 8.	Bond order

Bond ellipticity $\epsilon$	Defined by the curvature $\lambda_1$ and $\lambda_2$ of $\rho_b$ perpendicular to the bond according to Eq. 9.	$\pi$ -Character
Shift parameter $\Delta$	Deviation of $\mathbf{r}_b$ from the geometrical center of the bond path.	Bond polarity
Distance $d$	Deviation of bond path from the inter-atomic connection line (together with $R_b$ and $\beta$ ).	Bent bond character

## 2.2 From Atoms to Chemical Bonds

Analyzing  $\rho(\mathbf{r})$  reveals that there are as many  $(3, -1)$  saddle points, zero-flux surfaces, and MED paths as there are bonds in a molecule. For example, in  $\text{CH}_3^+$  (Figs. 1 and 2) only the C and H atoms are connected by MED paths but not the H atoms among themselves. If a bond is broken in a molecule the corresponding MED path will vanish in the electron density distribution. It will reappear if the bond is formed again [21]. These observations have led to the conclusion that there is a one to one correspondence between MED paths, saddle points  $\mathbf{r}_b$ , and zero-flux surfaces  $S$  on the one hand and chemical bonds on the other hand. As a consequence, the existence of a saddle point  $\mathbf{r}_b$  accompanied by the existence of a MED path linking the two nuclei of the adjoining atomic subspaces can be considered to be a necessary condition for the existence of a chemical bond [22, 26–28].

However, not every MED path represents a covalent chemical bond. MED paths are also found in case of van der Waals complexes, hydrogen bonds or electrostatic (ionic) interactions [22], i.e. in all cases of closed shell interactions. In order to uniquely define a covalent bond and to distinguish it from ionic and other bonds, a second, sufficient condition has to complement the first one. According to the variation principle the molecular charge distribution is such as to minimize the energy and bonding is intimately connected with an energy gain relative to the separated atoms. Therefore it seems reasonable to base a sufficient condition for chemical bonding on energetic grounds.

It has been shown that the gain in energy,  $\Delta E$ , resulting from bond formation is due to a complex interplay of kinetic and potential energy contributions [56–59]. When two bonded atoms share their electrons in a chemical bond, the space which the electrons can occupy has been increased with regard to that of the isolated atoms. The electrons *delocalize* and, as a consequence, the uncertainty of position of each electron increases. According to the Heisenberg uncertainty principle, this leads to a decrease of the momentum uncertainty. Since the kinetic energy is proportional to the square of the momentum uncertainty [60], delocalization of electrons causes a drop in the kinetic energy and, hence, a stabilization of the molecule [61].

In the case of the  $\text{H}_2$  molecule, the form of the molecular wavefunction  $\Psi$  is characterized by the bonding  $\sigma_g$  MO that results from an in-phase overlap of the  $1s$  AOs. Along the bond axis ( $z$ -axis), the  $\sigma_g$  MO takes the form qualitatively shown in Fig. 3a. Bonding overlap implies a flattening of the wavefunction in the bond

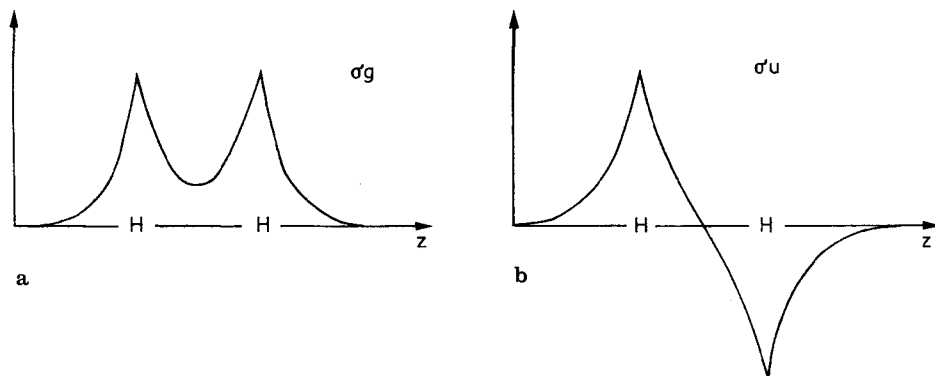


Fig. 3a, b. Schematic representation of **a** the bonding  $\sigma_g$  MO and **b** the antibonding  $\sigma_u$  MO of the  $H_2$  molecule shown along the bond axis (z-axis)

region reflected by a decrease in  $\partial\Psi/\partial z$  and an increase in  $\partial\Psi/\partial x$  and  $\partial\Psi/\partial y$ . Since the kinetic energy parallel to the H—H bond may be expressed as a function of  $\partial\Psi/\partial z$ , bonding overlap and delocalization of electrons leads to a reduction of the kinetic energy in the direction of the bond [57–59]. At the same time, components of the kinetic energy perpendicular to the bond increase yielding an overall, though minimal, increase of the kinetic energy.

Similar observations can be made for the three components of  $\varrho(\mathbf{r})$  namely,  $\varrho(x)$ ,  $\varrho(y)$ , and  $\varrho(z)$ . Delocalization of charge into the bonding region (occupation of the  $\sigma_g$  MO) causes a decrease in the curvature  $\lambda_3$  of  $\varrho(\mathbf{r})$  along the bond path while the two curvatures perpendicular to the bond path,  $\lambda_1$  and  $\lambda_2$ , increase. Since  $\lambda_3 > 0$  and  $\lambda_1, \lambda_2 < 0$ , their sum becomes more negative, which is indicative of a concentration of electronic charge in the bonding region (see Sect. 3). These observations suggest that covalent bonding is accompanied by a decrease of the kinetic energy (parallel to the bond) with respect to the free atoms and by a concentration of negative charge in the bonding region [62].

If heavy atoms are bonded, the situation will be far more complicated. Occupied antibonding orbitals cause an increase rather than a decrease of  $\nabla\Psi$  (see, e.g. Fig. 3b) and, hence, an increase in the kinetic energy parallel to the bond. At the same time, the sum of the curvatures  $\lambda_i$  may become positive, indicative of a depletion of charge in the bonding region. Studies on  $A_2$  and AH molecules [20, 63], suggest that there are regions with a drop in the kinetic energy, but they can be located anywhere, even in nonbonding regions.

In order to derive a more general model of the chemical bond valid for systems with and without hydrogen atoms, Ruedenberg [64] has proposed a conceptual partitioning of the binding energy, which is the difference of the total molecular energy and the sum of the energies of the atoms in their ground states. According to this scheme, the binding energy comprises five contributions that result from

1. promotion energy,
2. quasi-classical interaction energy,
3. sharing penetration,
4. sharing interference energy, and
5. charge transfer energy.

Although this partitioning of the binding energy provides valuable insight into the mechanism of bonding of small molecules, it is difficult to apply in general. This has to do with the choice of the atomic ground state, and some arbitrariness in the construction of the hybrid orbitals, which are necessary for the evaluation of the promotion energy. For larger molecules, an inflation of numbers will impede a clear description of chemical bonds [65]. Also, it remains to be seen how this description performs in the case of nonclassical bonds. — Other schemes have been proposed to describe chemical bonds by partitioning the energy [66, 67]. However, none of these descriptions is simultaneously simple, generally applicable, and free of shortcomings.

### 2.3 Distinction Between Covalent Bonds and Closed Shell Interactions

In view of the complications inherent to the various bonding analyses that are based on the total energy, it is better to turn to local properties of the energy and analyze them in a way similar to that employed for the analysis of the electron density distribution  $\rho(\mathbf{r})$ . For this purpose, the energy density  $H(\mathbf{r})$  has been defined [22, 26, 28]:

$$H(\mathbf{r}) = G(\mathbf{r}) + V(\mathbf{r}) \quad (4)$$

$G(\mathbf{r})$  is a local kinetic energy density [68] given by:

$$G(\mathbf{r}) = 1/2 \nabla \nabla' \Gamma^1(\mathbf{r}; \mathbf{r}')|_{\mathbf{r}=\mathbf{r}'}, \quad (5)$$

with  $\Gamma^1(\mathbf{r}; \mathbf{r}')|_{\mathbf{r}=\mathbf{r}'}$  being the first order density matrix [69].  $V(\mathbf{r})$  is the average field experienced by one electron in a many particle system [70]:

$$V(\mathbf{r}) = N \int [\Psi^*(-\mathbf{r} \nabla \nabla') \Psi] d\tau' \quad (6)$$

where  $d\tau'$  denotes integration over spin coordinates of all  $N$  electrons and integration over all  $N$  electrons but one. Integrated over the total molecular space,  $H(\mathbf{r})$  yields the molecular electronic energy  $E$

$$E = \int H(\mathbf{r}) d\mathbf{r} = \int G(\mathbf{r}) d\mathbf{r} + \int V(\mathbf{r}) d\mathbf{r} = T + V \quad (7)$$

$G(\mathbf{r})$  is always positive and  $V(\mathbf{r})$  is always negative. The sign of  $H(\mathbf{r})$  determines whether accumulation of charge at a point  $\mathbf{r}$  is stabilizing [ $H(\mathbf{r}) < 0$ ] or destabilizing [ $H(\mathbf{r}) > 0$ ]. Investigation of a variety of different chemical bonds [22] has revealed that covalent bonding is characterized by a predominance of the local potential energy density  $V(\mathbf{r})$  in the interatomic region reflected by  $H(\mathbf{r}_b) \equiv H_b < 0$ . For closed shell interaction, van der Waals complexes, or ionic bonds,  $H_b > 0$  has been found [22]. Therefore, it is reasonable to base a *sufficient* condition for covalent bonding on the properties of  $H(\mathbf{r})$  in the bond region. In view of these considerations, one can speak of a covalent bond between two atoms A and B if [22, 26, 28]

1. a MED path links A and B, i.e. the atomic basins  $\Omega_A$  and  $\Omega_B$  are adjoined, only separated by an interatomic surface  $S(A, B)$  (*necessary condition*), and

2. the local energy density  $H(\mathbf{r})$  at the saddle point  $\mathbf{r}_b$  is smaller than zero (*sufficient condition*).

If both conditions are fulfilled we will call the MED path a “*bond path*” and the saddle point  $\mathbf{r}_b$  a bond critical point [71]. If, however,  $H_b$  is  $\geq 0$ , there will be a closed shell interaction between A and B leading to either ionic bonding, van der Waals interactions, or other forms of noncovalent bonding.

It is clear that a reduction of the kinetic energy (density) in the bonding region is a prerequisite of a negative  $H(\mathbf{r})$ , i.e. the definition given above is in line with the idea that chemical bonding (mostly) implies a decrease in the kinetic energy in the direction of the bond. But since  $H(\mathbf{r})$  comprises the effects of both local kinetic and local potential energy, it is also indicative of bonding in those cases where the kinetic energy decrease in the bonding region is disguised by other effects as found for  $N_2$ ,  $O_2$ , and  $F_2$  [72] or cyclopropane [73]. We will corroborate on this point further when discussing the Laplacian of  $q(\mathbf{r})$  (see Sect. 3).

## 2.4 Description of the Covalent Bond

The definition of the covalent bond provides a basis for its characterization in terms of the properties of  $q(\mathbf{r})$  along the bond path or at the bond critical point. For example, the value of  $q(\mathbf{r})$  at  $\mathbf{r}_b$ ,  $q_b$ , can be used to determine a bond order and its position can serve as a measure for the bond polarity. Further, the anisotropy of  $q_b$  can be related to the  $\pi$ -character of a bond. In the case of strained molecules, the curvature of the bond path reflects the bent bond character of a bond [22, 23].

For a variety of hydrocarbon compounds with single, double and triple bonds, aromatic, strained and unstrained bonds a linear relationship between  $q_b$  and the CC bond distance  $R$  has been found [21, 22]. This relationship has been utilized to establish a definition for the bond order  $n$  [21] (see Fig. 4a):

$$n = \exp [a(q_b - b)] . \quad (8)$$

The constants  $a$  and  $b$  have been determined by assigning Lewis bond orders 1, 2, and 3 to ethane, ethylene, and acetylene. Bond orders for molecules containing nitrogen, oxygen or other hetero atoms can be defined in a similar way [22]. It has to be stressed that a bond order defined in terms of  $q_b$  does not suffer from the ambiguities of an analysis of chemical bonding in terms of molecular orbitals. It is simple to evaluate and simple to use [74].

In case of a hetero polar bond, the basin of the more electropositive atom is smaller than that of its bonding partner because it has lost part of its negative charge. As a consequence, the bond critical point  $\mathbf{r}_b$  is always closer to the more electropositive atom. For the  $AH_n$  series with  $A = Li, Be, B, C, N, O$  a linear relationship between the deviation  $\Delta$  of the bond critical point  $\mathbf{r}_b$  from the center of the bond path and the electronegativity difference between  $A$  and  $H$  has been found [22]. With increasing electronegativity of  $A$  the bond critical point moves toward the  $H$  atom which is indicative of a continuous compression of the  $H$  basin. However, for  $H_2O$  a natural compressibility limit of  $H$  is reached that cannot be surpassed. Bearing this in mind, the position of the bond critical point can be used as measure of the bond polarity [75].

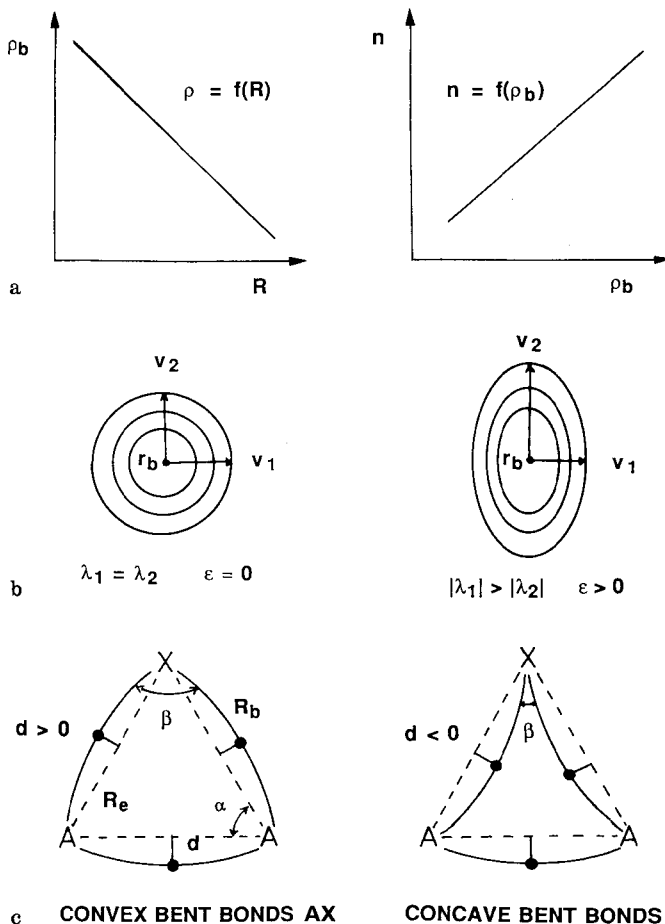


**Fig. 4a-c.** Description of a covalent bond in terms of the properties of the electron density distribution  $\rho(r)$ . **a** Schematic representation of the relationship between the electron density  $\rho_b$  at the bond critical point and the bond length  $R$  (left side) and of the relationship between the bond order  $n$  and  $\rho_b$  (right side). **b** Qualitative contourline diagrams of  $\rho(r)$  in the plane that contains the bond critical point  $r_b$  and is perpendicular to a CC single bond (left side) and a CC double bond (right side). Ellipticities  $\epsilon$  and eigenvectors  $v_1$  and  $v_2$  that indicate the direction of steep ( $\lambda_1$ ) and soft curvature ( $\lambda_2$ ) are given.  $v_2$  is the major axis. **c** Definition of parameters  $R_b$ ,  $d$ , and  $\beta$  describing the curved MED path (solid line) of a bent bond in strained rings. Outwardly (inwardly) curved bond paths denote convex (concave) bent bonds.  $R_b$  is larger than the geometrical distance  $R_e$ . The angle  $\beta$  is larger (convex bent bonds) or smaller (concave bent bonds) than the geometrical angle  $\alpha$ .

The density distribution at the bond critical point in the plane perpendicular to the bond may be isotropical or anisotropical [21, 22]. The ratio of the curvatures  $\lambda_1$  and  $\lambda_2$  is a measure of the anisotropy of  $\rho_b$  [21]. In case of the CC single bond in ethane, the negative charge distribution at  $r_b$  is isotropical and, hence,  $\lambda_1 = \lambda_2$ . However, for ethylene (or other hydrocarbons with CC double bonds) the density distribution at  $r_b$  is anisotropical ( $\lambda_1 < \lambda_2$ ). The electron density extends farther in the space above and below the molecular plane, i.e. in the direction of the  $\pi$  MOs,

than in the molecular plane perpendicular to the  $\sigma$  bond. The curvature  $\lambda_2$  associated with the  $\pi$ -direction is called *soft curvature* while  $\lambda_1$  is called *steep curvature*. The corresponding eigenvectors of the Hessian matrix, the directions of  $\lambda_1$  and  $\lambda_2$ , are given by  $\mathbf{v}_1$  and  $\mathbf{v}_2$  (see Fig. 4b). The ratio  $\lambda_1$  to  $\lambda_2$  has been used to define the bond ellipticity  $\varepsilon$  [21]:

$$\varepsilon = \lambda_1/\lambda_2 - 1. \quad (9)$$

For bonds with (partial)  $\pi$ -character  $\varepsilon$ -values larger than zero are found [21, 22]. Therefore, the ellipticity  $\varepsilon$  has been related to the  $\pi$ -character of a (partial) double bond.

For triple bonds,  $\varepsilon$  is equal or close to zero since there are now two soft curvatures ( $\lambda_1 \approx \lambda_2$ ). It is useful in this case to define effective ellipticities  $\varepsilon'_i$  by comparing  $\lambda_i$  ( $i = 1, 2$ ) with  $\lambda_i(A - B)$ , where  $\lambda_i(A - B)$  are the curvatures of the single bond  $A - B$  [22].

Another interesting feature of the chemical bond, is its bent bond character [22]. The analysis of  $\varrho(\mathbf{r})$  provides a basis for a quantitative description of this phenomena. In case of strained molecules, the bond path may not coincide with the interatomic connection line. It can be inwardly or outwardly curved, as schematically shown in Fig. 4c. The bond critical point  $\mathbf{r}_b$  is shifted from the interatomic connection line by a distance  $d$ . The shift parameter  $d$  has a positive sign in case of outwardly curved bonds (convex bent bonds) and a negative sign in case of inwardly curved bonds (concave bent bonds). For a bent bond, the bond path length  $R_b$  is longer than the internuclear distance  $R_c$ . Similarly, the interpath angle  $\beta$  is larger (for outwardly curved bonds) or smaller (for inwardly curved bonds) than the geometrical angle  $\alpha$  as shown in Fig. 4c. Thus, the bent bond character, i.e. the curvature of a bond path is quantitatively described by the ratio  $R_b/R_c$ , the interpath angle  $\beta$ , and the shift parameter  $d$ .

Table 1 summarizes the various definitions based on the properties of  $\varrho(\mathbf{r})$ .

## 2.5 Definition of Molecular Structure and Structural Changes

Once an atom in a molecule and the chemical bond have been defined, it is straightforward to define a molecule and molecular structure. Before doing this we have to characterize other types of stationary (critical) points of  $\varrho(\mathbf{r})$  that can be found in the molecular charge distribution. Apart from the the saddle points  $\mathbf{r}_b$  of  $\varrho(\mathbf{r})$  in the bond region (bond critical points), there are three other types of stationary points, namely the local maxima  $\mathbf{r}_a$  of  $\varrho(\mathbf{r})$  that occur at the position of the nuclei [53], ring critical points  $\mathbf{r}_r$ , and cage critical points  $\mathbf{r}_c$ . A ring critical point is found in the center of a ring while cage critical points are inside a cage. The number of positive and negative eigenvalues  $\lambda_i$  given by the signature  $s$  of the Hessian matrix (see Eq. (1)) for each of these critical points is given in Table 2. Hence,  $\mathbf{r}_a$  is a (3, -3) critical point (maximum),  $\mathbf{r}_b$  is a (3, -1) critical point (saddle point),  $\mathbf{r}_r$  a (3, +1) critical point (saddle point), and  $\mathbf{r}_c$  a (3, +3) critical point (minimum). The number and types of gradient vector paths terminating (springing) at each critical point are also given in Table 2. Further, each point can be classified as a 1-dimensional attractor (3-1-di-



**Table 2.** Description of critical (stationary) points of  $\rho(\mathbf{r})$ 

Notation	$\mathbf{r}_a$	$\mathbf{r}_b$	$\mathbf{r}_r$	$\mathbf{r}_c$
Critical point	Nucleus	Bond <sup>f</sup>	Ring	Cage
Eigenvalues of the Hessian Matrix	$\lambda_1, \lambda_2, \lambda_3 < 0$	$\lambda_1, \lambda_2 < 0, \lambda_3 > 0$	$\lambda_1 < 0, \lambda_2, \lambda_3 > 0$	$\lambda_1, \lambda_2, \lambda_3 > 0$
Rank, Signature <sup>a</sup>	(3, -3) <sup>e</sup>	(3, -1)	(3, +1)	(3, +3)
Mathematical Description	Maximum	Saddle point	Saddle point	Minimum
Topological Description <sup>b</sup>	3-dimensional attractor	2-dimensional attractor	1-dimensional attractor	Repeller
Trajectories <sup>c, d</sup>				
terminating	$\infty$ type I	$\infty$ type III	2 type III	—
originating	—	2 type II	$\infty$ ( $n_b$ I + $n_b$ II)	$\infty$ ( $n_a$ I) + $\infty$ ( $n_b$ II)
Associated Element <sup>d</sup>	basin $\Omega$	Zero-flux surface S	Edge of $n_b$ surfaces	Corner of $n_b$ surfaces
Chemical Relevance	Nucleus <sup>e</sup>	Bond path <sup>f</sup>	Ring structure	Cage structure

<sup>a</sup> The rank of the Hessian matrix is given by the number of eigenvalues  $\lambda_i$  unequal zero. The signature is defined by Eq. (1).

<sup>b</sup> An attractor “attracts” gradient paths (trajectories). They terminate at the attractor. A repeller “repels” gradient paths. They originate at the repeller. An 1-dimensional attractor is at the same time a (3-D)-dimensional repeller.

<sup>c</sup> Type I trajectories fill the basin  $\Omega$ , type II trajectories form the bond path, and type III trajectories form the zero-flux surface.

<sup>d</sup>  $n_a$  denotes the number of adjoining atomic basins,  $n_b$  the number of bonds in a ring or in a cage.  $n_a \geq 1$ ,  $n_b(\text{ring}) \geq 3$ ,  $n_b(\text{cage}) \geq 6$  where the equal sign would apply to a diatomic molecule, a three-membered ring, and a tetrahedral cage structure.

<sup>e</sup> The nucleus is a pseudo maximum. See Ref. [53].

<sup>f</sup> Since not each point  $\mathbf{r}_i$  is a bond critical point, the correct notation would be MED-critical point. For reasons of simplicity, we use a term that best fits in the list of structural elements associated with the critical points of  $\rho(\mathbf{r})$ .

mensional repeller) in view of the trajectories being “attracted” (being “repelled”) by it. The chemical relevance of each point is also given in Table 2.

The number  $n$  and type of critical points that can exist in a molecule is determined by the Poincare-Hopf relationship [54]:

$$n_a - n_b + n_r - n_c = 1, \quad (10)$$

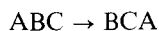
Utilizing the structural assignments given in Table 2 for each critical point,  $n_a$  denotes the number of nuclei,  $n_b$  the number of bonds and closed shell interactions,  $n_r$  the number of rings, and  $n_c$  the number of cages in a molecule.

Utilizing the definitions given above, a molecule is defined as a collection of 3-dimensional attractors, i.e. atoms, linked by a network of bond paths, i.e. chemical bonds. For a given nuclear configuration  $\mathbf{R}$  (geometry) of the molecule, it is characterized by the molecular graph, i.e. by the critical points of  $\rho(\mathbf{r}, \mathbf{R})$  and the associated MED paths connecting the atomic nuclei. Molecular graphs that possess the same number of MED paths linking the same nuclei form an equivalent class [76]. They

represent a single molecular structure, which in turn is associated with a structural region of the configuration space. For a given molecular state, there exists a finite number of classes of equivalent graphs (structures) and associated structural regions. Accordingly, the molecular configuration space is partitioned into a finite number of structural regions. Within a structural region, molecular structure does not change (is structurally stable [77]) with respect to differential changes of geometry). However, at the boundaries between two structural regions, a differential change in geometry leads to a discontinuous change in the molecular graph. Hence, at these boundaries the unstable structures of a molecule are located. A point  $\mathbf{R}$  of nuclear configuration space that is structurally stable is called a regular point. In contrast, a point  $\mathbf{R}_c$  on the boundary between two stable structures is called catastrophe point. Point  $\mathbf{R}_c$  will be a catastrophe point of bifurcation type if  $q(\mathbf{r}, \mathbf{R}_c)$  possesses at least one singularity, i.e. one critical point with a rank less than three; otherwise it is a catastrophe point of conflict type. An example for both cases is given below.

The collection of all structural regions together with their boundaries is called a structure diagram. For a given system, the structure diagram embodies all information concerning possible structures and their possible changes. Therefore, it should contain information to elucidate the mechanism of possible chemical reactions.

A change in structure necessitates passage of the system through a catastrophe point. This is a discontinuous process which can be best described with catastrophe theory [78]. For example, with catastrophe theory, one can predict that for the isomerization reaction



there should exist two different reaction mechanisms depending on what kind of catastrophe points are passed during the course of the reaction. The first possible

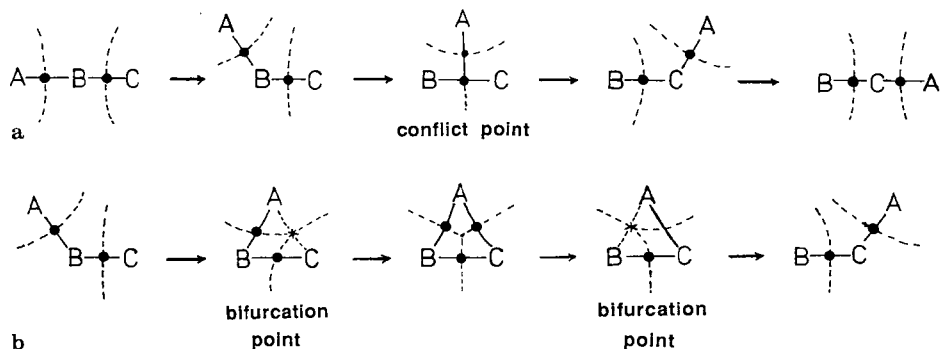


**Fig. 5a, b.** Qualitative molecular graphs representing the sequence of structural changes during the course of the isomerization reaction  $ABC \rightarrow BCA$ . Bond critical points are denoted by dots, MEP paths by solid lines and the traces of the zero-flux surfaces by dashed lines. **a** Bond switching mechanism. The system passes through one catastrophe point of the conflict type. **b** Mechanism involving ring formation. Singularities in  $q(\mathbf{r})$  are denoted by stars. The system passes through two catastrophe points of the bifurcation type. A dashed line between A and C (B) denotes the onset of bond formation (rupture)

mechanism is a simple switching of bond paths from one atom (attractor) to the other. As shown in Fig. 5a, atom A remains bonded to atom B until a catastrophe point of the conflict type is reached. This conflict point is caused by a direct link of atom A to the bond critical point  $r_b(B, C)$ . An infinitesimal movement of A in direction of C causes an abrupt switch of the A, (BC) path to nucleus C and the formation of BCA as indicated in Fig. 5a.

The second possible mechanism involves ring formation during the course of the reaction. The series of structural changes in this reaction is illustrated in Fig. 5b. Here, atom A moves toward C until a bifurcation catastrophe point is reached. This bifurcation point is caused by the birth of a new bond and ring critical point yielding a singularity in  $\varrho(\mathbf{r})$  in form of a (2, 0) critical point. An infinitesimal displacement of A toward C causes this bifurcation point to transform into the bond critical point  $r_b(AC)$  and the ring critical point  $r_r(ABC)$ . A ring structure is formed. When A moves further toward C a second catastrophe point is passed, at which  $r_b(AB)$  and  $r_r(ABC)$  disappear. Finally, the product BCA is formed. The two bifurcation catastrophe points may correspond to the transition states leading from the reaction and product side to the ring structure, which in turn may be a true intermediate.

It is appealing to associate the catastrophe points in the structure diagram with the transition states of the corresponding reaction. A limited number of investigations suggest that there may be a one-to-one relationship between catastrophe points and transition states encountered in a reaction. There even could exist a relationship between the coordinates of the catastrophe point and the nuclear configuration of the transition state [79]. In this case it would be possible to transform energy propensity rules such as the Hammond postulate into the electron density picture. However, no proof for the existence of a relationship between the number of catastrophe points and the number of transition states or between  $R_c$  and the transition state geometry has been given so far.

### 3 The Laplace Field of the Electron Density Distribution $\varrho(\mathbf{r})$

The electron density distribution  $\varrho(\mathbf{r})$  exhibits a simple pattern. Local maxima only occur at the position of the nuclei and local minima only in the interior of cage structures. Saddle points can be found inside rings and at the MED paths linking the nuclei of neighboring atoms. These properties of  $\varrho(\mathbf{r})$  lead to definition of the atom in a molecule, the chemical bond, molecular structure, and structural changes.

However, important features and useful models that describe the electronic structure of atoms and molecules are not reflected in any obvious way by  $\varrho(\mathbf{r})$ . Noteworthy are the shell structure of the electrons in an atom and the usual dissection of the electrons of a molecule into inner shell, bond, and lone electron pairs. It seems difficult to associate molecular stability and reactivity with these features of the electronic structure within an analysis of  $\varrho(\mathbf{r})$ . Shell structure and electron pair model, however, can also be extracted from the properties of  $\varrho(\mathbf{r})$  if the Laplacian of  $\varrho(\mathbf{r})$ ,  $\nabla^2\varrho(\mathbf{r})$ , is analyzed.

### 3.1 Mathematical Meaning of the Laplace Field of a Scalar Function

The Laplacian of any scalar field  $f(\mathbf{r})$ ,  $\nabla^2 f(\mathbf{r})$ , is given by the second derivatives of  $f(\mathbf{r})$  with regard to  $\mathbf{r}$ . It is obtained as the sum of the eigenvalues or the trace of the rank 3 Hessian matrix of  $f(\mathbf{r})$  with regard to the three components  $x, y, z$  of the vector  $\mathbf{r}$ . The Laplacian is an important property of a scalar field [80]. It is negative where the scalar field concentrates. In particular,  $\nabla^2 f(\mathbf{r})$  adopts a minimum where  $f(\mathbf{r})$  possesses a maximum. As shown for the one-dimensional scalar function  $f(x)$  in Fig. 6, the Laplacian of  $f$  at a point  $x$  provides a measure of the difference between the value of  $f$  at  $x$  and the average value of  $f$  at all neighboring points  $x + \Delta x$ . For  $\nabla^2 f(x) < 0$ ,  $f(x)$  is greater than the average value and the opposite holds for  $\nabla^2 f(x) > 0$ . Hence the Laplacian  $\nabla^2 f(\mathbf{r})$  is a measure of local concentration and depletion

$$\begin{aligned} & \lim_{\Delta x \rightarrow 0} \left\{ f(x) - \frac{1}{2} [f(x - \Delta x) + f(x + \Delta x)] \right\} = \\ & - \frac{1}{2} \lim_{\Delta x \rightarrow 0} \left\{ [f(x + \Delta x) - f(x)] - [f(x) - f(x - \Delta x)] \right\} = \\ & - \frac{1}{2} \left( \frac{d^2 f}{dx^2} \right) dx^2 = - \frac{1}{2} \nabla^2 f(x) dx^2 \end{aligned}$$

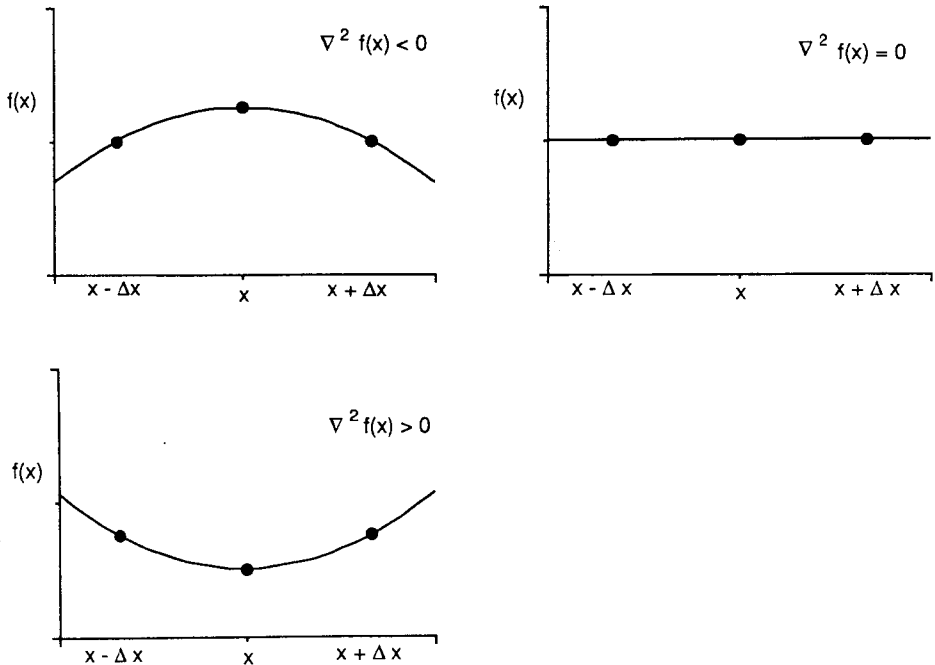
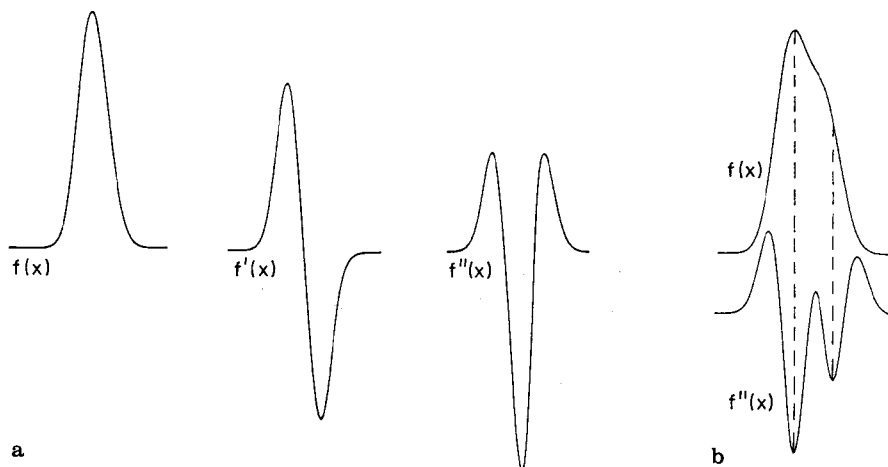


Fig. 6. Definition of the Laplacian  $\nabla^2 f(x)$  of a one-dimensional scalar function  $f(x)$  and a schematic representation of the behavior of  $f(x)$  in case of  $\nabla^2 f(x) = 0$ ,  $\nabla^2 f(x) < 0$ , and  $\nabla^2 f(x) > 0$



**Fig. 7. a** Characterization of a spectral band by the first and second derivatives of the enveloping function  $f(x)$ . **b** Determination of the positions of two overlapping bands in a spectrum

of the scalar field  $f(\mathbf{r})$ . Since the behavior of  $f(\mathbf{r})$  at  $\mathbf{r}$  is determined by comparison with an internal standard, namely the average value of all neighboring points this definition of concentration and depletion is completely independent of an arbitrary reference function [81].

The properties of the Laplacian are used to specify the local behavior of  $f(\mathbf{r})$ . For example, in derivative spectroscopy [82] the maximum of the function  $f(x)$  enveloping a spectral band is determined by the position of the minimum of the second derivative  $d^2f/dx^2 = f''(x) = \nabla^2 f(x)$ , i.e. the minimum in  $f''(x)$  determines a maximal concentration of the enveloping function  $f(x)$  (Fig. 7a). This looks trivial but turns out to be extremely useful if two bands overlap in a spectrum (Fig. 7b). From  $f(x)$  it is not possible to determine the positions of the maxima. On the other hand, the minimum of  $f''(x)$  clearly reveals the positions of maximum concentration of  $f(x)$ .

An investigation of the properties of the Laplace field is particularly useful when a three-dimensional function such as  $\varrho(\mathbf{r})$  is analyzed. For example, the strong exponential decay of  $\varrho(\mathbf{r})$  in the off-nucleus direction disguises any local properties of  $\varrho(\mathbf{r})$ . These are unearthed by the Laplacian of  $\varrho(\mathbf{r})$ .

### 3.2 Physical Meaning of the Laplace Field of $\varrho(\mathbf{r})$

The analysis of the Laplacian of the electron density  $\varrho(\mathbf{r})$ ,  $\nabla^2 \varrho(\mathbf{r})$ , is more than a convenient way of describing the distribution  $\varrho(\mathbf{r})$  with an appropriate mathematical tool. The Laplacian  $\nabla^2 \varrho(\mathbf{r})$  is of fundamental physical significance. It determines the one-particle Lagrangian density  $L(\mathbf{r})$  of a quantum mechanical system [19]:

$$L(\mathbf{r}) = -\hbar^2/4m\nabla^2 \varrho(\mathbf{r}) . \quad (11)$$

The Lagrangian, integrated over all space, vanishes for an isolated quantum system, e.g. a molecule [19]:

$$\int_{\infty} L(\mathbf{r}) \, d\mathbf{r} = 0. \quad (12)$$

For an open quantum system, e.g. an arbitrarily defined atom in a molecule the integral attains a finite nonzero value. However, for a virial atom defined by the zero flux condition (Eq. (2)), integration over the atomic subspace  $\Omega$  also leads to zero. This can be seen by applying the Gaussian theorem [83]

$$\int_{\Omega} \nabla^2 f \, d\omega = \oint_S \nabla f \, d\sigma = 0, \quad (13)$$

( $d\omega$  denotes integration of a  $n$ -dimensional function  $f$  over a volume element  $\Omega$  and  $d\sigma = \mathbf{n} \, ds$  denotes integration over a surface element  $S$ ) to the Laplacian of  $\varrho(\mathbf{r})$ :

$$\int_{\Omega} \nabla^2 \varrho(\mathbf{r}) \, d\mathbf{r} = \oint_S \nabla \varrho(\mathbf{r}) \, \mathbf{n}(\mathbf{r}) \, d\mathbf{r} = 0. \quad (14)$$

Because of Eqs. (11) and (14) the integral (15) vanishes:

$$\int_{\Omega} L(\mathbf{r}) \, d\mathbf{r} = 0. \quad (15)$$

It is because of this common property of the virial atom and the total molecule that a unique quantum mechanical description exists both for the total molecule and for the virial atoms within it [19].

Another important feature of the Laplacian  $\nabla^2 \varrho(\mathbf{r})$  is that it provides a link between the distribution of  $\varrho(\mathbf{r})$  and the forces acting on the system. The force density  $\mathbf{F}(\mathbf{r})$  defined as:

$$\mathbf{F}(\mathbf{r}) = -\nabla \sigma(\mathbf{r}), \quad (16)$$

in which  $\sigma(\mathbf{r})$  is the quantum stress tensor first introduced by Pauli [84]:

$$\sigma(\mathbf{r}) = \hbar^2/4m[(\nabla\nabla + \nabla'\nabla') - (\nabla\nabla' + \nabla'\nabla)] \Gamma^1(\mathbf{r}, \mathbf{r}')|_{\mathbf{r}=\mathbf{r}'}. \quad (17)$$

Noting the form of  $\mathbf{G}(\mathbf{r})$  (Eq. (5)) and that of  $\mathbf{L}(\mathbf{r})$  (Eq. (11)), the following relationship is established:

$$\text{tr } \sigma(\mathbf{r}) = -2\mathbf{G}(\mathbf{r}) - \mathbf{L}(\mathbf{r}). \quad (18)$$

Since the following relationship holds between the trace of the stress tensor and the potential energy density  $V(\mathbf{r})$  [85]:

$$V(\mathbf{r}) = \text{tr } \sigma(\mathbf{r}), \quad (19)$$

the *local virial theorem* results [19]

$$2\mathbf{G}(\mathbf{r}) + V(\mathbf{r}) = -\mathbf{L}(\mathbf{r}) = \hbar^2/4m \nabla^2 \varrho(\mathbf{r}). \quad (20)$$

Because of Eq. (15) integration over total space or an atomic subspace  $\Omega$  leads to the virial theorem

$$2 \int_{\Omega} G(\mathbf{r}) d\mathbf{r} + \int_{\Omega} V(\mathbf{r}) d\mathbf{r} = 2T_{\Omega} + V_{\Omega} = 0. \quad (21)$$

The local virial theorem locally connects the Laplacian with the kinetic energy density and the potential energy density. Since  $G(\mathbf{r})$  is always positive and  $V(\mathbf{r})$  is always negative, the sign of the Laplacian of  $\rho(\mathbf{r})$  determines the relative magnitudes of the local values of the potential and kinetic energy densities. In regions with  $\nabla^2 \rho(\mathbf{r}) < 0$ , the potential energy density is dominant. This leads to a concentration of negative charge. In contrast, in regions with  $\nabla^2 \rho(\mathbf{r}) > 0$  the kinetic energy density dominates and causes a depletion of negative charge.

The Laplacian of  $\rho(\mathbf{r})$  is directly related to the local contributions to the electronic energy of a system. The local virial theorem can be used to elucidate the sufficient condition for covalent bonding described in Sect. 2.3. From Eq. (20) it follows that

$$H(\mathbf{r}) = \hbar^2/4m \nabla^2 \rho(\mathbf{r}) - \dot{p}G(\mathbf{r}) \quad (22)$$

and

$$2H(\mathbf{r}) = \hbar^2/4m \nabla^2 \rho(\mathbf{r}) + V(\mathbf{r}). \quad (23)$$

Eqs. (22) and (23) show that  $H(\mathbf{r})$  will always be negative in the bonding region if  $\nabla^2 \rho(\mathbf{r}) < 0$ , i.e. if the electrons concentrate in the bonding region. On the other hand, for a homonuclear diatomic molecule there will always be electron concentration in the internuclear region if bonding MOs are occupied. Occupation of antibonding MOs leads to a depletion of negative charge. It depends on the number of occupied (anti)bonding MOs and their shape whether the Laplace concentration,  $-\nabla^2 \rho(\mathbf{r})$ , is larger or smaller than zero. If there is depletion, *the actual electron density in the internuclear region may still lead to bonding* when the magnitude of the potential energy density  $V(\mathbf{r})$  is so large (due to relatively high atomic number and concomitant strong electron, nucleus attraction) that electrons in the bonding region stabilize the system, i.e. decrease the total energy.

### 3.3 Chemical Meaning of the Laplace Field of $\rho(\mathbf{r})$

Since negative charge is concentrated in regions where  $\nabla^2 \rho(\mathbf{r}) < 0$ , it is convenient to refer to  $-\nabla^2 \rho(\mathbf{r})$  as the *Laplace concentration of  $\rho(\mathbf{r})$* . The Laplacian concentration exhibits a maximum parallel to a maximum in  $\rho(\mathbf{r})$ .

The vanishing of the Laplacian integrated over the total molecular space or over an atomic subspace  $\Omega$  defined by the zero-flux surface (Eq. (2)) has an important consequence. All fluctuations in  $\nabla^2 \rho(\mathbf{r})$  are such that local depletion or concentration of electronic charge cancel each other out for the molecule and for an atom in a molecule as well. If electrons concentrate at one position of the molecule, e.g. at the site of an electron lone pair, negative charge will be depleted at another site of

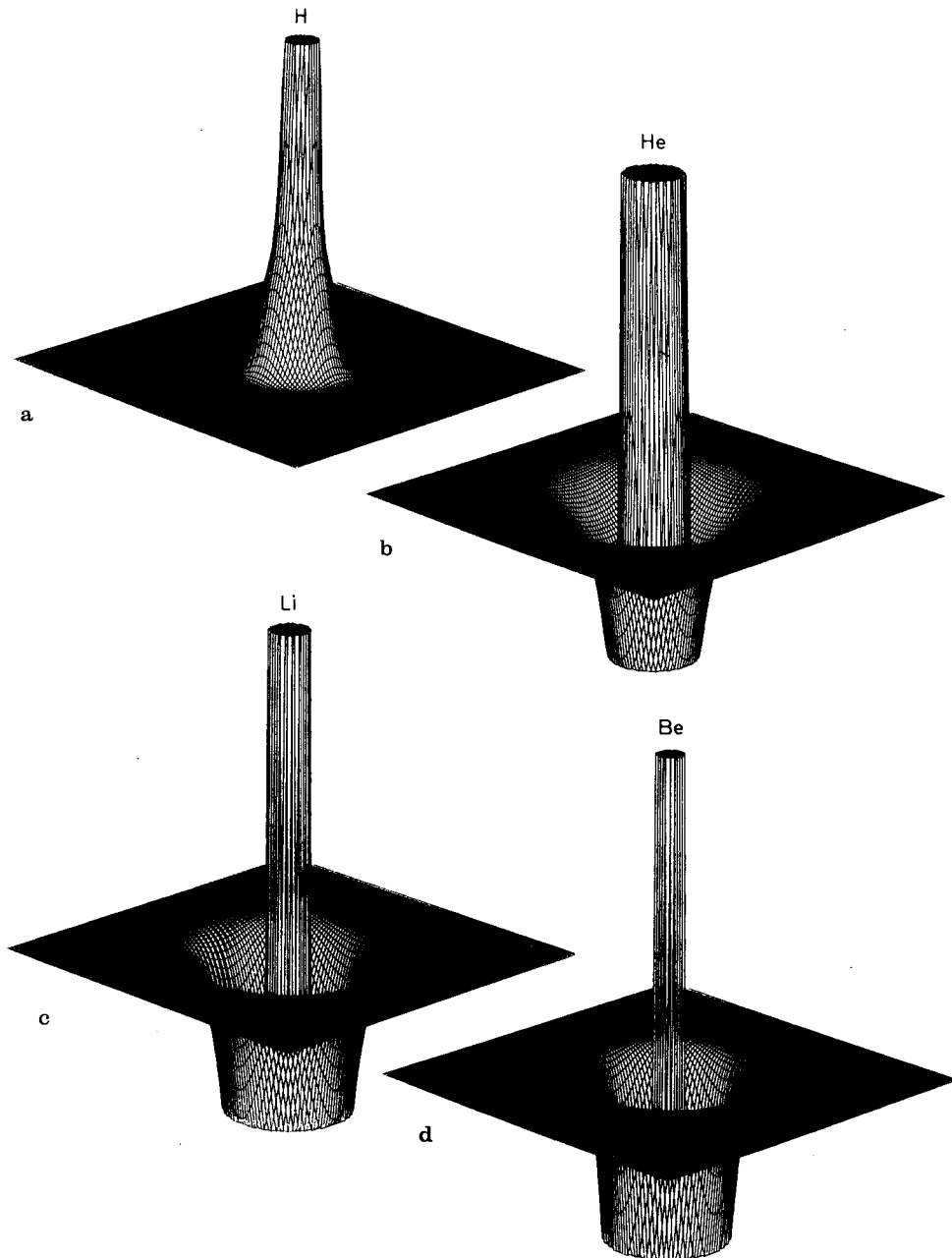


**Fig. 8a-j.** Perspective drawings of the Laplace concentration  $-\nabla^2\rho(\mathbf{r})$  of H, He, and the first row atoms Li through Ne. The inner concentration peaks are assigned to the  $1s$  electrons and the outer concentration spheres to the valence shell electrons. For a better presentation values above and below a threshold are cut off. Different scaling factors are used depending on the number of electrons. **a**  $\text{H}(^2\text{S})$ . **b**  $\text{He}(^1\text{S})$ . **c**  $\text{Li}(^2\text{S})$ . **d**  $\text{Be}(^1\text{S})$ . **e**  $\text{B}(^2\text{P}; 1s^2 2s^2 2p_x)$  (reference plane is the  $xy$  plane). **f**  $\text{C}(^3\text{P}; 1s^2 2s^2 2p_x 2p_y)$  (in the  $xz$  plane). **g**  $\text{N}(^4\text{S})$ . **h**  $\text{O}(^3\text{P}; 1s^2 2s^2 2p_x^2 2p_y 2p_z)$  (in the  $xy$  plane). **i**  $\text{F}(^2\text{P}; 1s^2 2s^2 2p_x^2 2p_y^2 2p_z)$  (in the  $xz$  plane). **j**  $\text{Ne}(^1\text{S})$ . (UHF/6-31G(d) calculations)



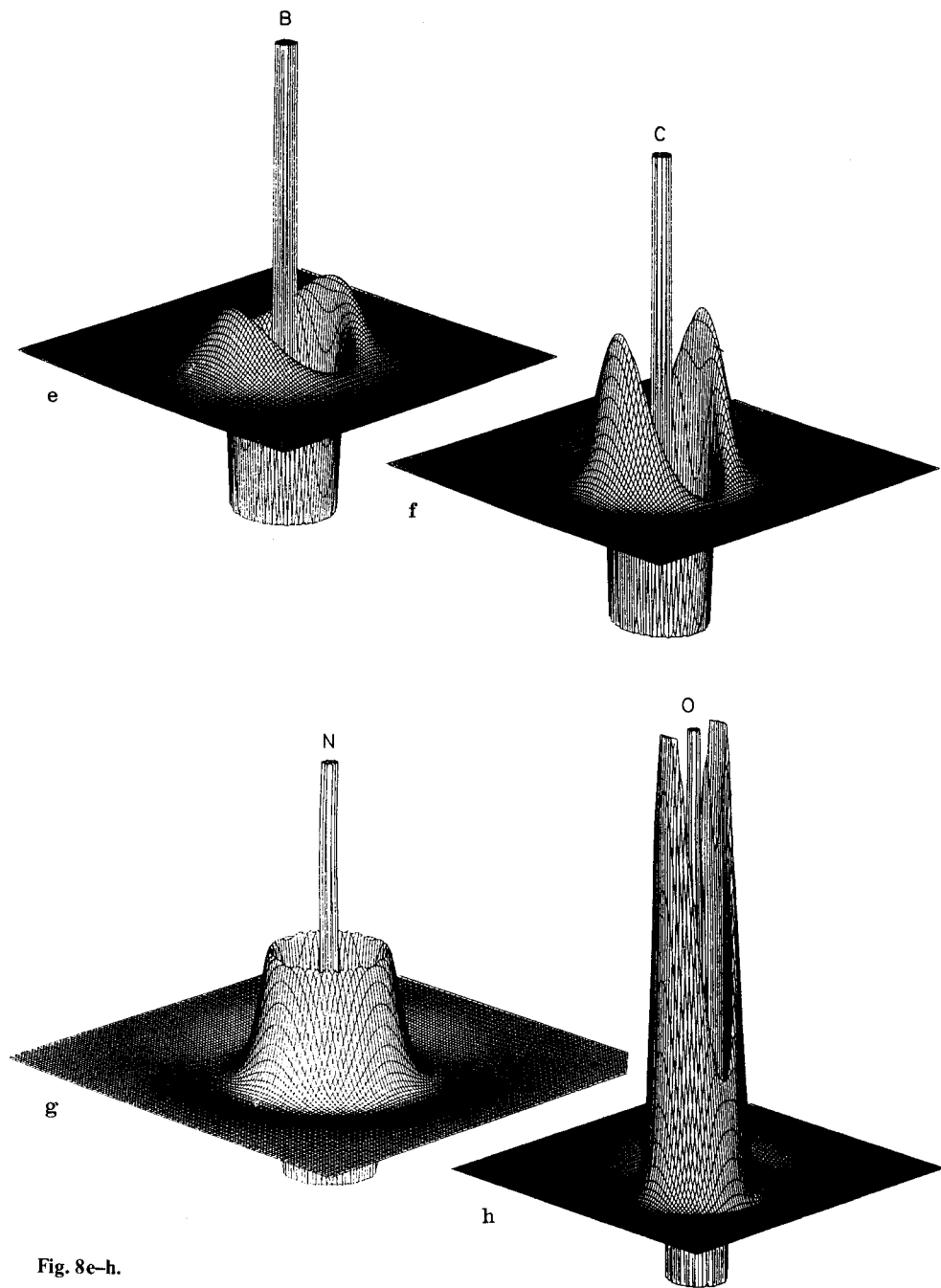


Fig. 8e-h.

the molecule, e.g. at the site of a possible nucleophilic attack. While the charge distribution  $\rho(\mathbf{r})$  of an isolated atom with spherical electron density distribution is characterized by one single local maximum at the position of the nucleus and an

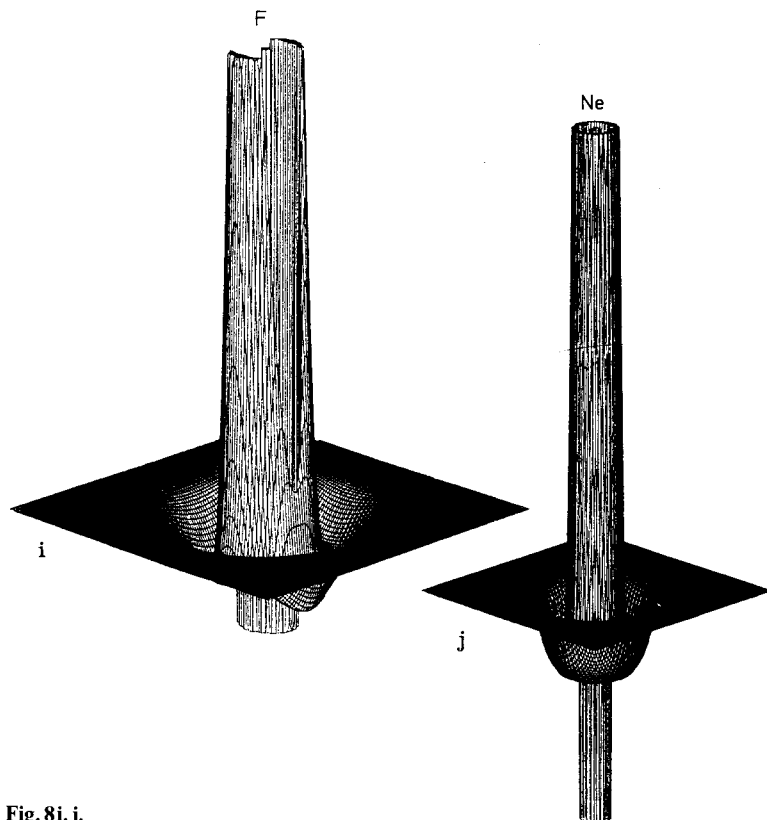


Fig. 8i, j.

exponential decay of  $\varrho(\mathbf{r})$  in the off-nucleus direction, the associated Laplace concentration adopts a much more complex pattern as is demonstrated in Fig. 8 for H, He, and the first row atoms Li—Ne. Picking the N atom, the following observations can be made. At the position of the nucleus a compact sphere with high concentration of negative charge is found. This inner sphere of charge concentration is surrounded by a sphere of charge depletion. In the region where one would expect the valence electrons a second sphere with relatively large electron concentration can be found followed by a relatively flat sphere of charge depletion. Obviously, one can distinguish between an inner and an outer sphere of electron concentration. It is appealing to assign the  $1s$  electron of N to the inner sphere and the valence electrons to the outer sphere and to speak of *inner shell and valence shell concentrations*. In other words, the Laplacian of  $\varrho(\mathbf{r})$  reflects the shell structure of the electrons in an atom. Each quantum shell can be associated with a pair of shells of  $\nabla^2\varrho(\mathbf{r})$ , one with charge concentration and one with charge depletion.

The fluctuations in the Laplacian of  $\varrho(\mathbf{r})$  must vanish if the Laplacian is integrated over the total space of the atom, i.e. spheres of electron concentration and electron depletion are a necessary consequence of the quantum mechanics of the atom. The Laplacian reveals that regions with an excess of potential energy are followed by

regions with an excess of kinetic energy. Electrons stay longer in the former than in the latter.

The shell structure is clearly reflected in the case of atoms B to Ne (Fig. 8c–8j). For Li and Be, the valence shell concentration is very diffuse and can only be detected by a quantitative analysis of the Laplacian. Also, the outer sphere of charge depletion is very flat for atoms to the right of the periodic table. It develops within a row and is pronounced for atoms such as He, F, or Ne (see Fig. 8b, i, j).

The inner shell and the valence shell concentration contract with increasing atomic number. If the maximum concentration of  $\rho(\mathbf{r})$  in the valence shell is characterized by the distance  $p$  from the position of the nucleus, then  $p$  values decrease from 1.3 Å (Li) to 0.3 Å (Ne) in the first row. At the same time  $-\nabla^2\rho(\mathbf{r})$  increases from 0.048 (Li) to 368.368 e Å<sup>-5</sup> (Ne).

For an isolated atom with an anisotropical charge distribution, as in the case of the atoms B, C, O, and F, the Laplace concentration in the valence sphere is no longer spherical. Local maxima (lumps) and local minima (holes) emerge in the valence shell concentration. For example, in case of the C atom in its <sup>3</sup>P ( $1s^2 2s^2 2p_x 2p_y$ ) state (Fig. 8f), the lumps are found in the direction of the occupied  $p$  orbitals and the holes in the direction of the empty  $p$  orbital. It seems that the lumps and holes in the valence sphere of the Laplacian reflect the occupation of the valence orbitals. At least, this is suggested by the Laplacian concentration of B(<sup>2</sup>P), C(<sup>3</sup>P), O(<sup>3</sup>P), and F(<sup>2</sup>P).

### 3.4 The Laplace Field of a Molecule

When an isolated atom with a spherical charge distribution forms a bond, its valence sphere concentration is distorted in a characteristic way. A pattern of lumps and holes is formed in the valence shell. In particular, local concentration maxima ((3, -3) critical points of  $-\nabla^2\rho(\mathbf{r})$ ) develop in direction of a bond with a neighboring atom while saddle points ((3, -1) critical points of  $-\nabla^2\rho(\mathbf{r})$ ) emerge between the bonds. The pattern of maxima and saddle points of the Laplace concentration of an atom is characteristic for the number and type of bonds with neighboring atoms [39]. It can be described by an *atomic graph*, i.e. the network of lines connecting the nucleus with the local maxima in the valence sphere concentration of the Laplacian. A critical point  $\mathbf{r}_A$  in the valence sphere can be characterized quantitatively by the value  $I_A^{AB}$  of  $-\nabla^2\rho(\mathbf{r})$  at  $\mathbf{r}_A^{AB}$ , by the distance  $p$  from the nucleus, and by the angle  $\gamma$  between the lines connecting two valence sphere critical points with the nucleus.

While the valence sphere concentration of an  $sp^3$  hybridized C(<sup>5</sup>P) atom is spherical, that of the carbon atom in methane exhibits the pattern schematically given by the atomic graph of Fig. 9a. A perspective drawing of the Laplacian concentration of CH<sub>4</sub> (with respect to the plane containing the C atom and two H atoms) is shown in Fig. 9b. There are four concentration lumps, one along each of the CH bond paths, and six concentration holes, each between two CH bonds. Accordingly, the valence shell concentration of C is best characterized by a tetrahedral atomic graph (Fig. 9a).

The HOMO of methane is dominantly concentrated in the CH bonding region while the LUMO preferentially occupies the regions between the CH bonds (Fig. 10).

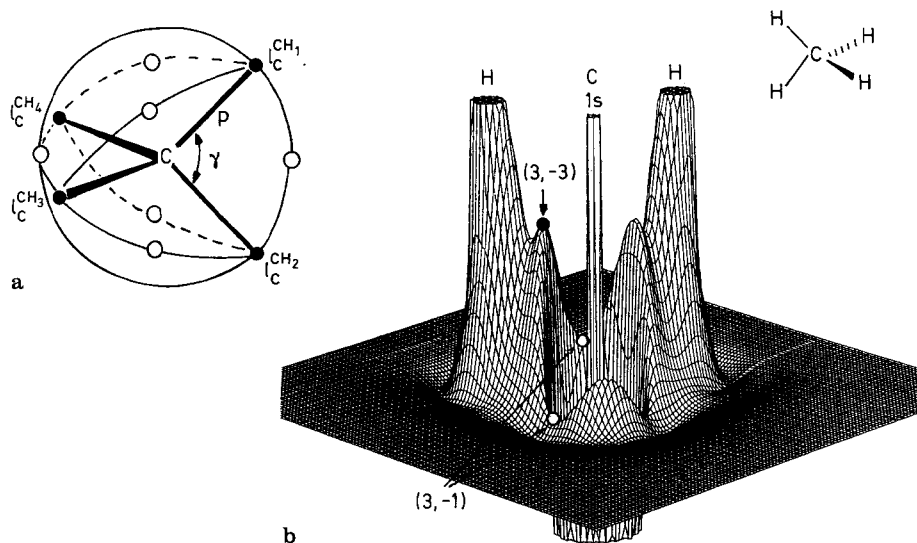


**Fig. 9.** **a** Schematic representation of the atomic graph of the C-atom in methane. Positions of concentration maxima  $l_{\text{C}}\text{CH}$  (3, -3) are denoted by *dots*, positions of saddle points (3, -1) are denoted by *open circles*. Distances  $p$  and angles  $\gamma$  determine the form of the atomic graph. **b** Perspective drawing of the Laplace concentration  $-\nabla^2\rho(\mathbf{r})$  of methane, depicted in the plane containing the C and two H atoms. Lumps (3, -3) and holes (3, -1) in the valence shell concentration of C are indicated. For a better presentation values above and below a threshold are cut off. (HF/6-31G( $d, p$ ) calculation)

Obviously, regions with concentration and depletion of negative charge coincide with the regions in which HOMO and LUMO possess their largest amplitude. Thus, in the same way as one can predict the sites of nucleophilic and electrophilic attack in a molecule by an analysis of the frontier orbitals (FOs), an investigation of the Laplacian  $\nabla^2\rho(\mathbf{r})$  yields information about the active sites of the molecule. Sites with

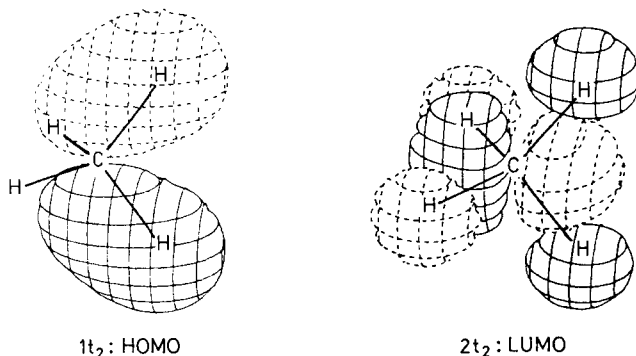


**Fig. 10.** Perspective drawing of the HOMO and LUMO of methane. Only one component of the  $1t_2$  and the  $2t_2$  sets are shown

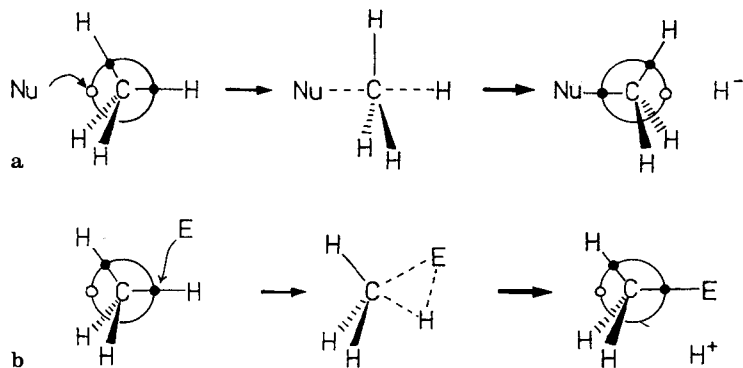


**Fig. 11.** **a** Schematic representation of a nucleophilic attack on methane. **b** Schematic representation of an electrophilic attack on methane

concentration holes in the valence sphere are prone to a nucleophilic attack while sites with concentration lumps in the valence sphere are prone to an electrophilic attack. A nucleophile will preferentially attack at a concentration hole between two CH bonds, i.e. the attack will take place at the C nucleus rather than at a CH bond. Formation of a bond weakens a CH bond at the opposite site of the valence sphere and the corresponding H will dissociate. Hence, a nucleophile leads to an inversion of the configuration at C. This is typical of a S<sub>N</sub>2 mechanism and is schematically shown in Fig. 11a.

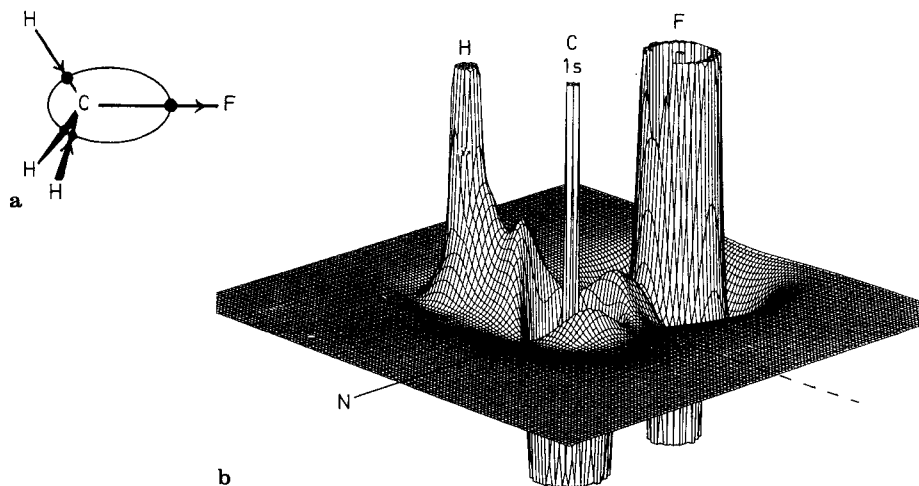


**Fig. 12.** **a** Distortion of the valence sphere of the C atom in methyl fluoride. The valence sphere is indicated by a large ellipse. The direction of the distortion is given by an arrow. Propagation of distortion effects is shown for the H atoms. **b** Perspective drawing of the Laplace concentration  $-\nabla^2 \rho(r)$  of methyl fluoride, depicted in the plane containing the C, the F, and one H atom. Lumps and holes in the valence shell concentration of C are indicated. For a better presentation values above and below a threshold are cut off. (HF/6-31G(d, p) calculation)

An electrophile will attack at the concentration maxima in the CH bond, i.e. contrary to the nucleophile the electrophile attacks the CH bond rather than the carbon nucleus. This leads to a 2-electron 3-center transition state typical of  $S_E2$  reactions with retention of configuration and is indicated in Fig. 11 b.

In the case of heteropolar bonding, charge transfer caused by the electronegativity difference between the bonding partners is reflected by a characteristic deformation of the valence sphere concentration of the atoms in question. This is depicted in Fig. 12 for methylfluoride,  $\text{CH}_3\text{F}$ . Due to the electronegativity of F, the valence sphere concentration of the C atom is pulled into the direction of F. The topology of the atomic graph remains unchanged, but the extent of charge<sup>+</sup> concentration and charge depletion in the CF and CH bond regions is strongly influenced. As a result of a charge transfer from C to F, the bond critical point of the CF bond is only 0.43 Å [86] from the carbon nucleus, i.e. the local charge concentration at carbon has been drawn into the subspace of the fluorine atom. This is in line with the low  $I_C^{\text{CF}}$  value of  $10.50 \text{ e } \text{Å}^{-5}$  and a large distance value  $p_C^{\text{CF}}$  of 0.555 Å. In comparison, the corresponding values for the CH bond in methane are  $I_C^{\text{CH}} = 28.62 \text{ e } \text{Å}^{-5}$  and  $p_C^{\text{CH}} = 0.519 \text{ Å}$ . Since all fluctuations in  $\nabla^2 \varrho(\mathbf{r})$  have to cancel each other out within the boundary of a bonded atom (compare with Eq. (15)), the decrease of concentration at C in direction of F is accompanied by an increase of charge concentration on the opposite side of the valence sphere (see Fig. 12). The three concentration maxima in the direction of the CH bonds are considerably larger and closer to the C nucleus than the corresponding ones in methane ( $I_C^{\text{CH}} = 34.32 \text{ e } \text{Å}^{-5}$ ,  $p_C^{\text{CH}} = 0.506 \text{ Å}$ ). In a chain of bonded atoms, distortions in the valence sphere caused by electronegativity differences between the bonding partners can propagate to some extent along the chain. This is reflected by the atomic graphs of the involved atoms.

Again, the pattern of the Laplace concentration in  $\text{CH}_3\text{F}$  correlates with the form of the corresponding frontier orbitals. Predictions made within the FO model can also be made by inspection of the Laplace concentration. Thus, the analysis of the Laplacian of  $\varrho(\mathbf{r})$  provides a link between the MO approach and the electron density approach for the description of molecules and their chemical behavior. Since *the Laplace concentration covers the effects of all occupied MOs*, it does not suffer from the ambiguities of FO theory with regard to the choice of the FOs (HOMO, second HOMO, third HOMO, etc.). The analysis of  $-\nabla^2 \varrho(\mathbf{r})$  leads to more reliable predictions. In those cases where the FOs are not dominant the shape of the Laplacian should differ from the shape of HOMO and LUMO and, in this way, should provide a basis to foresee the flaws of the FO model [87].

## 4 Description of $\pi$ -Conjugation

Conjugation of double bonds leads to  $\pi$ -electron delocalization. Although the distinction between  $\sigma$ - and  $\pi$ -electrons is no longer relevant when discussing  $\varrho(\mathbf{r})$ , features of the electron density in the bonding region can be related to features of the  $\sigma/\pi$ -model. A complete investigation of a conjugated bond AB would imply

1. an analysis of  $\rho(\mathbf{r})$  at the bond critical point  $\mathbf{r}_b(\text{AB})$ ;
2. an analysis of  $\rho(\mathbf{r})$  along the bond path AB starting at the valence shell of atom A and ending at the valence shell of atom B;
3. an analysis of  $\rho(\mathbf{r})$  in the internuclear surface  $S(\text{A}, \text{B})$ ;
4. an analysis of  $\rho(\mathbf{r})$  in the subspace of A and the subspace of B.

For reasons of simplicity the investigation of  $\rho(\mathbf{r})$  is constrained in most cases to the first step, namely an analysis of  $\rho_b$ , the electron density at the bond critical point  $\mathbf{r}_b$ . As noted in Sect. 2.4, the bond ellipticity  $\varepsilon$  can be related to the  $\pi$ -character of the bond. For example, by using the  $\pi$  double bond of ethylene as a suitable reference bond, the ratio  $\eta$  given in per cent gives the  $\pi$ -character of any other formal CC double or single bond once its bond ellipticity has been found:

$$\eta = 100 \varepsilon(\text{CC})/\varepsilon(\text{ethylene}) . \quad (24)$$

By definition,  $\eta$  of ethane (bond order  $n = 1$ ) and ethylene ( $n = 2$ ) are 0 and 100%. In the case of  $\pi$ -conjugation in polyenes or cyclopolyenes, the  $\pi$ -character  $\eta$  is decreased for the formal double bonds and increased for the formal single bonds. Accordingly, bond orders  $n < 2$  and  $n > 1$  result. Hence, bond order  $n$  and  $\pi$ -character  $\eta$  extracted from the properties of  $\rho_b$  allow a quantitative analysis of conjugative effects.

#### 4.1 Conjugation in Polyenes

In *trans*-1,3-butadiene, the  $\pi$ -character of the formal double bonds is decreased to  $\eta = 92.5\%$ , the bond order to  $n = 1.89$  (compare with Table 3) [88].  $\pi$ -electrons propagate along the C chain thus inducing partial  $\pi$ -character to the formal CC single bond. This is reflected by  $\eta = 15.1\%$  and  $n = 1.21$  for C2—C3. If the ratio

**Table 3.** Description of CC bonds in conjugated systems and appropriate reference molecules<sup>a</sup>

Molecules	Bond	Bond length R [Å]	Bond order $n^b$	Bond Ellipticity $\varepsilon$	$\pi$ -character $\eta^b$ [%]
Ethane	C—C	1.527	1.0	0	0
Ethylene	C=C	1.317	2.0	0.45	100
Benzene	C—C	1.386	1.5	0.23	50
<i>trans</i> -1,3-Butadiene ( $\tau = 180^\circ$ )					
	C=C	1.323	1.89	0.433	92
	C—C	1.467	1.21	0.070	15
<i>cis</i> -1,3-Butadiene ( $\tau = 0^\circ$ )					
	C=C	1.323	1.93	0.432	93
	C—C	1.479	1.14	0.066	14
orthogonal 1,3-Butadiene ( $\tau = 90^\circ$ )					
	C=C	1.319	1.96	0.463	100
	C—C	1.489	1.08	0	0

<sup>a</sup> HF/6-31G(d) calculations [30]. For a definition of parameters see text.

<sup>b</sup> All  $n$ - and  $\eta$ -values have been normalized to yield the proper number of bonds and electron pairs.

$Q = \eta(\text{C}=\text{C})/\eta(\text{C}-\text{C})$  is considered to be a quantitative measure for  $\pi$ -delocalization, then one can say that the  $\pi$  electrons of *trans*-1,3-butadiene are delocalized by 16%.

In general, the overlap between  $\pi$ -orbitals is a prerequisite for  $\pi$ -conjugation. Maximal overlap and effective  $\pi$ -delocalization is given by a parallel alignment of  $\pi$ -orbitals. Information that reflects the degree of overlap can also be extracted from  $\varrho_b$ . For this purpose, the direction of its major axis, i.e. the direction  $\mathbf{v}_2$  of the soft curvature  $\lambda_2$  is used (see Sect. 2.4). In *trans*-1,3-butadiene all major axes are perpendicular to the molecular plane, i.e. the major axis of the formal single bond is parallel to those of the formal double bonds (see Fig. 13a). We say that the major axes "overlap" completely as indicated by

$$\text{overlap}(\textit{trans}\text{-}1,3\text{-butadiene}) = \mathbf{u}_2(\text{C}1=\text{C}2) \mathbf{u}_2(\text{C}2-\text{C}3) = 1.0$$

$$\text{with } \mathbf{u}_2 = \mathbf{v}_2/|\mathbf{v}_2|.$$

For molecules such as allene or butatriene the major axes of the bond ellipticities of neighboring double bonds are perpendicular to each other, yielding

$$\text{overlap}(\text{allene}) = \mathbf{u}_2(\text{C}1=\text{C}2) \mathbf{u}_2(\text{C}2=\text{C}3) = 0$$

as is qualitatively shown in Fig. 13c, d. This is in line with the orbital description of  $\pi$ -conjugation.

For *cis*-1,3-butadiene the degree of  $\pi$ -delocalization is slightly lower ( $Q = 15\%$ ) as is indicated by  $n$ ,  $\varepsilon$ , and  $\eta$  values given in Table 3. This agrees with the MO description of the *cis* form. If  $\pi$ -delocalization is gradually disturbed by a rotation at the formal single bond of 1,3-butadiene either from  $\tau = 0^\circ$  (*cis* form) or from  $\tau = 180^\circ$  (*trans* form) to  $\tau = 90^\circ$  (*orthogonal* form), then the ellipticity of the single bond will decrease continuously to zero as is shown in Fig. 14.  $\pi$ -conjugation is no longer possible in the orthogonal form.

Inspection of the bond order  $n$  (Table 3), however, reveals that  $n(\text{C}-\text{C})$  for  $\tau = 90^\circ$  is 1.08 rather than 1.0. Obviously, there are other effects than  $\pi$ -conjugation that stabilize the central bond. First of all, C2 and C3 are  $sp^2$ -hybridized C atoms and, therefore the CC  $\sigma$ -bond is shorter and stronger than the  $\sigma$ -bond in ethane. Both  $\varrho_b$

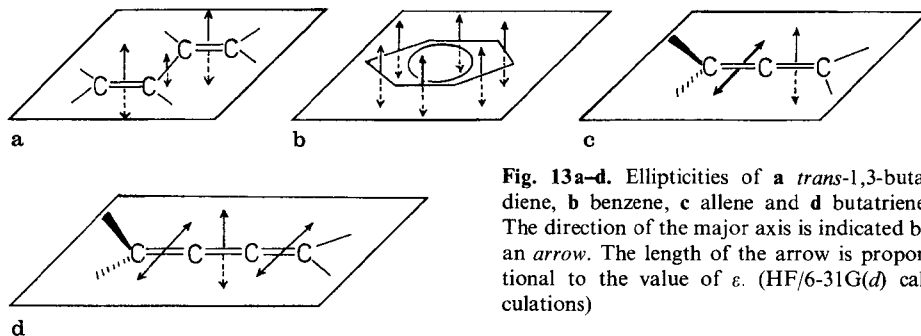


**Fig. 13a-d.** Ellipticities of **a** *trans*-1,3-butadiene, **b** benzene, **c** allene and **d** butatriene. The direction of the major axis is indicated by an arrow. The length of the arrow is proportional to the value of  $\varepsilon$ . (HF/6-31G(d) calculations)



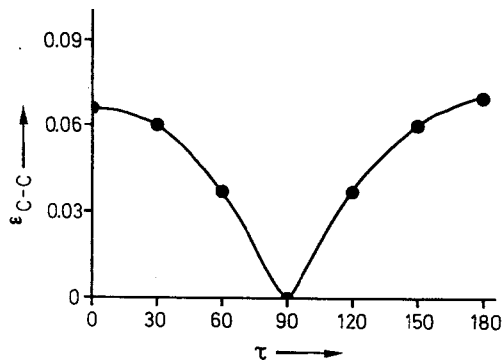


Fig. 14. Dependence of the bond ellipticity  $\varepsilon(\text{C2-C3})$  in 1,3-butadiene on the dihedral angle  $\tau(\text{C1C2-C3C4})$ . (HF/6-31G(d) calculations)

and  $n$  reflect this. Secondly, the curvatures  $\lambda_1$  and  $\lambda_2$  ( $-13.1$  and  $-13.0 \text{ e } \text{\AA}^{-5}$ ) perpendicular to the bond path are both softer than  $\lambda_1$  of C2-C3 in the *trans* form ( $-14.1 \text{ e } \text{\AA}^{-5}$ ), i.e. the effective ellipticities  $\varepsilon'$  (with regard to  $\varepsilon(\text{C2-C3 } \textit{trans})$ ) are  $< 1$  ( $\varepsilon' = 0.96$ ) as in the case of acetylene (0.86). This is indicative of hyperconjugative effects between C3-H or C3-C4 and the adjacent  $\pi$ -bond C1C2. By utilizing  $\varepsilon$ ,  $\varepsilon'$ , and  $n$  values other conjugative effects can be separated from  $\pi$ -effects thus leading to a unified description of conjugation.

Studies on conjugated polyenes have been focused on the question, whether or not the CC bond lengths converge to a common value with increasing chain length, i.e. whether or not electron delocalization increases to 100% for infinitely long polyenes [89]. Ab initio calculations on the geometries of polyenes have led to geo-

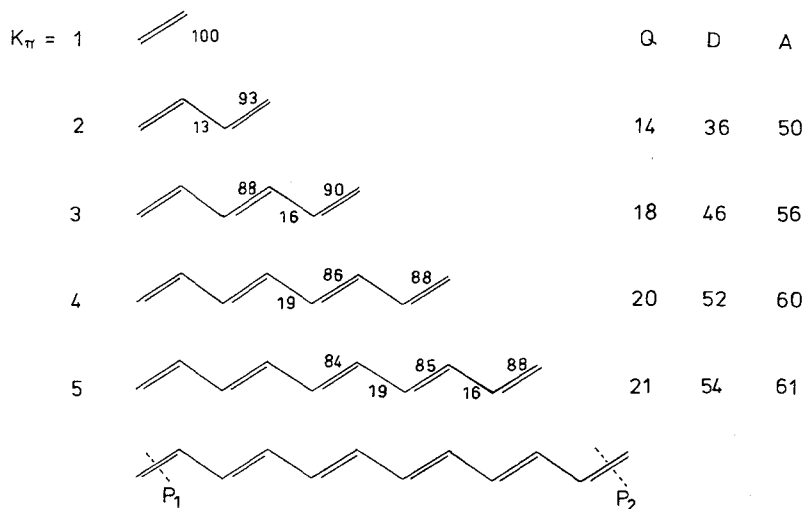


Fig. 15.  $\pi$ -character of polyenes with one to five double bonds. Values are given in per cent (see Eq. (24)) and are normalized to the total number of  $\pi$ -electrons. Delocalization of  $\pi$ -electrons is considered between the points  $P_1$  and  $P_2$ , i.e. the terminal  $\text{CH}_2$  groups are excluded. The degree of  $\pi$ -delocalization is measured by Q and D (Eq.s (25) and (26)), the degree of bond equalization by A (Eq. (29)). (HF/4-31G calculations from Ref. 30.)

metrical parameters that are indicative of increasing electron delocalization with increasing chain length. The double bonds close to the middle of the C chain are longer than those at the end, whereas the single bonds in the middle are shorter than those at the end. Hence, the  $\pi$ -character of the double bonds should decrease from the end to the middle of the C chain while that of the single bonds should increase in the same direction. Bond equalization should be more pronounced the larger the chain length is.

These findings can be verified quantitatively with the aid of calculated ratios  $\eta$ . According to the  $\eta$  values shown in Fig. 15, there is a progressive decrease in  $\pi$ -character toward the middle bond with increasing chain length [89].

The degree of delocalization  $Q$  (in per cent) in these polyenes may be calculated as the ratio of the averaged  $\pi$ -character in a formal single bond and the averaged  $\pi$ -character in a formal double bond:

$$Q = 100 K_{\pi}/K_{\sigma} \left[ \frac{\sum_i \eta(\text{C}-\text{C})}{1} \right] / \left[ \frac{\sum_j \eta(\text{C}=\text{C})}{3} \right]$$

$$= 100 \left[ \frac{\sum_i \eta(\text{C}-\text{C})}{1} \right] / \left[ \frac{\sum_j \eta(\text{C}=\text{C})}{3} \right], \quad (25)$$

where  $K_{\sigma}$  is the number of formal single bonds and  $K_{\pi}$  the number of formal double bonds. Since the number  $K_{\pi}$  of formal double bonds in a polyene is  $K_{\sigma} + 1$ , only properly averaged values  $\eta$  can be compared. On the other hand, the terminal groups in a polyene represent a wall that interrupts  $\pi$ -delocalization. Thus, it is reasonable to exclude the terminal groups and, thereby, the wall effect and to measure delocalization only between  $P_1$  and  $P_2$  as schematically shown in Fig. 15. Hence, the number of  $\pi$ -bonds is  $K'_{\pi} = K_{\sigma} - 1 + 1/2 + 1/2 = K_{\sigma}$ , i.e. the ratio of formal single and formal double bonds is one as in the case of conjugated monocyclic polyenes. This has been considered in Eq. (25).

$Q$  increases only very slowly with increasing bond equalization. Also, it is often difficult to distinguish e.g. in charged (cyclo) polyenes between formal single and double bonds. Therefore,  $\pi$ -electron delocalization should be measured by the parameter  $D$  (in per cent):

$$D = 100(1 - \sigma_{\eta}) \quad (26)$$

that is based on the average  $\pi$ -character  $\eta_{\text{av}}$  and the standard deviation  $\sigma_{\eta}$ :

$$\eta_{\text{av}} = 1/K \sum_i^K \eta(\text{AB}) \quad (27)$$

$$\sigma_{\eta} = 1/K \sum_i^K [\eta(\text{AB})_i - \eta_{\text{av}}]^2 / \eta_{\text{av}}^2, \quad (28)$$

where  $K$  denotes the total number of heavy atom bonds in the conjugated system.

If for some reason  $\varepsilon$  or  $\eta$  cannot be measured, the bond orders  $n(\text{AB})$  can be used to define a bond equalization parameter  $A$ :

$$A = 100(1 - 9\sigma_n) \quad (29)$$

with

$$n_{av} = 1/K \sum_i^K n(AB)_i \quad (30)$$

and

$$\sigma_n = 1/K \sum_i^K [n(AB)_i - n_{av}]^2 / n_{av}^2 \quad (31)$$

For a system with 100%  $\pi$ -delocalization leading to complete bond equalization as in benzene,  $\eta = 50\%$ ,  $\sigma_n = 0$ ,  $n = 1.5$ , and  $\sigma_n = 0$ .  $\pi$ -delocalization and bond equalization are zero for  $\eta_1 = 0$ ,  $\eta_2 = 100$ ,  $n_1 = 1$  and  $n_2 = 2$  as can be verified by applying Eqs. (26)–(31).

Both Q, D, and A values given in Fig. 15 for polyenes up to decapentaene confirm that  $\pi$ -electron delocalization and bond equalization increase with increasing chain length. In Fig. 16, the delocalization parameter D is plotted against the chain length K. Clearly, D approaches a limit value for increasing chain length. However, the available data suggest that convergence to a limit value of 100% is slow or may not be achieved at all.

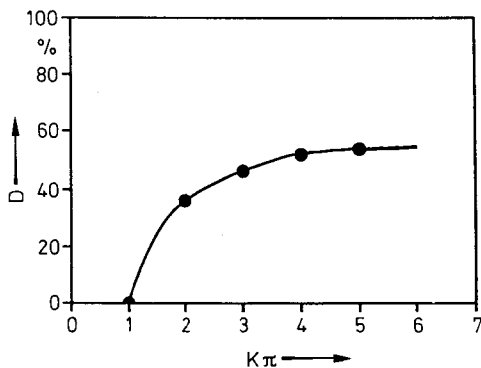


Fig. 16. Dependence of the degree of delocalization D on the number of double bonds  $K_\pi$  in a polyene. (Compare with Fig. 15)

## 4.2 Conjugation in Cyclic Systems — Aromaticity and Antiaromaticity

Cyclic conjugation involving  $(4q + 2)$   $\pi$ -electrons can lead to aromatic character. Aromaticity is reflected by the energetic, structural, and magnetic properties of the ground state of the compound in question. It can be determined by [90]

1. counting  $\pi$ -electrons and comparing their number with the Hückel  $4q + 2$  value,
2. calculating the Dewar resonance energy [91],
3. determining bond alternation or bond equalization parameters, and
4. relating magnetic properties to those of appropriate reference compounds.

All these criteria have been used in the literature. It has been found that criteria 1 and 2 are very useful for chemists while 3 and 4 are more difficult to apply [92].

Since the analysis of  $\rho(\mathbf{r})$  leads to a description of the chemical bond in terms of bond order and bond ellipticity, it is easy to determine the degree of bond equalization  $A$  and the degree of  $\pi$ -delocalization  $D$  in a potentially aromatic molecule and to use this as a measure of aromaticity.

As noted above, the bond order  $n$  covers all bond strengthening effects, not just those due to  $\pi$ -delocalization. For example, for the orthogonal form of 1,3-butadiene an  $A$  parameter of 32% is calculated although  $\pi$ -delocalization is no longer possible. Here,  $A$  reflects an increase in  $n(\text{C2C3})$  due to the shorter  $\text{C}(sp^2)\text{—C}(sp^2)$  bond and additional hyperconjugative effects. We note that any definition of aromaticity based on global properties of the bond such as bond length, bond energy, bond order (even though it has been derived from a local property of  $\rho(\mathbf{r})$ ) can only be used in a very qualitative way. Any quantitative use requires the separation of other effects not due to the delocalization of  $\pi$ -electrons.

The ellipticity  $\varepsilon$  of a bond and the  $\varepsilon$ -dependent parameter  $\eta$  may be better suited for a quantitative definition of the aromatic character of a molecule. Utilizing the delocalization parameter  $D$  (Eq. (26)) we expect aromatic character when

1. there is  $\pi$ -conjugation in a cyclic system as reflected by the overlap of the bond ellipticities,
2.  $(4q + 2)$   $\pi$ -electrons are delocalized in the conjugated cyclic system and
3. the degree of  $\pi$ -delocalization measured by  $D$  is significantly larger than in the appropriate acyclic reference compound(s) used to determine the Dewar resonance energy (*definition of aromaticity*).

It will be reasonable to consider  $\pi$ -overlap as sufficient if the overlap of the major axes of adjacent bonds is larger than 0.7, i.e. the angle enclosed by the major axes is larger than  $45^\circ$ . The number  $N$  of  $\pi$ -electrons is obtained by comparing the sum of (normalized) bond orders with the total number  $K$  of bonds:

$$N = 2 \left( \sum_i^K n_i - K \right). \quad (32)$$

For  $N \pm c = 4q + 2$  with  $c \leq 0.5$ , criterion 2 is considered to be fulfilled. For benzene,  $6\pi$  electrons are delocalized in the ring. All major axes of the CC bonds are perpendicular to the molecular plane, i.e. they overlap completely (see Fig. 13b). Each CC bond possesses the same value for  $n$ ,  $\varepsilon$ , and  $\eta$  (Table 3) which is indicative of complete delocalization with  $D = 100\%$ . Hence benzene is aromatic.

It is interesting to compare  $\pi$ -delocalization for benzene and 1,3-cyclobutadiene. Although the bond ellipticities of the latter also overlap completely (see Fig. 17a) the  $\pi$ -character of the CC bonds is 4 and 96%, and  $\pi$ -delocalization is just  $Q = 5\%$  ( $D = 17.7\%$ ), i.e. it is lower than in any polyene. The interaction of  $4q$   $\pi$ -electrons leads to a suppression of  $\pi$ -delocalization. Analogous to the definition of aromaticity, we can now give a definition for antiaromaticity. It is found when

1.  $4q$   $\pi$ -electrons are conjugated in a cyclic system and
2. the degree of  $\pi$ -delocalization measured by  $Q$  or  $D$  is suppressed as compared to that found for the appropriate acyclic reference compound(s) used to determine the Dewar resonance energy (*definition of antiaromaticity*).

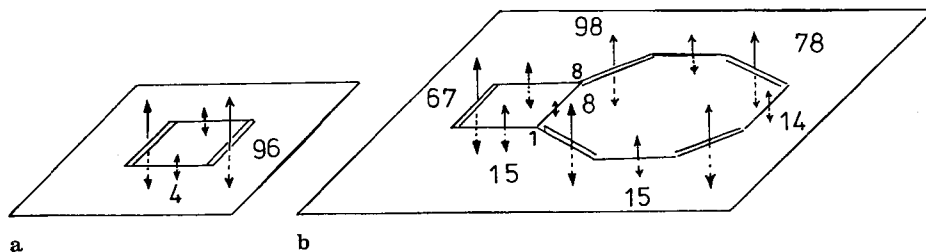


**Fig. 17 a, b.** Major axes of the bond ellipticities  $\epsilon$  (arrows) and  $\pi$ -character  $\eta$  for **a** 1,3-cyclobutadiene and **b** bicyclo[6.2.0]decapentaene. The length of the arrows is proportional to the value of  $\epsilon$ . Values of  $\eta$  in per cent and normalized to the total number of  $\pi$ -electrons. (HF/STO-3G calculations from Ref. [29])

With the  $\rho$ -based definitions of aromaticity and antiaromaticity the electronic nature of cyclopolynes can be investigated. To demonstrate this we discuss one example, namely bicyclo[6.2.0]decapentaene [29]. This compound has attracted interest by both experimentalists and theoreticians, in particular after its first successful synthesis by Oda and co-workers [93] and, independently, by Vogel and co-workers [94]. The component rings of bicyclo[6.2.0]decapentaene possess  $4q$   $\pi$ -electrons and, therefore, could be destabilized by antiaromatic character. On the other hand, there are  $(4q + 2)$   $\pi$ -electrons in the perimeter of bicyclo[6.2.0]decapentaene, possibly leading to aromatic stabilization provided bicyclo[6.2.0]decapentaene is planar or close to being so. The question is whether peripheral or monocyclic delocalization dominates the electronic nature of bicyclo[6.2.0]decapentaene, whether the  $\pi$ -system is stabilized by aromatic or destabilized by antiaromatic interactions that outweigh any aromatic effects.

Cremer and Schmidt [29] have carried out *ab initio* calculations on bicyclo[6.2.0]decapentaene which show that the molecule is essentially planar and that  $\pi$ -overlap is fully developed (Fig. 17b). Bicyclo[6.2.0]decapentaene contains a dimethylenecyclobutene unit rather than a cyclobutadiene unit in order to avoid  $4\pi$  electron interactions in the four-membered ring. Investigation of  $\rho(\mathbf{r})$  leads to the  $\eta$ -values shown in Fig. 17b. According to these data the central 1,8-bond of bicyclo[6.2.0]decapentaene possesses only low  $\pi$ -character ( $\eta = 8$ ), less than the central bond in 1,3-butadiene. Delocalization of  $\pi$ -electrons occurs essentially along the periphery of the bicyclic system. The  $\pi$ -character of the formal CC single bonds (15%) is somewhat higher, that of the formal CC double bonds (84%) is somewhat lower than that of *trans*-1,3-butadiene calculated at the same level of theory (13 and 93.5%) [29]. Hence, delocalization is slightly stronger in the periphery of bicyclo[6.2.0]decapentaene than in *trans*-1,3-butadiene.

This is confirmed by the calculated delocalization parameter  $D$ . For the four-membered ring  $D$  is as low as for cyclobutadiene itself (18.5 vs 17.7%) while for the eight-membered ring  $D$  is 42.7%. However,  $D$  is 52.8% in the periphery of bicyclo[6.2.0]decapentaene, clearly larger than  $D(\textit{trans}\text{-}1,3\text{-butadiene}) = 35\%$ .

The energetic consequences of peripheral  $\pi$ -delocalization have been estimated to be  $4.4 \pm 1.5$  kcal mol $^{-1}$ , i.e. bicyclo[6.2.0]decapentaene is slightly aromatic despite the fact that it contains antiaromatic ring units [29].

### 4.3 Hyperconjugation and Anomeric Effects

Interactions of properly aligned  $\sigma$ -bonds with an adjacent  $\pi$ -system lead to hyperconjugation. The extent of hyperconjugation is reflected by bond ellipticities  $\varepsilon$  larger than zero and a slight increase of bond orders  $n$  [21–23]. Figure 18 gives  $\varepsilon$  values for propene (Fig. 18a) and the ethyl cation (Fig. 18b).

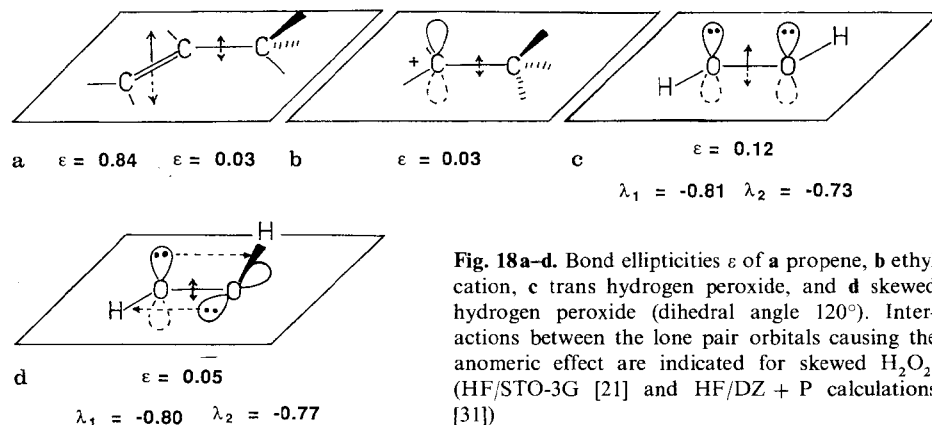


**Fig. 18a–d.** Bond ellipticities  $\varepsilon$  of **a** propene, **b** ethyl cation, **c** *trans* hydrogen peroxide, and **d** skewed hydrogen peroxide (dihedral angle  $120^\circ$ ). Interactions between the lone pair orbitals causing the anomeric effect are indicated for skewed  $\text{H}_2\text{O}_2$ . (HF/STO-3G [21] and HF/DZ + P calculations [31])

In the former molecule, the CC single bond possesses an ellipticity of 0.03. The major axis is parallel to that of the adjacent double bond, i.e. both ellipticities overlap completely. The bond order of the double bond is slightly increased ( $n = 2.1$ ). Its ellipticity is 14% larger than that of ethylene. Obviously, the methyl group of propene donates  $\pi$ -charge into the double bond. Similarly hyperconjugative interactions of the methyl group of the ethyl cation lead to a transfer of negative charge into the empty  $p$ -orbital. This is indicated by  $\varepsilon(\text{C}-\text{C}^+) = 0.03$  and a major axis parallel to the empty  $p$ -orbital at the positive C.

Anomeric interactions involve delocalization of negative charge from an electron lone pair to the  $\sigma^*$  orbital of a vicinal bond that is coplanar with the electron lone pair orbital. As a consequence, the  $\sigma$ -bond connecting the interacting centers adopts partial  $\pi$ -character.

In Fig. 18c and d  $\lambda$  and  $\varepsilon$  values of *trans* and skewed  $\text{H}_2\text{O}_2$  ( $\tau = 120^\circ$ ) are shown. In the planar form, the OO bond  $\text{H}_2\text{O}_2$  possesses  $\pi$ -character due to the occupation of  $\pi$  and  $\pi^*$  MOs. This electronic arrangement is unfavorable. Rotation about the OO bond leads to a coplanar arrangement of the lone pair orbitals at the vicinal O. Negative charge delocalizes into the  $\sigma^*(\text{OH})$  orbitals as indicated in Fig. 18d. Since this involves both OH bonds and lone pairs, the soft curvature ( $\lambda_2$ ) and the steep curvature ( $\lambda_1$ ) adjust leading to an electron arrangement similar to that of acetylene. Anomeric interactions are indicated by a nearly cylindrical density distribution at the OO  $\sigma$ -bond. The value of  $\varrho_b$  and, hence, the bond order  $n(\text{OO})$  increase indicating that the OO bond is strengthened and  $\text{H}_2\text{O}_2$  becomes more stable in line with experimental and theoretical observations [31]. The description of  $\text{H}_2\text{O}_2$  demonstrates that anomeric

effects similar as hyperconjugative effects can be quantitatively assessed from the properties of  $\rho(\mathbf{r})$  at the bond critical points of a molecule.

This has been used by LaBarge and co-workers to investigate anomeric effects in final ozonides (1,2,3-trioxolanes) [32, 33]. These authors determined the positions of the lone pair concentrations at the various O atoms for a given conformation of the molecule. Then, calculated  $\sigma^*$  MOs were associated with the bonds in  $\alpha$ -position to the O atoms and ordered according to their energy. Finally, the number of anomeric interactions, i.e. coplanar alignments of the lone pair concentrations at O and vicinal CX bonds were counted in dependence of the conformation of the final ozonid and weighted by the relative energy of the  $\sigma^*(CX)$  MO. In this way, the most stable conformations of substituted final ozonides were predicted and verified by ab initio calculations [32, 33].

## 5 Description of Homoconjugation

### 5.1 $\pi$ -Character of Three-membered Rings

As discussed in the previous section,  $\sigma$ -bonds can possess a bond ellipticity larger than zero due to hyperconjugative or anomeric effects. While these bond ellipticities generally are very small indicating less than 5%  $\pi$ -character, considerably larger bond ellipticities are calculated for formal single bonds in three-membered rings [21, 38, 39].

Table 4 gives relevant values which show that the  $\pi$ -character of the CC bonds in cyclopropane should be of the same magnitude as that of ethylene even though the bond order is close to  $n = 1$ .

There is, however, an important difference between the bond ellipticity in a polyene and in a three-membered ring. As indicated in Fig. 19, the major axes, i.e. the directions of the soft curvatures of the ring bonds, are not perpendicular but parallel to the plane of the carbon nuclei. This means that in the ring plane electron density

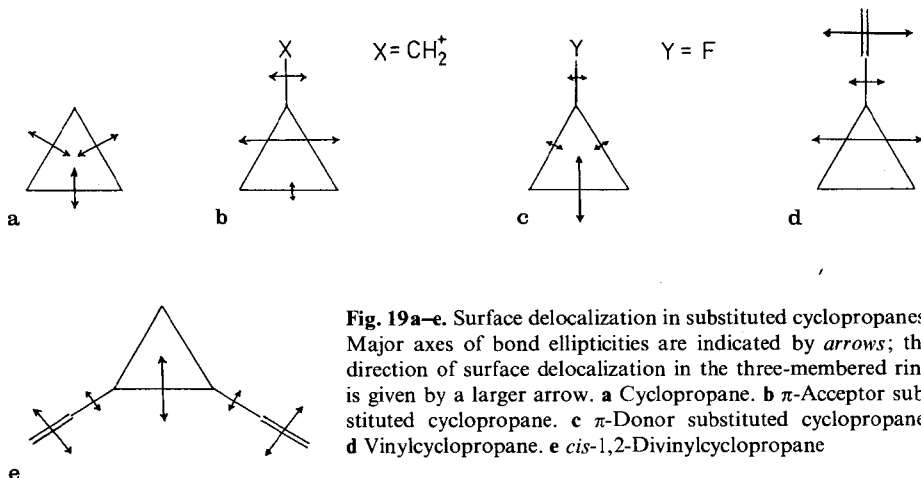
**Table 4.** Bond order  $n$ , bond ellipticity  $\epsilon_b$ , and degree of surface delocalization<sup>a</sup>

Molecule	CC			CX			Ring		
	$\rho_b$ [e Å <sup>-3</sup> ]	$n$	$\epsilon_b$	$\rho_b$ [e Å <sup>-3</sup> ]	$n$	$\epsilon_b$	$\rho_r$ [e Å <sup>-3</sup> ]	$\xi^b$ [%]	$\epsilon_r^c$
Cyclopropane	1.681	1.00	0.489				1.379	82.0	0
Aziridine	1.763	1.06	0.391	1.823	0.97	0.502	1.485	83.1	0.445
Oxirane	1.819	1.08	0.314	1.771	0.96	0.879	1.533	85.8	0.094
Cyclobutane		1.00	0.001				0.554	33	0
Benzene		1.50	0.231				0.141	7	0

<sup>a</sup> HF/6-31G(d) calculations [38]. All bond orders are normalized.

<sup>b</sup> Ratio ( $\rho_r/\rho_b(av)$ ) 100 where  $\rho_b(av)$  is the average of all  $\rho_b$  values.

<sup>c</sup> Ellipticity at the ring critical point.



extends both toward the ring center and toward the outside of the ring. This is unique for three-membered rings. For cyclobutane and larger rings the bond ellipticities are vanishingly small [38] (Table 4). The electron density distribution  $\rho(\mathbf{r})$  in the three-membered ring bonds clearly reveals features of the  $\pi$ -density of an alkene double bond. This is in line with experimental observations that suggest  $\pi$ -character for the three-membered ring bonds [95].

Due to the fact that the electron density extends into the ring,  $\rho(\mathbf{r})$  is considerably larger at the center of the three-membered ring than is usually observed at the center of other rings. For example, the density at the ring critical point of cyclopropane is still 82% of that at the bond critical point  $\mathbf{r}_b(\text{CC})$  ( $\xi$  in Table 4). In cyclobutane (benzene), there is just 33% (7%) of the density at the  $\mathbf{r}_b(\text{CC})$  points [38]. Hence, cyclopropane as well as other three-membered rings are unique in the sense that electron density is smeared out all over the ring plane in a similar manner as it is along the carbon framework of 1,3-butadiene or benzene. In order to distinguish between the various modes of electron delocalization, we speak of “ribbon delocalization”, when electrons delocalize along the “ribbon” of a  $\pi$ -conjugated system (see Sect. 4), and of “surface delocalization” when electrons delocalize in the ring surface [38, 40, 42].

Surface delocalization is characterized by  $\zeta$ , the percentage of negative charge at the ring critical point relative to that at the bond critical point [96], and the ring critical ellipticity  $\varepsilon_r$ . The latter parameter is zero for cyclopropane (Table 4) because both  $\lambda_{1r}$  and  $\lambda_{2r}$  possess the same value, i.e.  $\rho(\mathbf{r})$  is isotropical in the plane of the ring at  $\mathbf{r}_r$ .

For substituted cyclopropanes, interaction between ring and substituents influence the  $\pi$ -character of the CC bonds [39]. Depending on the nature of the substituent the bond ellipticity of the vicinal CC bonds exceeds that of the distal CC bond or vice versa. For the same reason,  $\rho(\mathbf{r})$  at the ring critical point becomes anisotropical, i.e.  $\varepsilon_r > 0$  and  $\lambda_1 \neq \lambda_2$ . *The major axis of the ring ellipticity  $\varepsilon_r$  always points to the CC bond(s) with the largest  $\pi$ -character.* Hence, a direction can be assigned to surface delocalization in substituted three-membered rings. This is the direction of the major axis of  $\varepsilon_r$  [38, 39].



Cremer and Kraka [38, 39] have shown that there is a direct relationship between orbital interactions in substituted cyclopropanes and the various modes of surface delocalization. For example, a  $\pi$ -acceptor substituent that leads to a depopulation of the antibonding Walsh MO of cyclopropane, and, hence, a shortening of the distal bond, causes the direction of surface delocalization to be parallel to the distal bond indicating that the  $\pi$ -character of the vicinal bonds is larger than that of the distal CC bond (Fig. 19b). Similarly, a  $\pi$ -donor substituent causes surface delocalization to be perpendicular to the distal CC bond. In this case, the  $\pi$ -character of the distal bond is larger than that of the vicinal bonds (Fig. 19c).

Due to the  $\pi$ -character of the CC bonds, the cyclopropane unit can both participate and close a gap between two  $\pi$ -conjugated systems. This is indicated in Fig. 19d for vinylcyclopropane. The major axis of the CC double bond is parallel to the direction of surface delocalization. The formal CC  $\sigma$ -bond linking double bond and ring adopts partial  $\pi$ -character. Its major axis overlaps with those of vinyl and cyclopropane, establishing a conjugated system. Obviously, the cyclopropane ring plays the role of a second ethylene unit. Vinylcyclopropane and 1,3-butadiene are isoconjugate.

If the substituent effects of two vinyl groups are superimposed as in *cis*-1,2-divinylcyclopropane, the  $\pi$ -character of the bond C1C2 will be larger than that of bonds C1C3 and C2C3. Surface delocalization takes the direction indicated in Fig. 19e. Again, the cyclopropane ring adopts the role of an ethylene unit that participates in conjugation. 1,2-Divinylcyclopropane is isoconjugate with 1,3,5-hexatriene.

These examples demonstrate that the union of a three-membered ring and one or more double bonds leads to  $\pi$ -conjugation. If two molecular entities that could form a conjugated system are separated by an isolating group X, this can be by-passed by the formation of a three-membered ring, in which X is the apex group and the basal bond connects the conjugated systems. Conjugation of this type has been called homoconjugation [97]. If homoconjugation leads to closure of a ring with  $(4q + 2)$   $\pi$ -electrons, a homoaromatic system will be established. Both homoconjugation and homoaromaticity are consequences of the peculiar properties of three-membered rings in general and cyclopropane in particular. In the same way, as the electronic features of three-membered rings are described with the aid of the properties of  $\rho(\mathbf{r})$ , homoconjugation and homoaromaticity can be described [34]. This is shown in the Subsections that follow.

## 5.2 Homoconjugation

A vinyl group and a carbenium ion that are separated by just one  $\text{CH}_2$  group can homoconjugate. The simplest system to possibly show this type of conjugation is the homoallyl cation,  $\text{C}_4\text{H}_7^+$  [97]. The most notable property of the homoallyl cation is its facile interconversion to the cyclopropylcarbinyl cation [98]. This can be anticipated from the electron density distribution of the homoallyl cation as reflected by bond orders and ellipticities [34] (Fig. 20a). The bond C2C3 is a slightly weakened ( $n = 0.9$ )  $\sigma$ -bond. Nevertheless, it possesses a substantial ellipticity ( $\epsilon = 0.3$ ) with its major axis lying in the plane C1C2C3 and being directed toward the region between

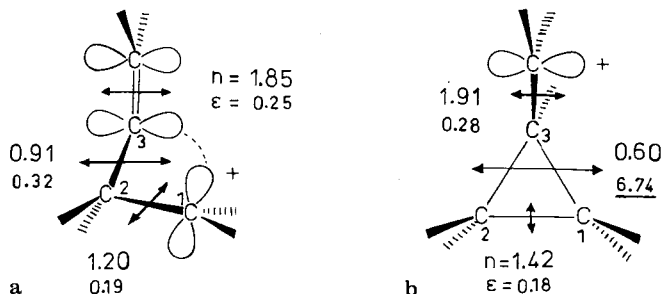


**Fig. 20 a, b.** Bond orders  $n$  and bond ellipticities  $\varepsilon$  of  $C_4H_7^+$ . **a** Homoallyl cation. **b** Cyclopropylcarbiny cation. (HF/6-31G(*d*) calculations [34])

C1 and C3. This is indicative of the onset of a C1C3 bond which is realized in the cyclopropylcarbiny cation.

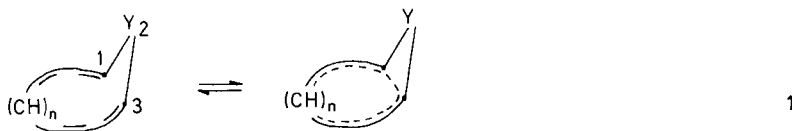
The cyclopropylcarbiny cation has two very labile ring bonds (Fig. 20b). The bond orders of C1C3 and C2C3 are just 0.6 and the ellipticities are extremely large ( $\varepsilon = 6.7$ ). The ring critical point lies almost on a line connecting the bond critical points  $r_b(C1C3)$  and  $r_b(C2C3)$ . Its density is marginally smaller than that at the two bond critical points, and in line with this, the negative curvature of  $\rho_r$  is close to zero. There is a trough in the distribution of negative charge in the plane of the ring linking  $r_r$  and the two bond critical points  $r_b$ . The trough gives the preferred direction of surface delocalization as parallel to the bond C1C2. Little energy is needed to break the ring structure and to merge the three critical points in the bond critical point  $r_b(C2C3)$  of the homoallyl cation.

In the cyclopropylcarbiny cation, the major axis of the bond ellipticity of bond C3C4 is parallel to the direction of surface delocalization. Three-membered ring and C3C4 bond form a conjugate system in which the cyclopropyl ring takes the part of an ethylene unit. The cyclopropylcarbiny cation is isoconjugate with the allyl cation. The onset of these interactions are already revealed by the density properties of the homoallyl cation as shown above.

Homoconjugation is generally considered to arise from  $\pi$ -overlap between non-bonded groups or atoms in a conjugated system. In terms of structure theory it implies the formation of a three-membered ring with enhanced bond ellipticities and a direction of surface delocalization that overlaps largely with the major axes of an adjacent  $\pi$ -system. In general, it is difficult to predict homoconjugative interactions just on the basis of orbital considerations (see Sect. 5.3). Therefore, homoconjugation is mostly postulated in an ad hoc manner to rationalize the properties or the reactivity of a given compound. By way of contrast, we will speak of homoconjugation only if conjugation, interrupt by an atom or group X, has been established by the formation of a labile bond with large  $\pi$ -character. A restriction of the term "homoconjugation" in this way helps to clarify the notion of homoaromaticity discussed in the next Subsection.

### 5.3 Homoaromaticity

The concept of homoaromaticity introduced into chemistry by Saul Winstein [97] is a useful tool to rationalize the chemical behavior of cyclic  $(4q + 2)$   $\pi$ -electron systems in which conjugation is interrupted by a  $sp^3$ -hybridized carbon atom or by any other saturated group Y [13]. Under certain circumstances these systems can circumvent the insulating group by 1,3-orbital interactions that close the conjugated system. Then, cyclic conjugation leads to homoaromatic character of the molecule.



The question is to which extent 1,3 orbital interactions have to be established to guarantee cyclic conjugation of  $4q + 2$  electrons and, hence, homoaromaticity.

There have been many experimental and theoretical investigations to answer this question [13]. Nevertheless, an unequivocal answer could not be found due to the fact that homoaromaticity is only a vaguely defined quantity. This becomes clear when scrutinizing Winstein's definition of homoaromaticity for hydrocarbons [97].



The potentially aromatic system A with  $(4q + 2)$   $\pi$ -electrons will be homoaromatic if

1. the system is closed by a 1,3 bond,
2. the bond order of the 1,3 bond is between 0 and 1,
3. orbital overlap between the participating p-AOs at centers 1 and 3 is neither  $\sigma$  nor  $\pi$ , but intermediate between  $\sigma$  and  $\pi$ , and



4. the  $(4q + 2)$   $\pi$ -electrons are fully delocalized in the resulting closed cycle.

On the basis of MO theory it is impossible to verify for any homoaromatic compound requirements 1 through 4. Although there have been many attempts to describe bonding in terms of MO theory, this has not led to a unified model of bonding that unequivocally distinguishes bonded and nonbonded interactions, that provides a unique definition of bond order, that defines a minimum overlap that is necessary for bonding or that quantifies the extent of  $\pi$ -delocalization in a cyclic system. The key question whether an overlap of 0.1 or even 0.03 is sufficient to establish a homoaromatic bond cannot be answered by MO-theory [99].

Also, experimental descriptions of potentially homoaromatic systems do not provide an unambiguous assessment of homoaromatic character. Does for example a 1,3-CC distance of 1.8 or 1.7 Å already imply bonding? How is homoaromatic stabilization measured in a system that contains both a strained cyclopropane unit and a conjugated  $\pi$ -system? How can magnetic properties be related to homoaromatic interactions? Despite all attempts to answer these questions, there has been only limited progress toward a quantitative description of homoaromaticity.

The analysis of  $\rho(\mathbf{r})$  provides a basis for a rigorous definition of homoaromaticity [34]. Utilizing the definitions of covalent bonding, bond order,  $\pi$ -character, and  $\pi$ -delocalization presented in Sects. 3 and 4, Winstein's definition of homoaromaticity can be translated into density language.

A potentially aromatic system with  $(4q + 2)$   $\pi$ -electrons will be homoaromatic if

1. the system is closed by a 1,3-bond path with a bond critical point  $\mathbf{r}_b(\text{C1}, \text{C3})$  and  $H_b < 0$ ;
2. the bond order  $n$  (see Eq. 8) of the 1,3 bond is  $0 < n < 1$ ,
3. the  $\pi$ -character of the 1,3-bond as measured by the bond ellipticity  $\varepsilon$  is larger than that of cyclopropane:  $\varepsilon(1,3) > \varepsilon(\text{cyclopropane})$ , and
4. the major axis of  $\varepsilon(1,3)$  overlaps effectively with those of the neighboring bonds.

This is a quantitative definition of homoaromaticity that is generally applicable, not only for hydrocarbons. However, this definition is much more stringent than Winstein's definition. It excludes all those systems with 1,3-interactions that do not lead to a bond path. Hence, it describes homoaromaticity in a restricted sense.

In the following the electron density description of homoaromaticity will be applied to the archetype of all homoaromatic compounds, namely the homotropylium cation [100]. In 1967 Winstein concluded that the available data on the homotropylium cation were in favor of a nonclassical homotropylium structure [97]. Childs and co-workers reached the same conclusion on the basis of a X-ray diffraction study of 2-hydroxy-homotropylium hexachloroantimonate [101]. Ab initio calculations carried out by Haddon [102] led to an equilibrium geometry that is in good agreement with the geometry found in the X-ray diffraction study [101].

Using the ab initio geometry of Haddon the bond orders and ellipticities shown in Fig. 21 have been obtained by Cremer and co-workers [34]. The most important result of this investigation is the observation of a 1,3 bond path with a bond order considerably lower than 1 ( $n = 0.71$ ) and a bond ellipticity that is considerably

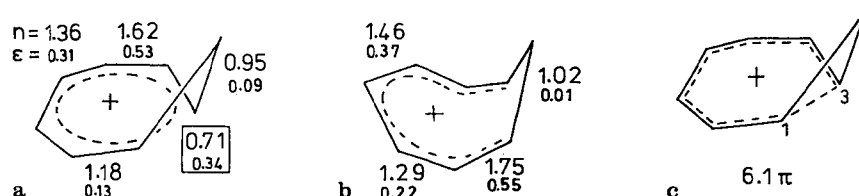


**Fig. 21a-c.** Bond orders  $n$  and bond ellipticities  $\varepsilon$  of  $\text{C}_8\text{H}_9^+$ . **a** Homotropylium cation. **b** Non-homoaromatic cyclooctatrienyl cation. **c** Number of  $\pi$ -electrons delocalized in the homotropylium cation. (HF/STO-3G calculations [34])

larger than that of cyclopropane obtained at the same level of theoretical accuracy. The corresponding  $\pi$ -character is 46%. Hence, *homotropylium cation possesses a homoaromatic bond*. The bond path is bent below the plane of the seven-membered ring which is in line with a 1,3 overlap that is intermediate between  $\sigma$  and  $\pi$ . For full realization of an aromatic system, all seven bond orders  $n$  and ellipticities  $\varepsilon$  should be equal and all major axes should be parallel and perpendicular to the ring plane as in the case of the tropylium cation. In the homotropylium cation, the bond orders alternate between 0.7 (C1C3), 1.2 (C3C4), 1.6 (C4C5), and 1.4 (C5C6). The  $\pi$ -character of the ring bonds is 45, 17, 70, and 41%. The dot products of the unit vectors defining neighboring major axes (see Sect. 4) are 0.89 (C2C3, C3C4), 0.98 (C3C4, C4C5), 0.99 (C4C5, C5C6), and 0.97 (C5C6, C6,C7). Hence, overlap of the major axes is close to 100% [34].

The bond orders in the ring sum to 9.1, a value equivalent to six single bonds and six  $\pi$ -electrons delocalized in the ring. The degree of delocalization  $D$  (Eq. (26), Sect. 4) is 78%, much higher than that of any of the polyenes discussed in Sect. 4. From Fig. 21 it becomes obvious that full delocalization ( $D = 100\%$ ) is not achieved due to the low bond order and  $\pi$ -character of the bonds C3C4 and C1C8 that link the homoaromatic bond to the pentadienyl fragment.

According to the definition given above, the homotropylium cation is a true homoaromatic system [34]. In addition, the analysis of  $\rho(\mathbf{r})$  reveals that the homoaromatic bond C1C3 is rather labile. This is a consequence of the proximity of the ring critical point  $\mathbf{r}_r(\text{C1C2C3})$  and the bond critical point  $\mathbf{r}_b(\text{C1C3})$ . Both points are just 0.44 Å apart and the density at these points differ by only 0.015 e Å<sup>-3</sup>. The other two three-membered ring bonds, C1C2 and C2C3 possess relatively small ellipticities. Their properties are closer to those of normal  $\sigma$ -bonds rather than to those of cyclopropane bonds. This is also a consequence of the migration of the ring critical point  $\mathbf{r}_r$  toward the homoaromatic bond C1C3. Obviously, surface delocalization in the cyclopropane unit is largely reduced in favor of  $\pi$ -character of the bridging bond C1C3.

Any lengthening of the C1C3 distance (1.58 Å) leads to further migration of  $\mathbf{r}_r$  toward  $\mathbf{r}_b(\text{C1C3})$ . Coalescence of these points (yielding a catastrophe point) causes a rupture of the homoaromatic bond. A second isomere of C<sub>8</sub>H<sub>9</sub><sup>+</sup> can exist with a C1C3 distance of 2.324 Å. It is 6.4 kcal mol<sup>-1</sup> less stable than the homotropylium cation [102], does no longer possess a cyclopropane unit and is best described as a heptatrienyl cation which is part of an eight-membered ring [34]. In conclusion, the analysis of  $\rho(\mathbf{r})$  along the lines established in Sect. 2, facilitates the characterization of potentially homoaromatic compounds. Utilizing the definitions given above a clear distinction between true homoaromatic and nonhomoaromatic systems can be made.

## 5.4 Do Neutral Homoaromatic Compounds Exist?

In the fifties, even before Winstein developed the concept of homoaromaticity, Turner and co-workers [103] pointed out that according to measured heats of hydrogenation 1,3,5-cycloheptatriene should be stabilized by about 9 kcal mol<sup>-1</sup>. Later this value was refined to 4 kcal mol<sup>-1</sup> by Roth and co-workers who analyzed heats of hydro-

generation with the aid of force field calculations [104]. The stabilization of 1,3,5-cycloheptatriene was considered to arise from 1,6-homoconjugative interactions and resultant homoaromaticity of a cyclic triene with  $6\pi$  electrons.

There have been many experimental and theoretical investigations on the question of homoaromaticity in cycloheptatriene, partially supporting partially rejecting this possibility [105]. In the late seventies Christoph, Paquette, Gleiter, Houk, and others raised the principal question whether homoaromatic character is possible in neutral compounds [106, 107]. Christoph and co-workers [106] investigated a select group of trienes, including  $C_{16}$ -hexaquinacene, triquinacene, and *cis*<sup>3</sup>-1,4,7-cyclo-nonatriene, the constituent double bonds of which adopt an arrangement potentially suitable for effective pp-overlap. From their investigation the authors concluded that *one can rule out the likelihood that neutral homoaromatic character will ever be discovered* [106]. Houk and co-workers [107] pointed out that homoconjugative interactions between  $\pi$ -systems should be destabilizing due to closed-shell repulsion and, therefore, the existence of neutral homoaromatic molecules is rather limited [108]. To scrutinize these arguments and to resolve their contradiction with the apparent stabilization of 1,3,5-cycloheptatriene, Cremer and co-workers investigated the latter molecule with the aid of ab initio methods [35, 36].

In its equilibrium geometry 1,3,5-cycloheptatriene adopts a boat conformation with dihedral angles as large as  $60^\circ$ . The distance between C1 and C6 is 2.5 Å. For this form, bond orders and ellipticities typical of a cyclopolyene with partial  $\pi$  delocalization are found (see Fig. 22). There is no indication of homoconjugative 1,6-interactions. 1,3,5-Cycloheptatriene is not a homoaromatic system.

It is, however, striking that despite the nonplanarity of 1,3,5-cycloheptatriene,  $\pi$ -delocalization is as large as in planar 1,3-butadiene. Analysis of the conformation of cycloheptatriene with the aid of Cremer-Pople puckering coordinates [109] revealed that cycloheptatriene in its equilibrium geometry does not represent a pure boat form but a mixed conformation comprising 77% boat and 23% chair form, as schematically shown in Fig. 23. The admixture of the chair form leads to a perturbed boat conformation, which is flattened in the triene part of the seven-membered ring as reflected by folding angles of  $27^\circ$  (stern of the boat) and  $49^\circ$  (bow of the boat) [35]. In this way,  $\pi$ -delocalization is improved and 1,3,5-cycloheptatriene stabilized. Also, hyperconjugative effects reflected by the small ellipticities of bonds C1C7 and C6C7 ( $\epsilon = 0.04$ ) add to the stability of the system. *There is no need to invoke homoaromaticity to explain the stability of 1,3,5-cycloheptatriene.* However, this finding not necessarily implies that homoaromaticity is not possible for a neutral molecule.

Upon decreasing the distance C1C6, the energy of cycloheptatriene increases and electron density is redistributed in the ring. In particular, there is a build up of electron

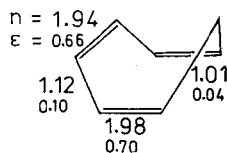
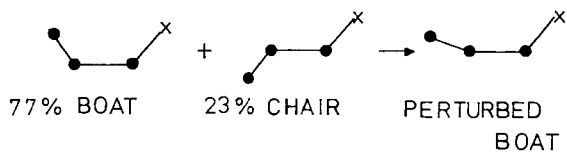
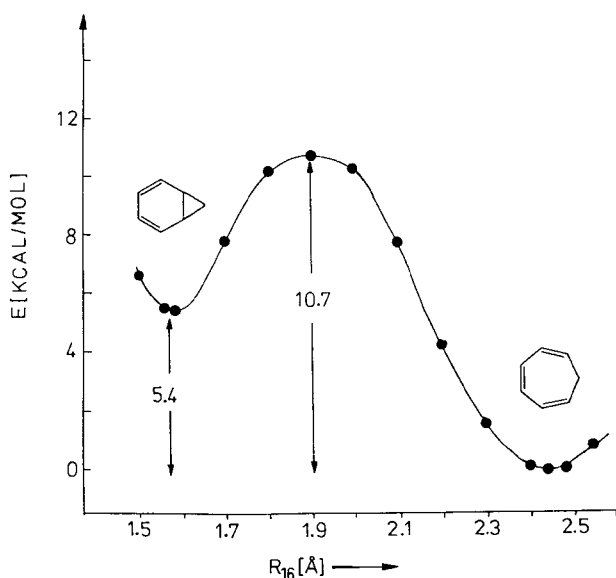


Fig. 22. Bond orders  $n$  and bond ellipticities  $\epsilon$  of cycloheptatriene. (HF/6-31G(d) calculations)



**Fig. 23.** Representation of the perturbed boat conformation of 1,3,5-cycloheptatriene (side view) as a linear combination of boat and chair form of the seven-membered ring ( $X = \text{CH}_2$ )

density between C1 and C6 indicating the onset of a bond formation. 1,3,5-Cycloheptatriene rearranges to its valence tautomer norcaradiene. The energy change along the reaction path as determined by ab initio calculations [36], is shown in Fig. 24. According to these calculations the activation energy is  $10.7 \text{ kcal mol}^{-1}$  and the reaction is endothermic by  $5.4 \text{ kcal mol}^{-1}$  (Fig. 24).



**Fig. 24.** Potential energy surface calculated for the valence tautomerization of 1,3,5-cycloheptatriene to norcaradiene. As a reaction coordinate the 1,6-distance ( $R_{16}$ ) has been taken. Dots denote calculated energies for fixed  $R_{16}$  values. (MP2/6-31G(d) calculations)

In view of the fact that norcaradiene contains a strained  $\text{C}_3$  ring (the strain energy of cyclopropane is  $27.5 \text{ kcal mol}^{-1}$  [110], see Sect. 6), the energy gap of just  $5 \text{ kcal mol}^{-1}$  between the two valence tautomers appears extremely small. An explanation for the surprising stability of norcaradiene emerges from its bond orders and ellipticities as obtained from the analysis of  $\rho(\mathbf{r})$  (see Fig. 25). The bond C1C6 is labile ( $n = 0.85$ ) with a rather large ellipticity indicating substantial  $\pi$ -character. If one assumes the electrons forming this bond to interact with the other  $\pi$ -electrons of the six-membered ring, an ensemble of six  $\pi$ -electrons will be formed that can delocalize in the ring. According to the definition given above *norcaradiene is a*

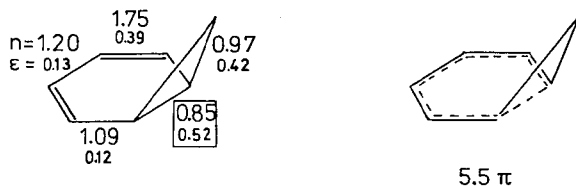


**Fig. 25.** Bond orders  $n$  and ellipticities  $\epsilon$  of norcaradiene. The number of  $\pi$ -electrons delocalized in the six-membered ring are given

*neutral homoaromatic system.* Homoaromatic stabilization leads to a partial compensation of the strain induced by the cyclopropane unit. Hence, the energy difference between norcaradiene and cycloheptatriene is less than expected [111].

Neutral homoaromatic compounds exist! Possible candidates are norcaradiene or compounds containing norcaradiene such as bisnorcaradiene (tricyclo[4.4.1.0<sup>1,6</sup>]-undeca-2,4,7,9-tetraene), the valence tautomer of 1,6-methano[10]annulene [36, 112].

### 5.5 Homoantiaromaticity — Fact or Fiction?

If one extends the concept of homoconjugation in a purely schematic way, one might expect that homoconjugative interactions also lead to cyclic delocalization of  $4q$   $\pi$ -electrons. In this case, one could speak of homoantiaromaticity. However, this is a definition according to pattern probably without any chemical relevance. Since delocalization of  $(4q)$   $\pi$ -electrons should lead to destabilization, there is no reason why homoconjugative interactions should take place at all.

Cremer and co-workers [34] have investigated the bicyclo[3.1.0]hexenyl cation (Fig. 26a), which has been described as being homoantiaromatic [113]. An interaction of the allylic  $2\pi$  system with the cyclopropane unit similarly as encountered in nor-

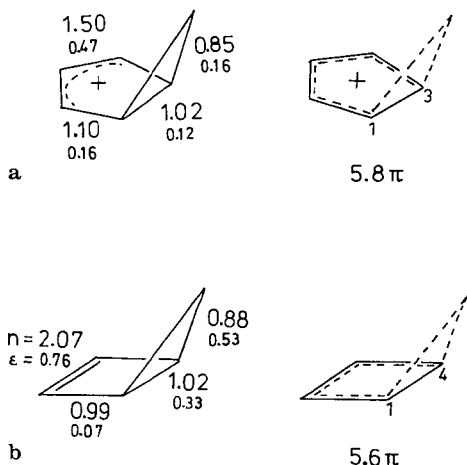


**Fig. 26.** Bond orders  $n$  and bond ellipticities  $\epsilon$  of potentially homoantiaromatic molecules. **a** Bicyclo[3.1.0]hexenyl cation. (HF/STO-3G calculations [34]) **b** Bicyclo[2.1.0]pen-2-tene. (HF/6-31G(*d*) calculations) Number of electrons delocalized in the two molecules are given on the right side



caradiene (Section 5.3) would entail destabilizing  $4\pi$  electron interactions. However, the bicyclo[3.1.0]hexenyl cation avoids homoantiaromatic  $4\pi$  electron delocalization as is clearly revealed by calculated  $n$  and  $\epsilon$  values (Fig. 26a). The properties of the bond C1C3, including its length (1.501 Å) [34] are those of a CC bond in an isolated cyclopropane. On the other hand, the two external bonds of the three-membered ring, C1C2 and C2C3, are extended (1.535 Å) and are the most labile bonds in the cation with  $n$  being just 0.85. They possess ellipticities whose major axes have substantial overlaps with the corresponding axes of the neighboring bonds in the five-membered ring. Their properties are similar to, but less extreme than, those of the homoaromatic bond in the homotropylium cation.

The analysis of  $g(r)$  of bicyclo[3.1.0]hexenyl cation suggests that the ring of the six outer bonds forms a conjugated system. Their bond orders sum to 6.8, equivalent to four single bonds and a  $\pi$ -system of approximately six electrons. The labile character of bonds C1C2 and C2C3 accounts for the perambulatory properties of the cyclopropane ring. For methyl-substituted derivatives of the bicyclo[3.1.0]hexenyl cation it has been found that C2 and, hence, the cyclopropane ring migrates around the five-membered ring by a series of sigmatropic 1,4-rearrangements [114]. Unlike the homotropylium cation, in which the external bonds of the three-membered ring are effectively moved from the conjugated system, delocalization of negative charge persists over the entire surface of the three-membered ring and this surface is conjugated with the  $\pi$ -system of the five-membered ring. The direction of surface delocalization is parallel rather than perpendicular to the bond C1C3 indicating that the latter is excluded from conjugation.

Similar observations can also be made for other potentially homoantiaromatic compounds. For example, a molecule for which one could expect  $4\pi$  electron delocalization similar to the  $6\pi$  delocalization in norcaradiene (Sect. 5.3) is bicyclo[2.1.0]pent-2-ene [113] (Fig. 26b). Again, the external bonds rather than the bridging bond of the three-membered ring are labile as reflected by  $n = 0.88$  and  $\epsilon = 0.53$ . Approximately six electrons are delocalized on the perimeter of the six-membered ring.

In conclusion, potentially homoconjugative systems with  $(4q)$   $\pi$ -electrons clearly avoid homoantiaromaticity by adopting an electronic situation with  $(4q + 2)$  delocalized electrons. This is possible because surface delocalization in the three-membered ring can be both perpendicular and parallel to the 1,3-bond. It seems that the preferred direction of surface delocalization is always as such that a  $(4q + 2)$  system of delocalized  $\pi$ -electrons is formed and a homoantiaromatic system is avoided. The question remains whether homoantiaromaticity will also be avoided if steric factors enforce interactions of  $4q$  electrons. These interactions will clearly be destabilizing. In this situation, the molecule will adopt a geometry that minimizes destabilizing interactions, i.e. it will avoid a homoconjugative bond. In view of these considerations *it is unlikely that homoantiaromaticity exists*. This does not exclude that through-space (or through-bond) interactions are still destabilizing to some extent leading to molecular properties different from those expected [115].

## 5.6 Distinction Between Homoconjugation and Through-Space Interactions

The definition of homoaromaticity given in Sect. 5.3 is based on changes of molecular structure as reflected by the network of bond paths. Compounds that possess a

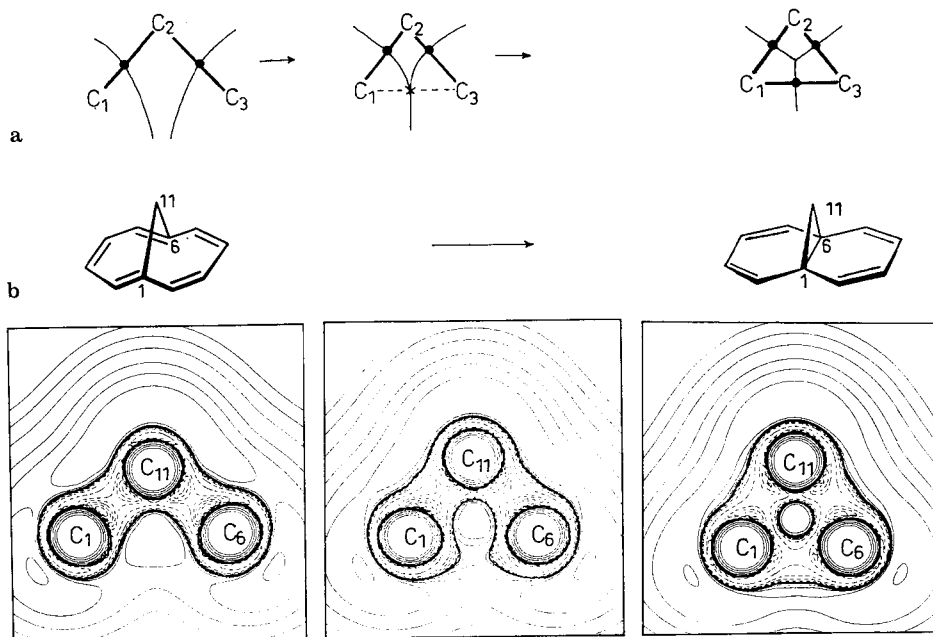


**Fig. 27.** **a** Schematic view of the changes of the atomic subspaces upon the approach of C1 and C3 in a potentially homoaromatic system. *Heavy solid lines* denote bond paths, *dots* bond critical points, *a star* a catastrophe point. The traces of the zero-flux surfaces in the plane are given by *light solid lines*. **b** Change of the Laplace concentration (shown in form of contour-line diagrams) for the rearrangement of 1,6-methano[10]annulene to bisnorcaradiene (tricyclo[4.4.1.0<sup>1,6</sup>]undeca-2,4,7,9-tetraene). The reference plane contains nuclei C1, C6, and C11. *Dashed contour-lines* denote concentration of charge ( $\nabla^2 \rho(\mathbf{r}) < 0$ ) and *solid contour-lines* denote depletion of charge ( $\nabla^2 \rho(\mathbf{r}) > 0$ ). (HF/6-31G(*p*, *d*) calculations)

homoaromatic bond in a cyclic  $(4q + 2)$   $\pi$ -system are homoaromatic in the closer sense. However, there are other compounds that exhibit 1,3-interactions that do not lead to a 1,3-bond path but affect the properties of the molecule. An example for such a case is the cyclobutenyl cation. The spectroscopic properties of this cation are often quoted to emphasize its "homoaromatic" character [13]. Yet, none of the ab initio calculations carried out so far leads to an electron density distribution with a 1,3 homoaromatic bond path [34] despite the fact that other properties of the cation such as geometry and conformation are well reproduced by ab initio theory [116].

The question is which properties of  $\rho(\mathbf{r})$  indicate through-space interactions and the stepwise formation of a chemical bond. Fig. 27a presents a schematic view of how the atomic subspaces  $\Omega$  change on an approach of C1 and C3. Clearly, the subspace C2 extends less and less in the region between C1 and C3 until the surfaces of C1 and C3 coincide and a bond path between C1 and C3 is formed. At the same time the Laplace concentration between C1 and C3 gradually increases and converges to the one found for a three-membered ring. This is shown in Fig. 27b for the case of the valence tautomerism of 1,6-methano[10]annulene to bisnorcaradiene [36].

An analysis of the Laplace concentration,  $-\nabla^2 \rho(\mathbf{r})$ , yields information about the

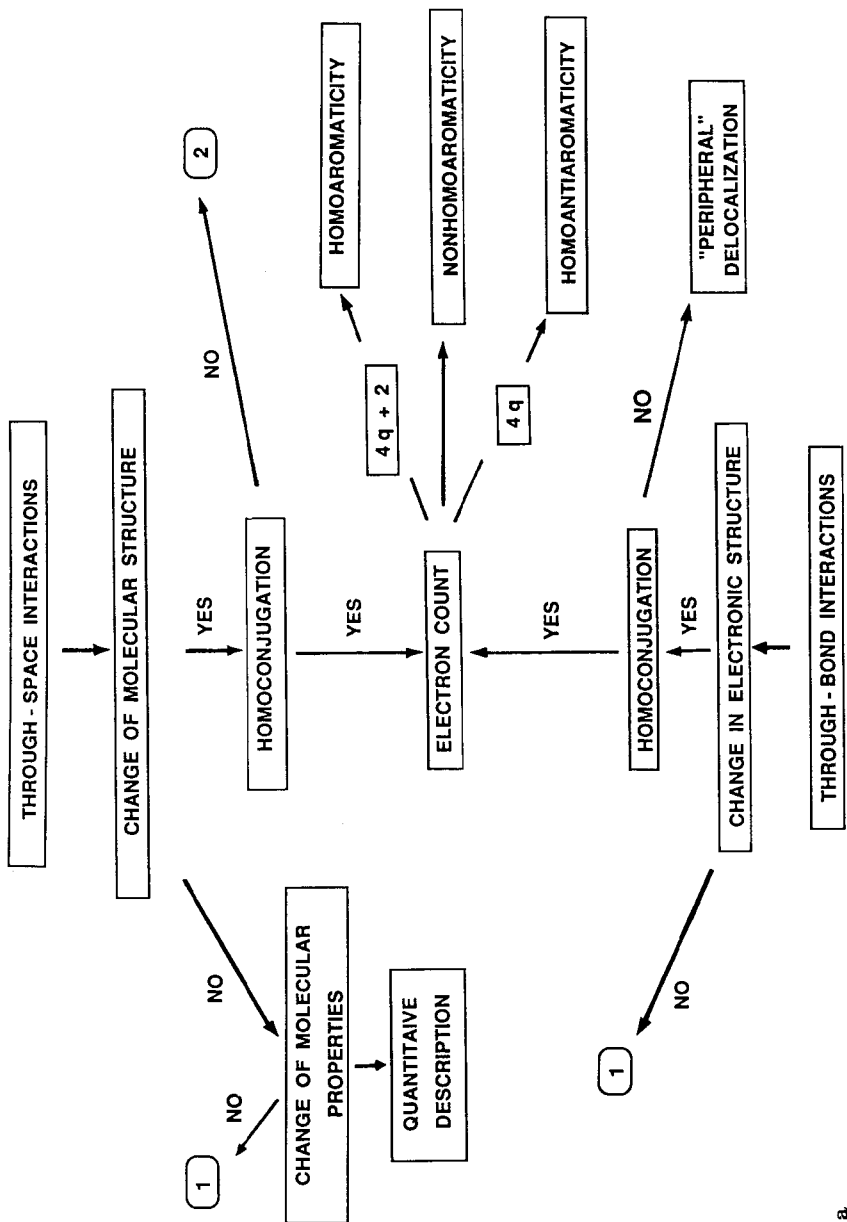
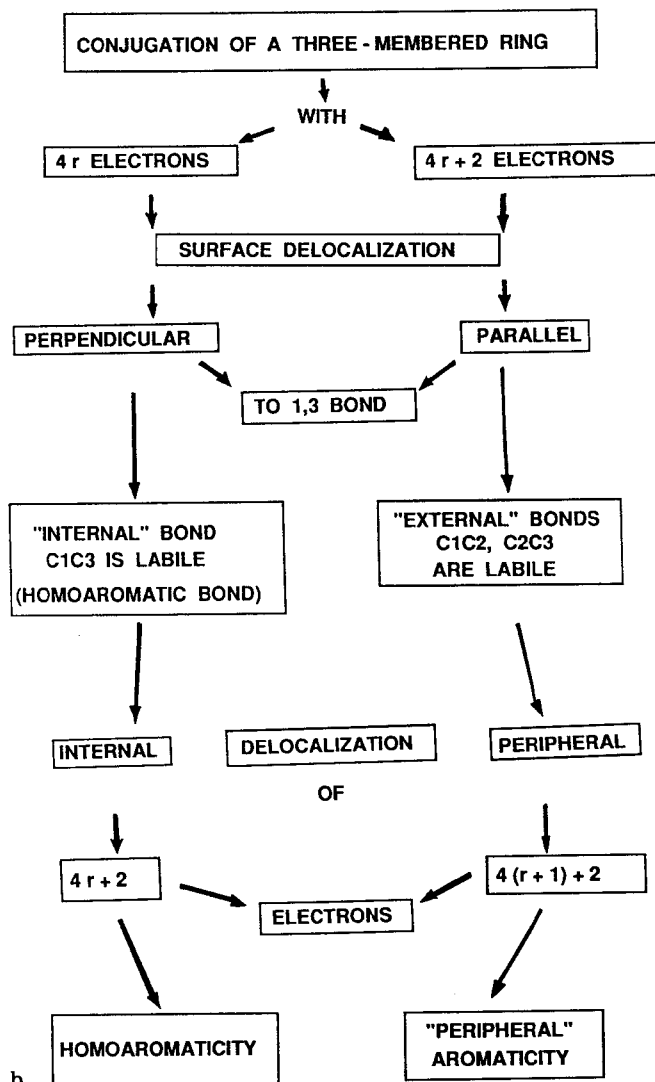


**Fig. 28. a** Flow chart diagram for the distinction of through-space, through-bond, and homoconjugative interactions utilizing the properties of  $\rho(r)$ . The numbers have the following meaning. 1: Through-space or through-bond interactions are negligible. 2: Other nonclassical structures are formed. **b** Flow chart diagram showing the two possible modes of conjugation between a three-membered ring and an adjoining  $\pi$ -system



extent of through-space interactions and the concomitant changes in the molecular properties. Hence, a clear distinction between the various modes of intermolecular interactions is possible. This is shown in form of a flow chart diagram in Fig. 28a. Through-space interactions can lead to a change in molecular structure, in particular a 1,3 bond may be established due to homoconjugative interactions. An electron count will reveal whether a homoaromatic system is formed. If the molecular structure is not changed, i.e. no new bond path is established, the molecular properties will change to some degree. Strong changes in typical parameters such as NMR shifts have led to the denotation of "homoaromaticity" in the broader sense [13]. Examples are the cyclobutenyl cation or the isoelectronic 1,2-dihydro-borete [37].

Alternatively, homoaromaticity may be caused by through-bond interactions. The latter do not cause a change in molecular structure (if they would change molecular structure, the interaction would have to be considered as through-space interaction), but a change in the electronic structure which in turn may lead to a homoconjugative bond and to a conjugated cyclic system. "Internal" delocalization of  $(4q + 2)$   $\pi$ -electrons involving a 1,3 bond yields homoaromaticity as in norcaradiene while "external" delocalization of  $(4q + 2)$   $\pi$ -electrons involving bonds 1,2 and 2,3 results in a labilization of these bonds and "peripheral aromaticity" (Fig. 28b).

Homoaromaticity requires conjugation of a three-membered ring with an adjoined  $\pi$ -system. A four-membered ring (bridging of two saturated groups) does not lead to homoaromatic character. This is due to the fact that surface delocalization of electrons is found just for three-membered rings and not for larger ones [38, 42].

Depending on the number of  $\pi$ -electrons in the adjoining  $\pi$ -system, the preferred direction of surface delocalization is perpendicular or parallel to the 1,3-bond to yield in any case an  $(4q + 2)$  ensemble of delocalized electrons. Only in the former case is the  $\pi$ -character of the 1,3 bond increased and a homoaromatic system formed. Noteworthy is that both ionic and neutral homoaromatic compounds exist. Homoantiaromaticity, however, is not possible.

Obviously, homoconjugation is the result of the exceptional electronic structure of a three-membered ring. One could expect that homoconjugation first leads to a destabilization of the molecule since formation of a three-membered ring results in increased ring strain. Since this is not the case, ring strain must be outweighed or at least be compensated largely by the stabilizing effects of surface delocalization. We will consider this question in Sect. 6.

## 6 Description of Strain

In general, one distinguishes between four major types of strain [117], namely

1. bond stretching strain,
2. bond angle or Baeyer strain,
3. torsional or Pitzer strain, and
4. nonbonded or Dunitz-Schomaker strain.

Strain is caused by deviations from the strain-free molecular geometry, e.g. by deviations of the bond lengths from ideal values, by deformation of the tetrahedral, trigonal or linear bond angles, by bond eclipsing as opposed to bond staggering, and by nonbonded distances that are smaller than ideal van der Waals distances. Since an extensive discussion of the various types of strain can be found in Ref. 40, we refrain from repeating this discussion. Instead we focus on the question how strain affects the properties of  $q(\mathbf{r})$ . If this is known, a quantitative description of strained molecules with the properties of  $q(\mathbf{r})$  is straightforward.

Actually, the description of an elongated bond in terms of the properties of  $q(\mathbf{r})$  is trivial. As discussed in Sect. 2.4 an increase in the bond distance  $R$  leads to a linear decrease of  $q_b$ , the electron density at the bond critical point  $\mathbf{r}_b$ . More interesting

are the changes in  $\varrho(\mathbf{r})$  caused by a compression of bond angles. Angle bending as encountered, e.g. in small cycloalkanes leads to bent bonds. The bend of the ring bonds should reflect the amount of Baeyer strain induced by angle compression. Therefore, a realistic and quantitative description of bent bonds is a prerequisite for an assessment of ring strain in small rings.

## 6.1 Baeyer Strain — Description of Bent Bonds

The bond paths are images of the covalent bonds of a molecule [22, 23]. Any deviation of the bond path from the internuclear connection line is indicative of bond bending. The bent bond character is quantitatively assessed by determining the bond path length  $R_b$ , the interpath angle  $\beta$ , and the shift parameter  $d$  (for a definition of these parameters see Sect. 2, Fig. 4c).

In Table 5, bent bond parameters of some strained rings are compared. For cyclopropane, the CC bond paths are 0.009 Å longer than the  $R_e$  distances [38, 41]. The shift parameter is positive (0.06 Å, Table 5), reflecting that the bent bonds in cyclopropane are convex, i.e. outwardly curved. The interpath angle  $\beta$  is 19° larger than the geometrical angle  $\alpha$  of 60°. The corresponding values for cyclobutane (Table 5) indicate that going from a three- to a four-membered ring leads to a significant decrease in bond bending. For example,  $\beta(\text{CCC})$  in cyclobutane is just 7° larger than  $\alpha(\text{CCC})$  (Table 5). Bond bending is negligible for five-membered or larger rings.

If one of the C atoms in cyclopropane is replaced by a more electronegative atom X, the bend of the distal CC bond will increase while that of the vicinal CX bonds decreases, i.e. the CX bonds approach the internuclear connection lines. These trends are reflected by the bent bond parameters given in Table 5 for oxirane (X = O). The corresponding molecular graphs are depicted in Fig. 29.

For a further increase of the electronegativity of X, the CX bond paths curve inwardly into the ring, i.e. the bent bonds become concave and  $d < 0$ ,  $\beta < \alpha$  are found

Table 5. Bent bond parameters of strained rings in comparison with geometrical parameters<sup>a</sup>

Molecule	Bond	$R_e$ [Å]	$\Delta R^b$ [10 <sup>3</sup> Å]	$d$ [Å]	$\epsilon$	Angle	$\alpha$	$\beta$
Cyclopropane	CC	1.497	9	0.06	0.49	CCC	60	78.8
	CC	1.453	23	0.094	0.31	CCO	58.8	72.8
Oxirane	CO	1.401	3	0.004	0.88	COC	62.4	75.8
	CO	1.401	3	0.004	0.88	COC	62.4	75.8
Protonated Oxirane	CC	1.446	18	0.087	0.05	CCO	61.1	56.7
	CO	1.498	184	-0.171	2.16	COC	57.7	19.9
Fluoro-ethyl cation	CC	1.445	15	0.083	0.03	CCF	61.9	4.3
	CF	1.533	537	-0.455	> 10 <sup>2</sup>	CFC	56.2	0.02
Bicyclobutane	CC <sup>c</sup>	1.484	18	0.089	0.36	CCC <sup>c</sup>	58.8	73.6
	CC	1.513	9	0.056	0.49	CCC	60.6	77.4
Cyclobutane	CC	1.544	3	0.038	< 0.01	CCC	88.6	95.6

<sup>a</sup> All values from HF/6-31G(d) calculation [38, 43].

<sup>b</sup>  $\Delta R = 1000 (R_b - R_e)$ .

<sup>c</sup> Central bond and angle opposite to central bond, respectively.

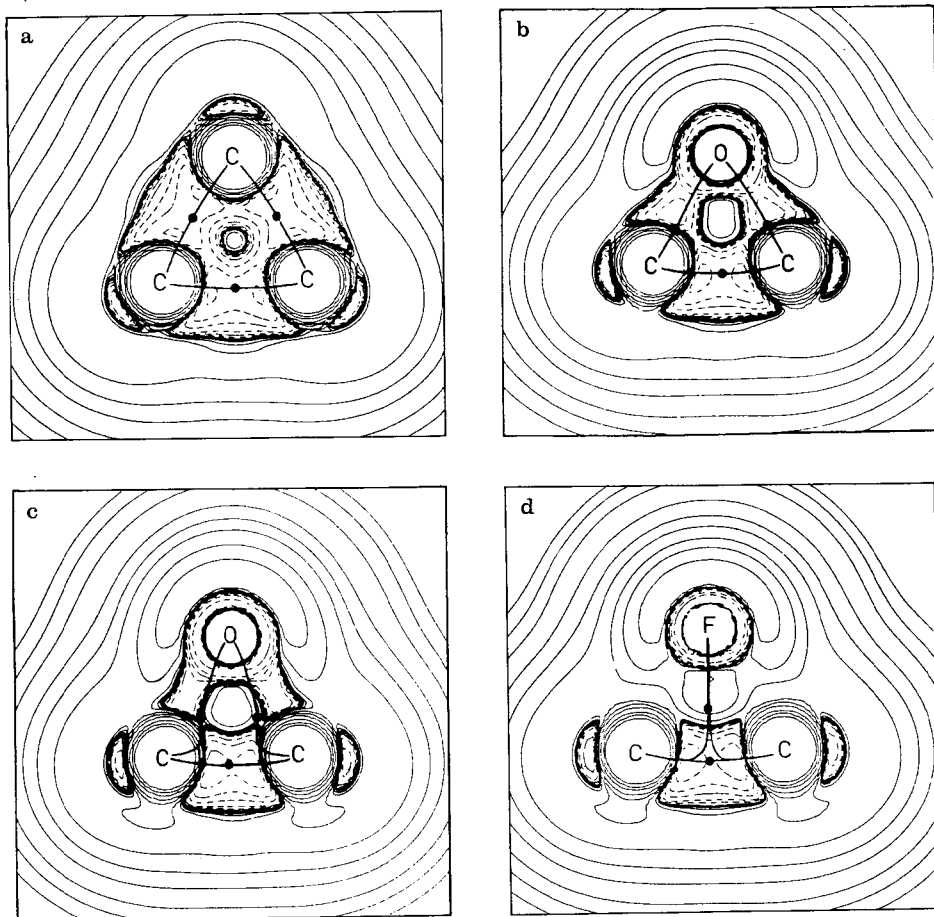


**Fig. 29 a-d.** Molecular graphs and Laplace concentrations,  $-\nabla^2 \rho(\mathbf{r})$ , of **a** cyclopropane, **b** oxirane, **c** protonated oxirane, and **d** halogen-bridged fluoroethyl cation. The reference plane contains the nuclei of the heavy atoms. Bond paths are indicated by *heavy solid lines* and bond critical points by *dots*. *Dashed lines* are in regions where electronic charge is concentrated ( $\nabla^2 \rho(\mathbf{r}) < 0$ ) and *solid lines* in regions where charge is depleted ( $\nabla^2 \rho(\mathbf{r}) > 0$ ). Inner shell concentrations are not shown. (HF/6-31G(d) calculations [38])

[38]. At the same time the bending of the CC bond is reduced. This is the case for  $X = \text{OH}^+$  and  $X = \text{F}^+$  (Table 5 and Fig. 29). For  $X = \text{F}^+$ , the vicinal bond paths are so extremely inwardly curved that they coincide largely. The CFC interpath angle  $\beta$  is just  $0.02^\circ$  and the shift parameter  $d$  is  $-0.455 \text{ \AA}$ . The corresponding molecular graph (Fig. 29) resembles no longer a three-membered ring but a  $\pi$ -complex [38].

## 6.2 From Three-membered Rings to $\pi$ -Complexes — Limits of the Concept of Strain

The molecular graphs given in Fig. 29 reveal that there is a continuous transition from three-membered rings to  $\pi$ -complexes depending on the electronegativity of the constituent atoms. This has been observed not only for C-containing but also for Si-containing three-membered rings [44].

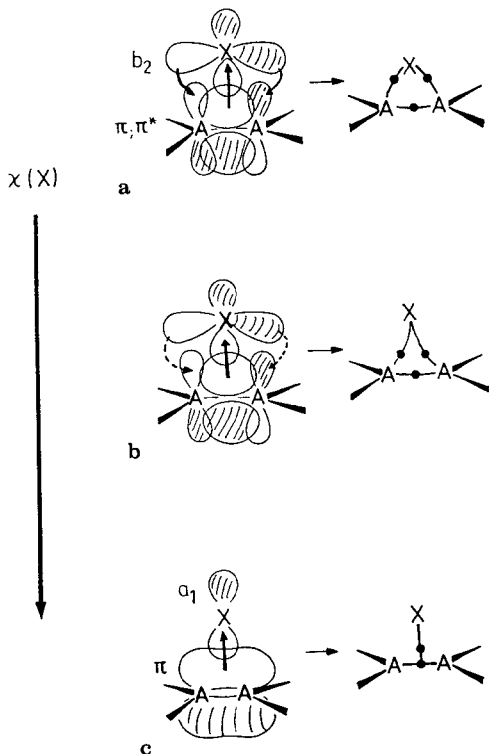


**Fig. 30a-c.** MO description of donor-acceptor interactions between the basal group  $A_2H_4$  ( $A = C, Si, \text{etc.}$ ) and the apex group  $X$ . The relevant orbitals ( $a_1$  and  $b_2$  symmetry) are shown on the left side and the corresponding molecular graphs on the right side of each diagram. The direction of charge transfer is indicated by arrows (dashed arrows indicate reduced charge transfer). **a** Three-membered ring with convex bent bonds. **b** Three-membered ring with concave bent bonds. **c**  $\pi$ -Complex. The electronegativity  $\chi$  of  $X$  increases from a) to c). Reprinted with Permission from J. Mol. Structure (Theochem), 169 (1988) 531. Copyright (1988) Elsevier Science Publishers, Amsterdam

Dewar was the first to point out a relationship between three-membered rings and  $\pi$ -complexes [118]. Combining the MO model developed by Dewar and Ford [119] and an electron density model developed by Cremer and Kraka [38], the following picture emerges (Fig. 30). The curvature of the bond paths in three-membered rings can be rationalized by donor, acceptor interactions between the group (atom)  $X$  and the basal group  $A=A$  (with  $A = CH_2, SiH_2, \text{etc.}$ ). The basal group donates electrons from a  $\pi$  MO into a suitable low lying  $a_1$  MO ( $C_{2v}$  symmetry assumed) thus establishing a build up of electron density in the center of the ring. Back donation from a high lying  $b_2$  MO into the  $\pi^*$  MO of  $A=A$  leads to a peripheral accumulation of electron density, mainly responsible for the curvature of the bond paths (Fig. 30).

1. If donation and back-donation are comparable, a three-membered ring with convex bent bonds will result (Fig. 30a).
2. If back-donation is reduced due to the electronegativity  $\chi$  of  $X$  (reduced donor capacity of  $X$ ), a three-membered ring with concave bent bonds results (Fig. 30b). As a further consequence, the vicinal  $AX$  bonds are weakened.
3. In the extreme case, back-donation becomes negligible and the interaction between  $X$  and  $A_2$  is characterized by the amount of negative charge transferred from  $A_2$  to  $X$ . The T-structure of a  $\pi$ -complex is formed with  $X$  being "bound" to the bond critical point  $r_b(A=A)$  (Fig. 30c).



The analysis of  $\rho(\mathbf{r})$  of a potential three-membered ring immediately reveals whether the structure is closer to a ring or a  $\pi$ -complex [38]. This is of importance in discussions of strain since it helps to avoid severe misinterpretations: It makes no sense to discuss the "strain" of a  $\pi$ -complex or a ring with large  $\pi$ -complex character (see, e.g., protonated oxirane [40]). For example, concave bending is indicative of inter-path angles considerably lower than ideal bond angles. Strain energies derived from these angles, e.g. with the aid of Hooke's law are extremely large, larger than bond dissociation energies. However, these strain energies are derived under the assumption that fully developed bonds are bent, an assumption that is not fulfilled for concave bent bonds, that are partial bonds with a bond order  $n < 1$ . *The concept of strain does not apply to partial bonds or any nonclassical bond. Therefore, it is useless to discuss the strain of three-membered rings with concave bonds and partial  $\pi$ -complex character [40].*

### 6.3 Pitzer Strain and Dunitz-Schomaker Strain

Bond eclipsing leads to changes in geometry, energy, and other molecular properties. It is also reflected by changes in  $\rho(\mathbf{r})$ , e.g.,  $\rho_b$  is increased in the eclipsed bonds contrary to expectations based on an electrostatic model of interacting bond electron pairs [39]. The increase in  $\rho_b$ , however, is a secondary effect caused by a) a significant lengthening of the bond that connects the eclipsed bonds and b) a concomitant small shortening of the latter bonds. Because of this, it is difficult to unearth the actual effect of bond eclipsing on  $\rho(\mathbf{r})$  and to distinguish between the cause and the effect.

A way to show the impact of bond eclipsing on  $\rho(\mathbf{r})$  is to compare the charge distributions in hydrogen fluoride, HF, and methyl fluoride,  $\text{CH}_3\text{F}$  [39]. In HF, the nonbonded electron pairs at F are arranged in form of a torus of negative charge. If H is replaced by  $\text{CH}_3$ , accumulation of electron density in the CH bonds will cause a change of the potential (V), kinetic (G), and total energy (H) densities in both the CF bonding region and the valence sphere of F. Off-nucleus positions that are staggered to the CH bonds possess lower  $V(\mathbf{r})$  and, hence,  $H(\mathbf{r})$  values than those that are eclipsed (Fig. 31 a). Correspondingly, higher  $\rho$ -values are found at points with lower  $H(\mathbf{r})$  values. This is illustrated by the difference density plot of the lone pair region at the F atom of  $\text{CH}_3\text{F}$  (Fig. 31 b). The preference for staggering of nonbonded charge distributions is obvious and holds also for the Laplace concentration (Fig. 31 c). From this and other observations it has been concluded that *bonded and nonbonded charge concentrations try to avoid each other (principle of avoidance of charge concentrations [39])*. If the molecular geometry forces vicinal charge concentrations to be eclipsed, Pitzer strain will result.

Avoidance of charge concentrations is also apparent in the distribution  $-\nabla^2 \rho(\mathbf{r})$  of cyclobutane [41]. Dunitz and Schomaker [120], pointed out as early as 1952 that repulsive 1,3-interactions between the C atoms in cyclobutane are responsible for a considerable part of its strain. Destabilizing 1,3 interactions lead to a depletion of electron density inside the cyclobutane ring. This can be visualized by plotting a contourline diagram of the Laplace concentration in the plane of the carbon

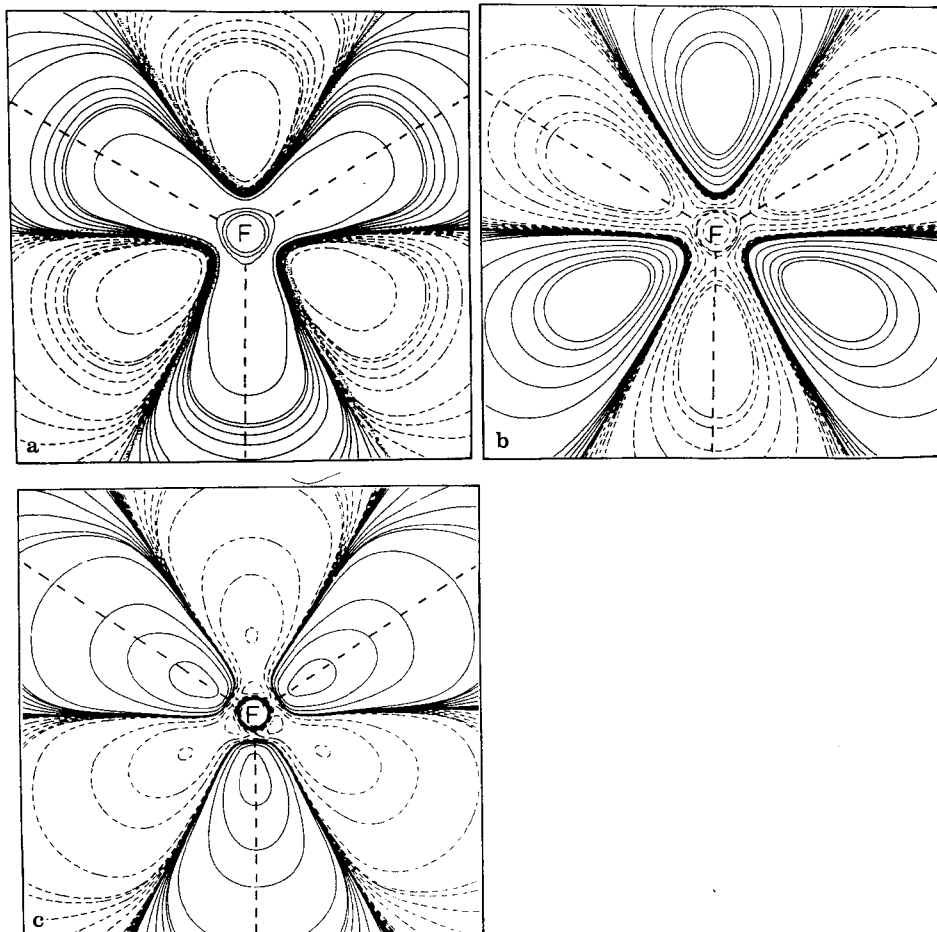


**Fig. 31 a-c.** Concentration of electron density in the lone pair regions of F in  $\text{CH}_3\text{F}$ . Contour-line diagrams have been drawn with regard to the plane that contains the F nucleus and is perpendicular to the CF bond axis. Positions of the methyl CH bonds are given by (*heavy dashed lines*). **a**  $H(\mathbf{r})$ . **b**  $q(\mathbf{r})$ . **c**  $\nabla^2 q(\mathbf{r})$ . In order to amplify effects, difference maps are used, i.e.  $H(\mathbf{r})$ ,  $q(\mathbf{r})$ , and  $\nabla^2 q(\mathbf{r})$  are plotted with regard to  $\text{CH}_3\text{F}$  with the methyl group rotated by  $60^\circ$  as reference. *Dashed lines* indicate areas with larger stabilizing energy density (lower electron density, larger concentration) and *solid lines* areas with lower stabilizing energy density (larger electron density, smaller charge concentration). (HF/6-31G(d) calculations [39]). Reprinted with Permission from J. Am. Chem Soc., 107 (1985) 3811. Copyright (1985) American Chemical Society.

nuclei of planar cyclobutane (Fig. 32). Contrary to cyclopropane (compare with the contourline diagram in Fig. 29a) negative charge is depleted in the center of the ring. Repulsive 1,3 interactions between the C atoms seem to impede surface delocalization of electrons in cyclobutane.

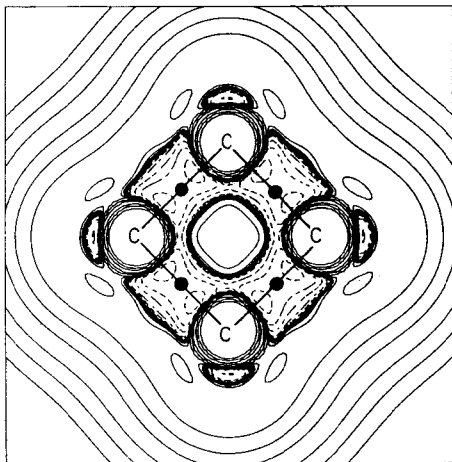


**Fig. 32.** Molecular graph and contour-line diagram of the Laplace concentration of cyclobutane. Bond paths are indicated by *heavy lines* and bond critical points by *dots*. *Dashed lines* are in regions where electronic charge is concentrated ( $\nabla^2 \rho(\mathbf{r}) < 0$ ) and *solid lines* in regions where charge is depleted ( $\nabla^2 \rho(\mathbf{r}) > 0$ ). Inner shell regions with  $\nabla^2 \rho(\mathbf{r}) < 0$  are not shown. (HF/6-31G(d) calculations)

## 6.4 Energetic Consequences of Strain

A dissection of strain into the various contributions provides a basis for the calculation of the strain energy. For this purpose, one has to define a set of suitable reference compounds and to use their properties to define a strain-free molecular state. Cremer and Gauss [41] have carried out such an analysis for cyclopropane and cyclobutane. They proceeded in the following way.

1. Stretching strain energies were estimated from Hooke's law and known  $k(\text{CC})$  and  $k(\text{CH})$  force constants.
2. Baeyer strain energies were determined with the aid of Hooke's law *utilizing calculated interpath angles  $\beta$  rather than physically meaningless geometrical angles  $\alpha$* . In addition, a CCC bending force constant was derived that does not contain effects arising from 1,3 CC repulsion.
3. Pitzer strain energies were evaluated directly from ab initio calculations using ethane as an appropriate reference compound.
4. The Dunitz-Schomaker strain energy for cyclobutane was taken from appropriately scaled CNDO/2 energies obtained for model calculations with and without C,C-nonbonded repulsion [21].
5. Stabilization effects due to strengthening of the external bonds were directly evaluated. For this purpose  $\rho(\mathbf{r})$  was integrated over the interatomic (zero-flux) surface  $S(\text{CH})$  and the resulting integral was related to the bond energy.

Strain energies obtained in this way are listed in Table 6. For cyclobutane, they add up to the conventional strain energy of  $27 \text{ kcal mol}^{-1}$  determined from thermochemical data [110]. In the case of cyclopropane, however, there is a discrepancy of  $16.4 \text{ kcal mol}^{-1}$  between the theoretical value ( $44.4 \text{ kcal mol}^{-1}$ , Table 6) and the conventional strain energy ( $28 \text{ kcal mol}^{-1}$  [110]). This energy difference has to be attributed to the stabilizing effects of surface delocalization of  $\sigma$ -electrons [38, 40–42]. Hence, *the energetic consequences of surface delocalization are responsible for the*

**Table 6.** Ab initio strain energies and stabilization energies of cyclopropane and cyclobutane<sup>a</sup>

Strain	Strain Energy [kcal mol <sup>-1</sup> ]	
	Cyclopropane	Cyclobutane
Destabilization Energies		
Stretching	0.5	1.0
Baeyer <sup>b</sup>	46.3	13.0
Pitzer	4.0	3.9
Dunitz-Schomaker	0	12.0
Total	50.8	29.9
Stabilization Energies		
CH Strengthening	6.4	2.8
$\sigma$ -Delocalization	x = 16.4	0
Conventional strain energy	28.0 = 44.4 + x	27.1

<sup>a</sup> From Ref. [41].

<sup>b</sup> Baeyer strain energy of cyclopropane calculated with Hooke's law (41.3 kcal mol<sup>-1</sup> [41]) plus energy increase from anharmonicity effects calculated from a bending function with and without a cubic term for an interpath angle  $\beta = 79^\circ$  (5 kcal mol<sup>-1</sup>). Note that the strain energy of propane has been set erroneously to 5.1 kcal mol<sup>-1</sup> in Ref. 41 (Table IX). This energy, however, is compensated by the increase in the CC bond energy relative to that of ethane (Table V, Ref. 41).

*puzzling similarity of the strain energies of cyclopropane and cyclobutane. In addition, they explain the existence of homoaromatic compounds as well as the relatively large stability of bicyclic molecules such as norcaradiene or bisnorcaradiene.*

## 7 $\sigma$ -Conjugation — Modes of $\sigma$ -Electron Delocalization

### 7.1 $\sigma$ -Conjugation

Over the last three decades various authors, in particular Dewar, have repeatedly pointed out the possibility and chemical consequences of  $\sigma$ -conjugative interactions [122, 123]. The concept of  $\sigma$ -conjugation is based on the fact that resonance integrals between different AOs of a given atom will not vanish even if the AOs are orthogonal. This applies also to the resonance integrals between geminal  $sp^n$  hybrid orbitals of a C atom, which are considerably larger than that between adjacent  $2p\pi$  AOs in the case of conjugated double bonds. Hence interactions between  $\sigma$ -bonds should be at least as strong as interactions between  $\pi$ -bonds.

Utilizing the concept of  $\sigma$ -conjugation Dewar was able to rationalize a number of apparent anomalies in organic chemistry that are difficult to explain in other ways [122]. These examples included, among others, the astonishing stability of three-membered rings, the pyramidal conformation of radicals and biradicals, bond staggering in saturated molecules, the gauche and anomeric effects, and the geometry of triplet carbene.

*There always is  $\sigma$ -conjugation in a molecule with three or more atoms.* Conjugative effects between adjacent  $\sigma$ -bonds are approximately constant in most cases and, therefore, they can be absorbed in the empirical values of appropriate reference compounds used within the concept of localized bonds.  $\sigma$ -Conjugation should influence the distribution  $\rho(\mathbf{r})$  in a molecule. For example, it has been found for many unstrained molecules in their equilibrium geometry that the bond paths do not coincide with the internuclear connection lines. They are slightly curved toward each other ( $\beta < \alpha$ ,  $|\beta - \alpha| < 1^\circ$ ) despite the fact that coulombic repulsion between the electron bond pairs should cause outwardly curved bent bonds. Bending of normal  $\sigma$ -bonds may be indicative of  $\sigma$ -conjugation. Also the Laplace concentration in the valence shell of an atom that is bonded to at least two neighboring atoms should reflect the degree of  $\sigma$ -conjugation. Probably, valence shell holes between concentration lumps in the direction of the bond paths and the geometrical arrangement of concentration lumps and holes depend on the extent of  $\sigma$ -conjugation.

From a practical point of view, however, a description of  $\sigma$ -conjugative effects in terms of the properties of  $\rho(\mathbf{r})$  is an enterprise without any basis. Since all molecules with three or more atoms always should benefit from  $\sigma$ -conjugation, it is impossible to assess the degree of  $\sigma$ -conjugation by comparison with a suitable reference molecule that does not possess  $\sigma$ -conjugation. A description of  $\sigma$ -conjugation will only be possible in those cases where  $\sigma$ -conjugation causes changes in the molecular properties that are no longer expected on the basis of normal  $\sigma$ -conjugative effects. The latter are absorbed in descriptions based on the localized bond model. If the localized bond model fails to describe the properties of a molecule, it will be reasonable to expect exceptional  $\sigma$ -conjugative effects. Such a case is encountered for three-membered rings [42]. But before discussing these effects it will be useful to describe orbitals and modes of  $\sigma$ -electron delocalization in cyclic systems.

## 7.2 Ribbon, Surface, and Volume Delocalization of $\sigma$ -Electrons

While for acyclic molecules it is not difficult to distinguish between  $\sigma$  and  $\pi$ -MOs, this may become problematic for cyclic compounds. Therefore, definitions have been introduced [41], which help to classify orbitals in cyclic systems and which allow a distinction between various modes of electron delocalization. In the following these rules are summarized for cycloalkanes, but a generalization to other N-membered rings is straightforward.

1. If a cycloalkane is considered to be made up of  $\text{CH}_2$  entities each possessing two singly occupied orbitals, two sets of orbitals can be distinguished: a) the  $r$ -set that consists of radially (toward the ring center) oriented  $sp^2$  hybrid orbitals and b) the  $t$ -set that consists of tangentially (with regard to the ring perimeter) oriented  $p$ -orbitals.

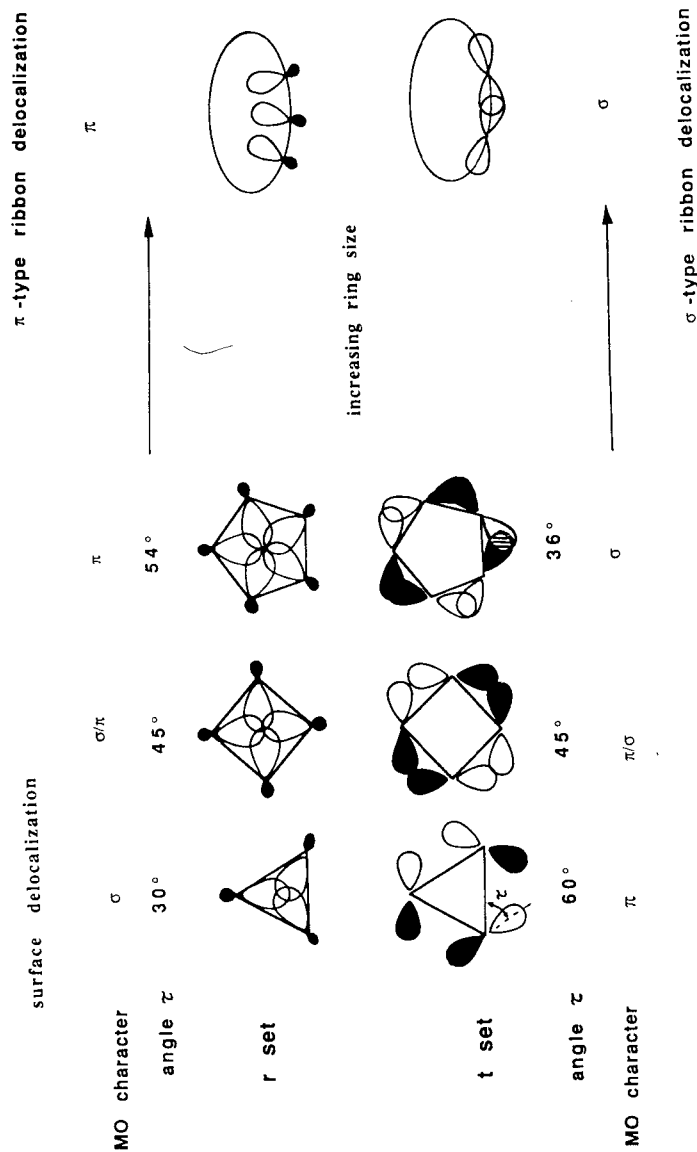


Fig. 33. Characterization of ring orbitals ( $\sigma$  or  $\pi$ ) with the aid of the angle  $\tau$



occupied by  $4q + 2$  electrons while ring MOs with dominant  $t$ -character (for odd  $N$ ) are occupied by  $4q$  electrons. In this way Hückel- or Möbius-aromatic subshells are formed. This is shown for cyclopropane and cyclobutane in Fig. 34.

2. If  $r$ -( $t$ -)orbitals enclose angles  $90^\circ \geq \tau > 45^\circ$  with the internuclear connection lines of a ring (see Fig. 33), then the orbitals will be classified as  $\pi$ -orbitals. For  $45^\circ > \tau \geq 0^\circ$ , they are classified as  $\sigma$ -orbitals. Accordingly, the  $r$ -orbitals are  $\sigma$ -MOs for  $N = 3$  while they are  $\pi$ -MOs for  $N > 4$ . For large  $N$ , the  $r\pi$ -MOs are topologically equivalent to the  $p\pi$ -MOs of a  $\pi$ -conjugated system such as a cyclopolyene (see Fig. 33).

The  $t$  orbitals correspond to  $\pi$ -MOs for  $N = 3$ . This is in line with the well-known  $\pi$ -character of the ring bonds of three-membered rings such as cyclopropane (see Section 5.1). For  $N > 4$  the  $t$ -orbitals form  $\sigma$ -MOs (Fig. 33). These definitions collapse in the case of the four-membered ring because both  $r$ - and  $t$ -orbitals enclose angles of  $45^\circ$  with the interatomic connection lines (Fig. 33).

3. Electrons occupying  $r$ -type orbitals can delocalize in the surface of the ring for small  $N$  or along the chain (ribbon) of ring atoms if  $N$  is large (Fig. 33). It is reasonable to distinguish between *surface delocalization* and *ribbon delocalization* of electrons [38, 42]. Electrons occupying  $t$ -type orbitals for  $N = 3$  delocalize on a circle enveloping the three-membered ring. For large  $N$ , they delocalize along the ribbon of atoms.

If  $N$  is small, overlap will be better for  $r$ -orbitals than  $t$ -orbitals while the reverse will be true for large  $N$  (see Fig. 33). This suggests that *surface delocalization of electrons can only be found for small rings*.

4. For a cage compound of the type  $(\text{CH})_N$  ( $N = 4$ : tetrahedrane),  $r$ -orbitals are oriented toward the center of the cage. At each C atom there are two tangentially oriented, mutually orthogonal  $p$ -orbitals. Both  $r$ - and  $t$ -orbitals can be classified using the rules given for monocyclic systems. For example, the  $r$ -MOs ( $t$ -MOs) of tetrahedrane correspond to  $\sigma$ -MOs ( $\pi$ -MOs) [42].

The actual cage MOs are formed as linear combinations of  $r$ - and  $t$ -orbitals. Cage MOs with dominant  $r$ -( $t$ -)character are occupied in such a way that "aromatic" subshells are formed similar as in the case of cycloalkanes. Electrons occupying MOs with dominant  $r$ -character can delocalize inside the cage provided  $N$  is small and there is strong overlap between the  $r$ -orbitals. In this case we speak of *volume delocalization of electrons* [41, 42].

One has to distinguish between three different modes of electron delocalization, namely

- i) ribbon delocalization of either  $\sigma$ - or  $\pi$ -electrons,
- ii) surface delocalization of  $\sigma$ -electrons or
- iii) volume delocalization of  $\sigma$ -electrons.

The three modes of  $\sigma$ -electron delocalization are shown in Fig. 35. The extent of surface delocalization depends on the overlap of the  $r$ -orbitals, i.e. it depends on the topology and the geometry of the ring. Inspection of the overlap in cycloalkanes reveals that significant effects resulting from surface delocalization can only be expected for three-membered rings [40, 41]. *Due to their topology, three-mem-*



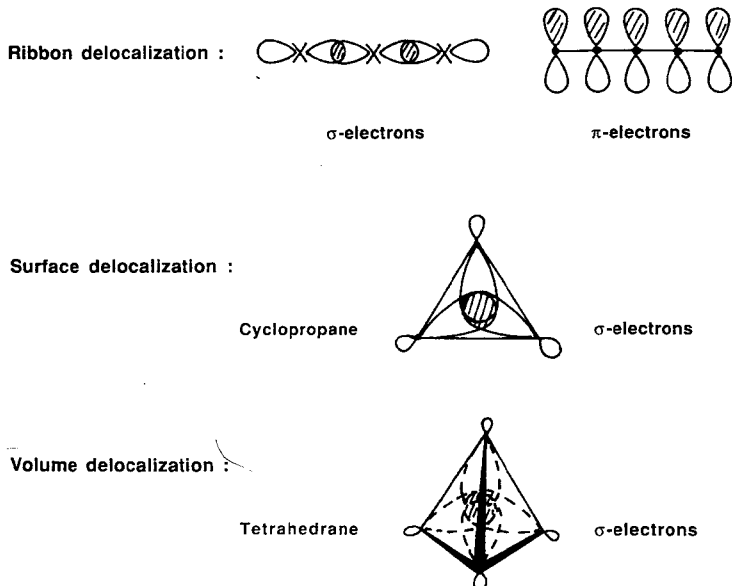


Fig. 35. Possible modes of electron delocalization

*bered rings are exceptional since they possess  $\sigma$ -electrons delocalized over the ring surface and  $\pi$ -electrons delocalized in peripheral bent bonds.*

Similar considerations apply to volume delocalization. If a cage consisting of three-membered rings is formed (e.g. tetrahedrane), *volume delocalization* of  $\sigma$ -electrons will be possible [41, 124].

### 7.3 Surface Delocalization and Bonding in Cyclopropane

There have been a number of clues indicating that the properties of cyclopropane are exceptional. Dewar [122] was the first to list these clues and to discuss them in view of  $\sigma$ -electron delocalization, which may cause or, at least, may influence the properties of cyclopropane. Later Cremer and co-workers [38–42] reinvestigated cyclopropane utilizing *ab initio* methods and the topological analysis of  $\rho(\mathbf{r})$ . According to these investigations, cyclopropane differs from other cycloalkanes by

1. its relatively low strain energy (SE) that is almost identical to that of cyclobutane (28 and 27 kcal mol<sup>-1</sup>, respectively),
2. its relatively high electron density in the center of the ring,
3. its relatively short CC distances,
4. its relatively high CC bond strength,
5. the upfield shifts of its proton and <sup>13</sup>C NMR signals,
6. its electronic interactions with substituents,
7. its ability to enhance conjugation in homoaromatic systems.

As was already pointed out above the relatively small strain energy of cyclopropane is a result of destabilizing Baeyer strain ( $46 \text{ kcal mol}^{-1}$ ) and stabilizing surface delocalization of  $\sigma$ -electrons ( $16 \text{ kcal mol}^{-1}$ ). Surface delocalization has to do with the existence of a doubly occupied low-lying *surface orbital* ( $a_{1g}$  in Fig. 34) that stems from the in-phase overlap of all  $r$ -orbitals inside the ring. Since overlap decreases exponentially with the size of the ring, the nature of the surface orbital changes dramatically when going to larger rings. Already for cyclobutane it does no longer bring sufficient electron density into the center of the ring. Also, the two 1,3 antibonding  $e_u$  orbitals (Fig. 34) that are responsible for Dunitz-Schomaker strain reduce the electron density in the center of the ring, thereby yielding the observed depletion of the Laplace concentration (Fig. 32).

For larger rings the surface orbital changes to a ribbon orbital which allows  $\sigma$ -electrons to delocalize along the ring framework. Occupation of the surface orbital in cyclopropane leads to the relatively high electron density inside the ring, is responsible for the observed CC bond properties, and may also cause the magnetic properties of cyclopropane. As discussed in Sect. 5, the interaction between substituents and cyclopropane as well as the special role of the three-membered ring in homoaromatic compounds can be understood in terms of surface delocalization of  $\sigma$ -electrons.

Surface delocalization of  $\sigma$ -electrons in cyclopropane is nicely reflected by the Laplace concentration of the electrons in the plane of the cyclopropane ring. In Fig. 36 a perspective drawing of the theoretically determined Laplace concentration is shown [38, 41]. The corresponding contourline diagram is given in Fig. 29a. Electrons are concentrated (dashed contourlines in Fig. 29a) along the CC bond

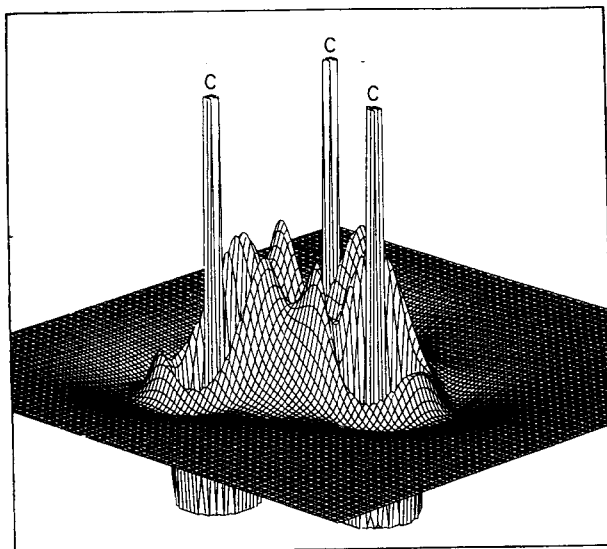


**Fig. 36.** Perspective drawing of the Laplace concentration  $-\nabla^2 \rho(\mathbf{r})$  of cyclopropane shown in the ring plane. Inner shell concentrations are indicated by the atomic symbol C. Laplace values above and below a threshold are cut off. (HF/6-31G(d) calculations)

paths (heavy solid lines in Fig. 29a) as well as inside the ring. For other cycloalkanes such as cyclobutane there is depletion rather than concentration of negative charge inside the ring (Fig. 32).

Various other authors have made similar observations when investigating the electron density distribution of cyclopropane. Coulson and Mofitt [125] were the first to note that there is a plateau of relatively high negative charge inside the  $C_3$  ring. In a more recent investigation, Schwarz and co-workers [73] found that the total electron density is increased by  $0.16 \text{ e } \text{Å}^{-3}$  in the center of cyclopropane as compared to the electron density of the promolecule formed by three spherical isolated carbon atoms. Delocalization of  $\sigma$ -electrons occupying the surface orbital leads to a strong reduction of their kinetic energy which in turn triggers enhanced AO contraction at the C atoms. This restores the virial relation, lowers the total energy, and leads to CC bond shortening [73]. Hence,  $\sigma$ -electron delocalization directly influences the length of the ring bonds.

Ahlrichs and Ehrhardt [126] have calculated shared electron numbers for alkenes. While bonding is reflected in these compounds by two-center contributions and negligible contributions from three- and four-center terms, a CCC shared electron number of 0.3 is calculated for cyclopropane, that is indicative of three-center bonding.

Putting all facts together, the following conclusions can be drawn. Bonding in cyclopropane is exceptional since the C atoms are linked by (see Fig. 37)

1. a central 2-electron 3-center bond ("super- $\sigma$  bond") and
2. two peripheral 4-electron 3-center bonds (" $\pi$ -bonds").

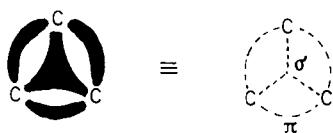


Fig. 37. Nonclassical 2-electron 3-center bond and 4-electron 3-center bonds in cyclopropane

The classical structure of cyclopropane is misleading. It does not reflect the high degree of  $\sigma$ -electron delocalization which influences stability, geometry, magnetic properties, etc. of cyclopropane.

#### 7.4 Pros and Cons of $\sigma$ -Aromaticity

Dewar has drawn an analogy between the  $=HC-CH=$  groups of a conjugated (cyclo)polyene and the  $-CH_2-$  groups of a cycloalkane [122]. He has argued that cyclopropane and benzene are isoconjugate; the latter possesses a system of six delocalized  $\pi$ -electrons, the former a system of six delocalized  $\sigma$ -electrons. Therefore, cyclopropane should be considered to be  $\sigma$ -aromatic and its properties should be seen to result or at least to be influenced by  $\sigma$ -aromaticity.

There is no question that the peculiar properties of cyclopropane in particular and three-membered rings in general are coupled with the unusual bond features encoun-

tered in these molecules. The question is only whether such a situation should be described with a term (aromaticity) that is heavily loaded with what has been found for cyclopolyenes with  $4q + 2\pi$ -electrons. Aromaticity is expected for those systems that can only be represented in form of two or more resonance structures [90–92]. For example, the electronic structure of benzene has to be described as a resonance hybrid of two classical cyclohexatriene structures. It is impossible to anticipate  $\pi$ -delocalization and  $\pi$ -aromaticity of benzene by just looking at one cyclohexatriene structure. It seems that there is a considerable difference between benzene and cyclopropane in so far as the latter molecule is normally represented by just one classical structure. However, does this structure provide a realistic image of bonding and electron delocalization in cyclopropane?

We have already discussed in Sect. 6 that there is a close electronic relationship between three-membered rings and  $\pi$ -complexes. According to this relationship, cyclopropane can be written as a resonance hybrid of three equivalent methylene, ethylene  $\pi$ -complexes as shown in Fig. 38 [118]. Of course, a methylene, ethylene  $\pi$ -complex does not exist but the same is also true for cyclohexatriene. One might argue that resonance structures used to describe  $\pi$ -aromatic compounds are all “classical” in the sense that they possess just single and double bonds. However, this argument can easily be refuted. Cremer and Kraka have demonstrated that the bond

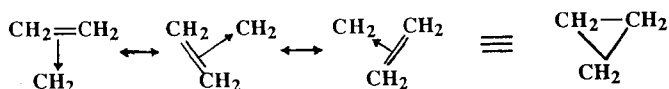


Fig. 38. “Resonance structures” of cyclopropane and shorthand notation

paths, i.e. the paths of maximum electron density between bonded atoms, nicely describe the bonds of three-membered rings and  $\pi$ -complexes [38]. For  $\pi$ -complexes a bond path is found where chemists draw the arrow between basal group, e.g. ethylene, and the apical group, e.g. a halogen cation. Hence, the  $\pi$ -complex notation is as realistic as any other representation of molecular structure and, accordingly, it can be placed at the same level with the “classical” structures.

Actually, the  $\pi$ -complex description of cyclopropane is better suited to reflect its properties than the notation normally used in chemistry. It indicates

1. that there are different types of CC bonds in cyclopropane,
2. the  $\pi$ -character of the CC bonds,
3. the possibility of resonance stabilization,
4. a possible shortening of the CC bonds,
5. increased s-character in the CH bonds and a corresponding CH bond strengthening, etc.

In conclusion, one can consider cyclopropane in the same way as a resonance hybrid as this is done for benzene. In this respect, the classical structure of cyclopropane is the shorthand notation for the three equivalent resonance structures shown in Fig. 38.

The discussion clearly shows that a rejection of the term  $\sigma$ -aromaticity on the

grounds that it is inconsistent with common understanding of the term aromaticity is not justified. Even if the usual criteria for  $\pi$ -aromaticity [90–92], namely (see Sect. 4.2)

1.  $4q + 2$   $\pi$ -electrons (Hückel rule),
2. the Dewar resonance energy,
3. partial or complete bond equalization, and
4. diatropicity of the NMR signals,

are applied, the term  $\sigma$ -aromaticity cannot be discarded.

1. There are six delocalized  $\sigma$ -electrons that form the ring bonds of cyclopropane. Two of them establish a Hückel-aromatic, the remaining four a Möbius-aromatic system (Fig. 34). In whatever way the electron count is carried out, an aromatic ensemble of electrons is obtained.
2. Calculation of the Dewar resonance energy implies a comparison with a suitable acyclic reference compound that contains the same number of CC  $\sigma$ -bonds. In addition, it requires the separation of energetic effects resulting from ring strain on the one hand and  $\sigma$ -aromaticity on the other hand. This has been done for cyclopropane and a delocalization energy of  $16 \text{ kcal mol}^{-1}$  has been obtained [41].
3. The CC bonds in cyclopropane are all equivalent. In addition, they are considerably shorter ( $0.03\text{--}0.05 \text{ \AA}$ ) than those of other (cyclo)alkanes.
4. Due to the high  $s$  character of the CH bonds, one would expect the  $^1\text{H}$ -NMR signal for cyclopropane to appear downfield from the signals of the  $\text{CH}_2$  protons of alkanes. However, it appears upfield by 1 ppm ( $\delta = 0.22 \text{ ppm}$ ) [127]. Also, the  $^{13}\text{C}$ -NMR signal is shifted by 20 ppm upfield from other aliphatic  $^{13}\text{C}$ -NMR signals [128]. It was found that the isotropic shift of  $-3.8 \text{ ppm}$  from  $\text{Me}_4\text{Si}$  is the consequence of that component of the chemical shift tensor for  $\text{CH}_2$  that is perpendicular to the ring plane. The value of this component ( $-36 \text{ ppm}$  from  $\text{Me}_4\text{Si}$ ) is indicative of strong circulation of electrons in the ring plane [128]. Both the  $^1\text{H}$ - and the  $^{13}\text{C}$ -NMR shifts of cyclopropane suggest  $\sigma$ -electron delocalization in the ring.

Looking at points 1 through 4 in one context, it seems to be appropriate to consider cyclopropane as being  $\sigma$ -aromatic. Accepting  $\sigma$ -aromaticity all properties of cyclopropane are easily rationalized while the rejection of this concept entails the unpleasant task of looking for additional explanations. Certainly, this is reason to lean on an acceptance of the notion of  $\sigma$ -aromaticity. Also, the concept of  $\sigma$ -aromaticity helps to rationalize the properties of substituted cyclopropanes [39], those of the Si, Ge, etc. analogues of cyclopropane [41, 44], and of homoaromatic compounds [34, 38].

## 8 Chemical Reactivity

To make predictions on the chemical reactivity of a molecule knowledge of its labile bonds and the sites prone to electrophilic or nucleophilic attack is needed. This information can be extracted from the density distribution  $\rho(\mathbf{r})$  of the molecule.

### 8.1 Chemical Reactivity as Reflected by Properties of $q(\mathbf{r})$

A labile bond is mostly indicated by a low bond order. Also, the shape of the bond path reveals whether a bond can easily be broken or not. A suitable example to demonstrate this is the differing behavior of oxiranes in basic, neutral or acidic media. The addition of nucleophiles to oxiranes to yield 1,2-disubstituted products, which is widely used in synthesis [129], is known to be considerably accelerated in acidic solutions. For an unsymmetrically substituted oxirane the nucleophilic attack

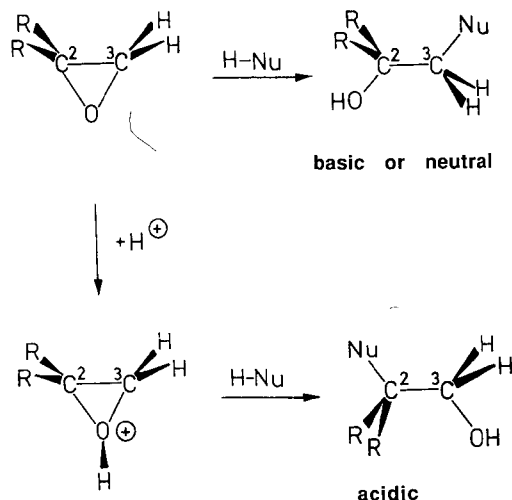


Fig. 39. Nucleophilic ring opening of an epoxide in basic, neutral or acidic solvents

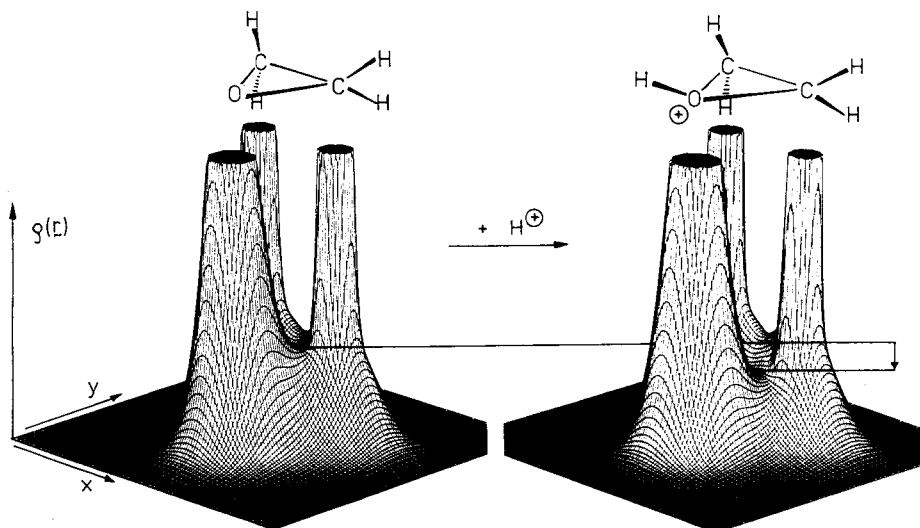


Fig. 40. Perspective drawing of the electron density distribution  $q(\mathbf{r})$  of oxirane and protonated oxirane shown with respect to the ring plane. The value of  $q(\mathbf{r})$  is cut off above a predetermined value to improve the representation. The weakening of the CO bonds upon protonation is indicated. (HF/6-31G(d) calculations)

occurs predominantly at the sterically less hindered C atom in neutral or basic media while in acid solution surprisingly the higher substituted C atom of oxirane is attacked (compare with Fig. 39). Since ring opening is always accompanied by a Walden inversion, a  $S_N1$  mechanism can be ruled out in acidic media [129].

In Fig. 40, the effect of protonation (or complexation with a Lewis acid) at the O atom of oxirane is shown with the aid of perspective drawings of  $\varrho(\mathbf{r})$  obtained for the plane of the three heavy atoms. There is a dramatic decrease of the electron density in the CO bond regions upon protonation. The corresponding bond orders decrease from 1.0 to 0.77 and the bond paths bend inside the ring, indicating that protonated oxirane attains partial  $\pi$ -complex-character (compare with Fig. 29c) [38]. All these observations suggest an acceleration of CO bond rupture in acidic media in line with experimental observations.

The preference of an attack on the sterically more hindered C atom of protonated oxirane seems to depend on three effects [38].

1. By increasing the  $\pi$ -complex character of the three-membered ring the alkyl groups bend backwards toward the CC axis to adopt the position they take in normal  $\pi$ -complexes. In this way, sterical shielding of C2 is reduced.
2. According to calculated bond orders for substituted protonated oxiranes [38] the bond C2O is more facile to bond rupture than the bond C3O.
3. The concentration holes in the valence sphere of C2 (see Fig. 41) are more prone to nucleophilic attack than those at C3.

Hence, the regioselectivity of the reaction can be elucidated from the electron density distribution  $\varrho(\mathbf{r})$  of oxirane and protonated oxirane without the need to speculate on the charge distribution in the transition state of the reaction.

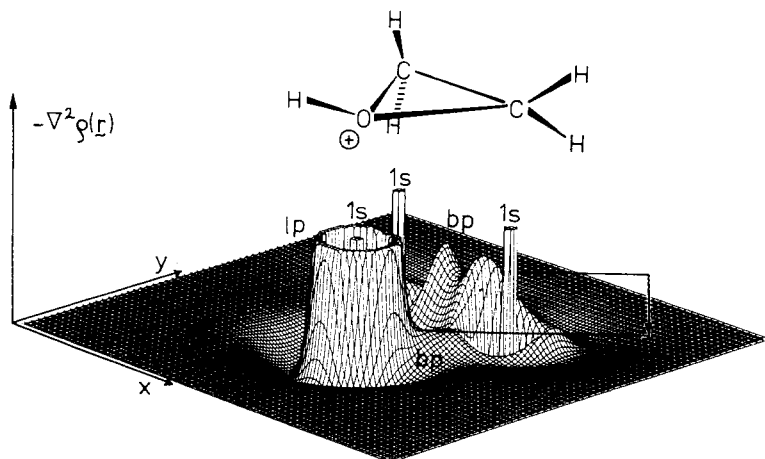


**Fig. 41.** Perspective drawing of the Laplace concentration  $-\nabla^2\varrho(\mathbf{r})$  of protonated oxirane in the plane of the ring. Inner shell (1s), bond (bp), and lone pair (lp) concentrations and the difference of the CC and CO bond concentrations are indicated. Laplace values above and below a threshold are cut off. (HF/6-31G(d) calculations)

## 8.2 The Structure Diagram

Reactions as the one discussed in Sect. 8.1 can be seen in a broader context if the structure diagram of the compound in question is analyzed (see Sect. 2.5). The structure diagram of a given system embeds all information concerning possible structures and their possible changes. To discuss structural changes of a molecule such as oxirane a control space  $W$  has to be defined, which is of the same dimension as the configuration space  $C$  of the corresponding system ( $W \subset C$ ). For example, if just changes of the heavy atom bonds in oxirane are considered,  $W$  will be a three-dimensional control space spanned by the control parameters  $u$ ,  $v$ ,  $w$ , and applies to any system of the general form  $A_2X$ .

In Fig. 42a the structure diagram of  $A_2X$  is shown in the plane spanned by the parameters  $u$ ,  $v$  located at a constant value of  $w$ . Control parameters  $u$  and  $v$  are chosen to describe the two independent coordinates of  $X$ . For each pair of  $(u, v)$  the third degree of freedom of  $A_2X$  is considered to be optimized. In this way,  $v$

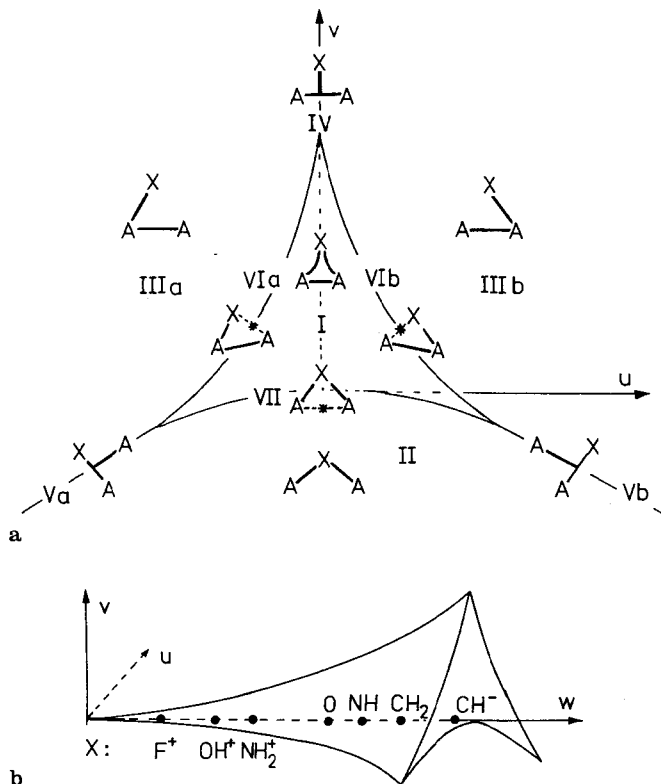



Fig. 42. Structure diagram of system  $A_2X$  shown in  $(u, v, w)$  space. **a** Control parameter  $w = \text{constant}$ . For each of the structural regions I–VII a molecular graph is given. Asterisks denote catastrophe points. **b** Three-dimensional display of the bifurcation set of the elliptic umbilic in  $(u, v, w)$  space for  $w \geq 0$ . The meaning of  $w$  as chemical control parameter is illustrated by giving the approximate positions of three-membered rings  $C_2H_4X$  on the positive  $w$  axis. Reprinted with Permission from J. Am. Chem. Soc., 107 (1985) 3800. Copyright (1985) American Chemical Society



Table 7. Description of structural regions of the  $A_2X$  structure diagram

Structural region	I	II	IIIa, IIIb	IV	Va, Vb	VIa, VIb	VII
Number of critical points of $q(\mathbf{r})^a$							
(3, -3) [atoms]	3	3	3	3	3	3	3
(3, -1) [bonds]	3	2	2	2	2	2	2
(3, +1) [rings]	1	0	0	0	0	0	0
(2,0) <sup>b</sup> [dissolved bonds]	0	0	0	0	0	0	0
Form of molecular graph	3MR <sup>c</sup> 	$C_{2v}$ chain	$C_1$ chain	$C_{2v}$ T-form	$C_5$ T-form	change from $C_1$ chain	3MR <sup>c</sup> to $C_{2v}$ chain
Structure of $A_2X$	$A-A$	$A-X-A$	$A-A-X$	$(A_2)-X$	$(AX)-A$	$C_1$ chain	$C_{2v}$ chain
Catastrophe	none	none	none	conflict	conflict	bifurcation	bifurcation

<sup>a</sup> Associated chemical unit is given in brackets.

<sup>b</sup> Singularity of  $q(\mathbf{r})$ .

<sup>c</sup> Three-membered ring.

represents the reaction path of a  $C_{2v}$  approach of X toward  $A_2$  (decreasing  $v$ ,  $a_1$  symmetrical displacement of X) while  $u$  describes  $b_2$  symmetrical displacements of X from this reaction path.

The topologically stable molecular graphs of  $A_2X$  belong to one of the structural regions I, II or III. The boundaries of these stable regions are formed by a set of all catastrophe points corresponding mathematically to the unfolding [130] of the elliptic umbilic catastrophe. Regions IV, and Va, b denote the positions of all conflict catastrophes, regions VIa, b and VII the position of all bifurcation catastrophes (compare with the isomerization mechanism described in Sect. 2.5). In Table 7a complete description of the structural region of the  $A_2X$  system, including molecular graphs (I–III) as well as catastrophe graphs (V–VII) is summarized. Transitions from I to II or III correspond to ring opening processes, and approach of X toward  $A_2$  along  $v$  results in the formation of a three-membered ring via a  $\pi$ -complex.

Similar structure diagrams are obtained for oxirane and protonated oxirane. For the latter, the area of the hypocycloid-shaped region I is smaller which is reflected by a decrease in the control parameter  $w$ . Hence, by the value of  $w$  the degree of  $\pi$ -complex character and an assessment of the stability of the three-membered rings can be made. Cremer and Kraka [38] have used  $w$  as a chemical control parameter reflecting the electronic nature of both A and X. The larger the electronegativity difference between A and X (for A, X not equal H), the smaller becomes the parameter  $w$ . On this basis, various combinations of A (carbon) and X have been placed at positive  $w$  values of the control space as is illustrated in Fig. 42b. The most labile three-membered rings with high  $\pi$ -complex character adopt small  $w$ -values (e.g.  $X = F^+$ ), a stable three-membered ring such as cyclopropane ( $X = CH_2$ ) a large  $w$  value. All catastrophe points leading to acyclic structures form the elliptic umbilic [78].

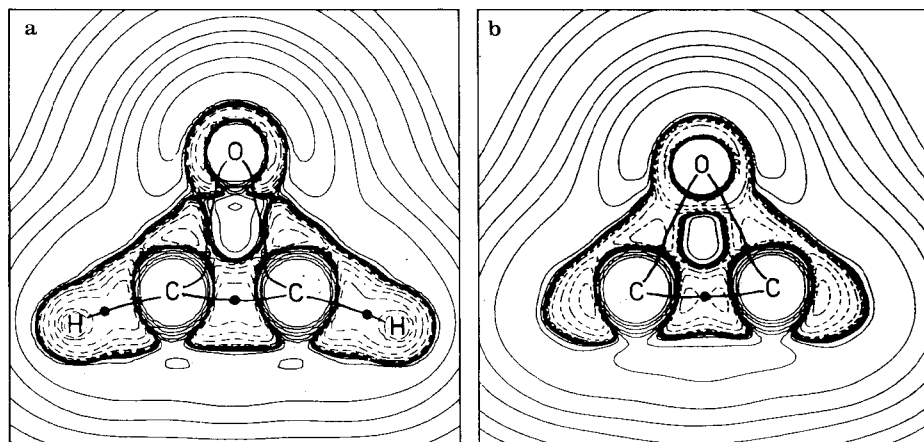


Fig. 43a, b. Molecular graphs and contour-line diagrams of the Laplace concentration  $-\nabla^2\rho(\mathbf{r})$  of a oxirene and b 1,3-dioxabicyclobutane. For oxirene, the reference plane is identical with the molecular plane. For 1,3-dioxabicyclobutane, the reference plane contains O1, C2, and C4. Heavy solid lines denote bond paths, dashed (solid) contour-lines are in regions with charge concentration (depletion). (HF/6-31G(d) calculations [43])

With a structure diagram such as that shown in Fig. 42b structural changes of a whole class of molecules can be discussed and a relationship between equilibrium properties and reaction behavior can be established. For example, analysis of  $\rho(\mathbf{r})$  of 1,3-dioxabicyclobutane and oxirene have revealed [43] that these systems possess lower  $w$  values and, hence, larger  $\pi$ -complex character than oxirane. This is clearly reflected by the molecular graphs of the two molecules shown in Fig. 43 (compare with Fig. 29b). The structure of oxirene is close to a  $\pi$ -complex between acetylene and oxygen. This can be understood in terms of the donor-acceptor model of three-membered rings discussed in Sect. 6.2. Acetylene is a weaker  $\pi$ -acceptor than ethylene because its  $\pi^*$  MOs are higher in energy than the  $\pi^*$  MO of ethylene. Accordingly, there is a dominance of  $\pi$ -donation from acetylene to a  $a_1$ -symmetrical p-orbital at O). As a consequence the CO bonds are labile and the stability of oxirene is low [43].

In the case of 1,3-dioxabicyclobutane, there are donor, acceptor interactions between acetylene and *two* O atoms. Acetylene donates electrons to both O atoms and, therefore, looses more charge than in oxirene. To compensate this loss,  $\pi$ -backdonation is stronger and the CO bonds are more developed (less concave). Hence, 1,3-dioxabicyclobutane takes an intermediate position between oxirane and oxirene. Its  $\pi$ -complex character is weaker and its stability higher than that of oxirene. Similar considerations apply to other bicyclic or unsaturated three-membered rings [43].

While molecular graph, structure diagram, and the value of  $w$  in that order represent an increasing wealth of information on the reactivity of the corresponding molecule, it is not clear at the moment whether this information can be used as a basis for predicting reaction dynamics. Future investigations have to show whether the catastrophe points of the structure diagram bear a direct chemical relevance, e.g. by giving the locations of the transition states that have to be passed when going from one stable nuclear configuration to another.

### 8.3 Chemical Reactivity as Reflected by the Laplace Field of $\rho(\mathbf{r})$

The determination of a structure diagram is a very costly way to assess the reactivity of a molecule because it requires many calculations before the dissection of  $\mathbf{W}$  into the various structural regions emerges. A simpler way to identify the reactive sites in a molecule is an approach that has amply been applied within MO theory. In Sect. 3 it has already been pointed out that the Laplace concentration in the valence shell of an atom can be related to the form of the frontier orbitals or, more general, to those MOs that are important to predict the course of the reaction. To demonstrate this we will discuss below some simple examples [27].

Figure 44 presents a perspective drawing of  $\rho(\mathbf{r})$  of HCN. Although it is easy to see that N possesses more electrons than C, detailed predictions with regard to the sites most prone to electrophilic or nucleophilic attack are only possible by a quantitative analysis of  $\rho(\mathbf{r})$  including integrations over the three atomic basins  $\Omega$ . Since this is very time consuming, the analysis of  $\rho(\mathbf{r})$  should be replaced by an inspection of Laplace field.

Figure 45 depicts the Laplace concentration  $-\nabla^2\rho(\mathbf{r})$  of HCN. The concentration

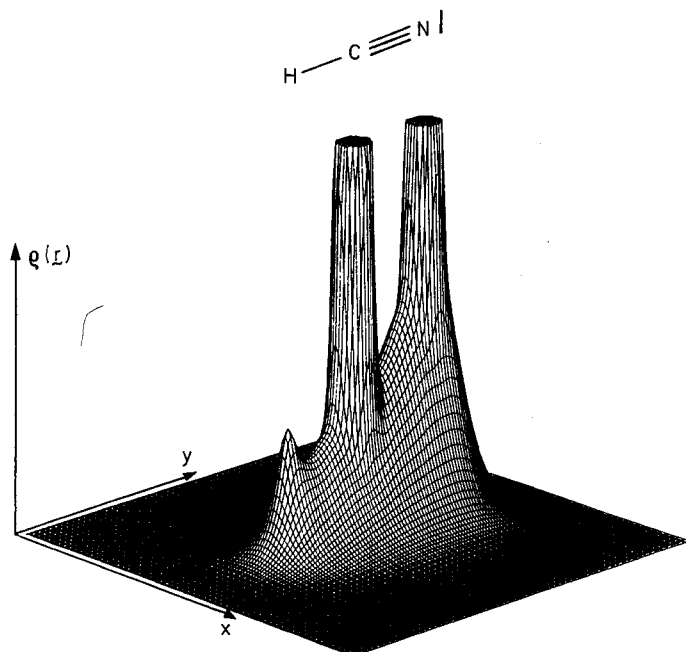


Fig. 44. Perspective drawing of the electron density distribution  $\rho(\mathbf{r})$  of HCN. The reference plane contains the three nuclei. The value of  $\rho(\mathbf{r})$  is cut off above a predetermined value to improve the representation. (HF/6-31G(d) calculations)

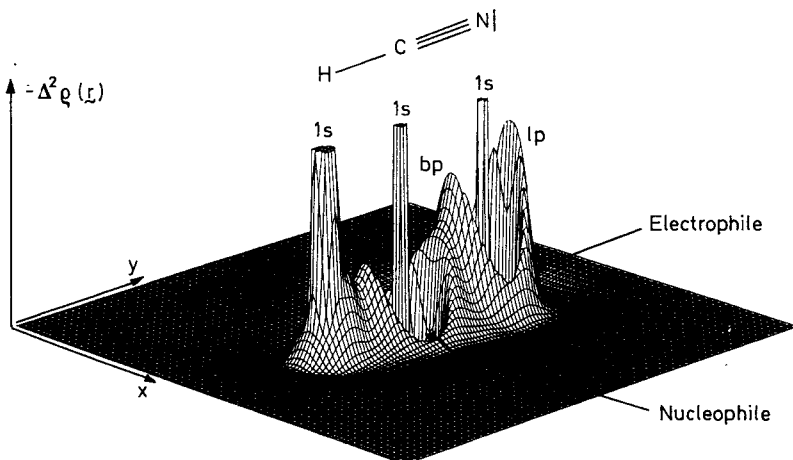


Fig. 45. Perspective drawing of the Laplace concentration  $-\nabla^2\rho(\mathbf{r})$  of HCN. Inner shell (1s), bond (bp), and lone pair (lp) concentrations as well as the positions of electrophilic and nucleophilic attack are indicated. The reference plane contains the three nuclei. Laplace values above and below a threshold are cut off. (HF/6-31G(d) calculations). Reprinted with Permission from *Modelling of Structure and Properties of Molecules*, Z. B. Maksic, Ed., published by Ellis Horwood Limited, Chichester, England 1987

lumps in the Laplace distribution can be associated with the inner shell electron pairs (1s), bond electron pairs (bp), and an electron lone pair (lp) at the N atom as indicated in Fig. 45. Clearly, an electrophile will attack at the back of the N atom where the lp concentration is found.

There are distinct holes in the valence shell of both the C and the N atom (Fig. 45). However, the hole at C is significantly deeper than that at the N atom, i.e. the C nucleus is less shielded than the N nucleus. A nucleophile will preferentially attack at the C atom, in line with experimental observations. Hence, inspection of the Laplace concentration of the electrons immediately reveals the reactive sites of a molecule.

This information can also be exploited in a quantitative way. The four aza compounds (Fig. 46) quinoline, isoquinoline, 2,7-methanoaza[10]annulene, and 3,8-methanoaza[10]annulene differ considerably with regard to their basicity although they are all isoconjugate  $10\pi$  systems [45]. 2,7-Methanoaza[10]annulene is a significantly weaker base ( $\text{p}K_a = 3.20$ ) than either pyridine or quinoline ( $\text{p}K_a = 5.23$  and 4.92, respectively). The perimeter of a bridged [10]annulene is slightly puckered and, as a consequence, a lone-pair orbital of an atom in  $\alpha$ -position to the bridge is no longer perpendicular to the  $\pi$ -orbitals. Accordingly, the lone pair orbital and  $\pi$ -orbitals overlap partially and the electron lone pair can delocalize to some extent into the annulene ring thus reducing the electron density, and hence, the basicity of the N-atom in 2,7-methanoaza[10]annulene [45].

This is nicely reflected by the perspective drawings of the Laplace concentrations of quinoline and 2,7-methanoaza[10]annulene taken in the plane defined by the N nucleus and the nuclei of the neighboring atoms (Fig. 47a, b). The lone pair concentration in the bridged annulene is clearly lower than that of quinoline. On the other hand, the lone pair concentration of the 3,8-methanoaza[10]annulene is comparable to that of isoquinoline (Fig. 47d, c).

If the value of  $-\nabla^2\rho(\mathbf{r})$  at the position of the lone pair concentration lumps is plotted against measured  $\text{p}K_a$  values, a linear relationship will result (Fig. 48). The larger the electron concentration at a lone pair site, the more basic the molecule. Utilizing this relationship the  $\text{p}K_a$  value of 3,8-methanoaza[10]annulene has been calculated to be 4.8 in good agreement with a value of  $4.7 \pm 0.5$  that was measured *after* the theoretical calculations had been carried out [45].

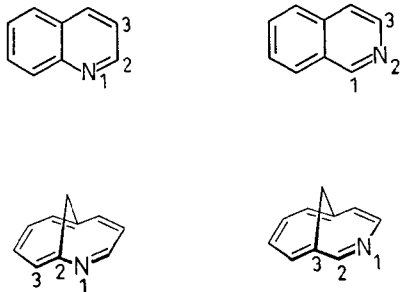
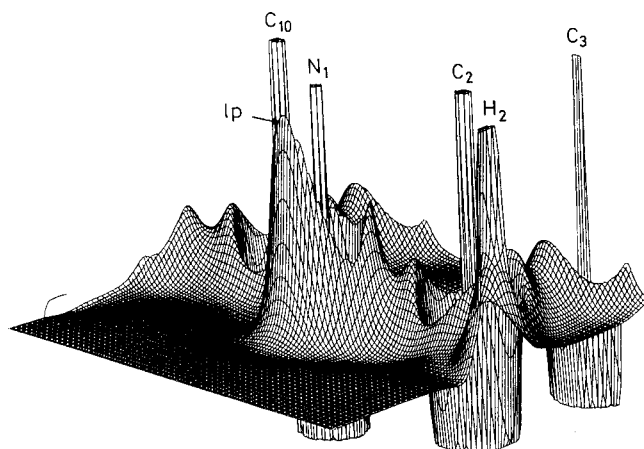
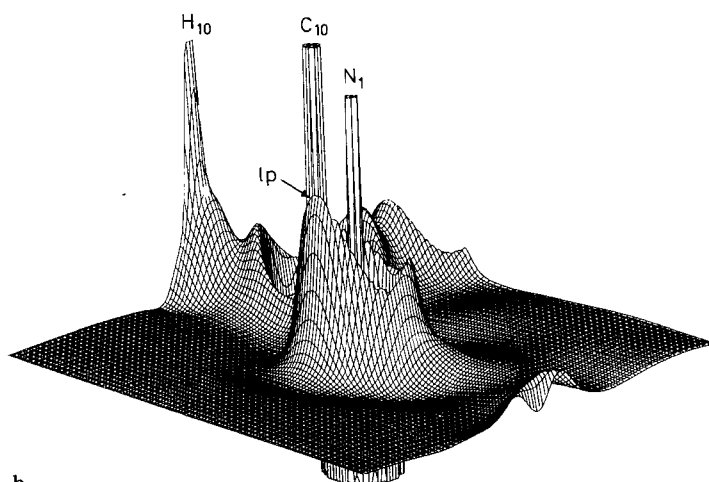


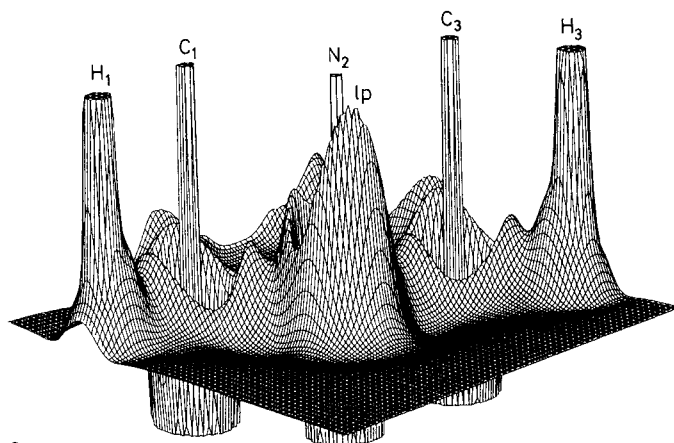
Fig. 46. Quinoline, isoquinoline, 2,7-methanoaza[10]annulene, and 3,7-methanoaza[10]annulene



a

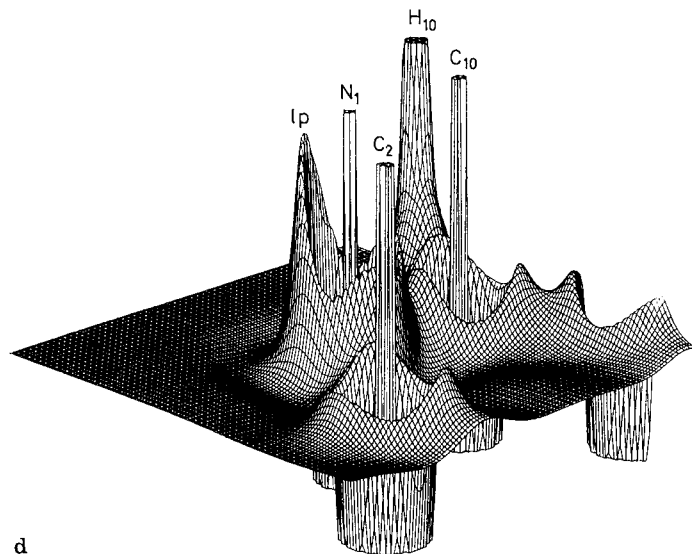


b



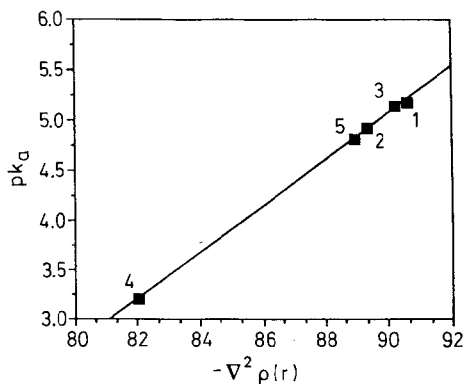
c

Fig. 47 a-c.



**Fig. 47 a-d.** Perspective drawing of the Laplace concentration  $-\nabla^2\rho(\mathbf{r})$  of **a** quinoline, **b** 2,7-methanoaza[10]annulene, **c** isoquinoline, and **d** 3,7-methanoaza[10]annulene. In each case, the plane containing the N nucleus and those of the neighboring atoms is chosen as a reference plane. Laplace values above and below a threshold are cut off. (HF/4-31G calculations [45])

Pearson has developed the concept of hard and soft acids and bases (HASB concept) [131], which is very useful to classify and to rationalize the reactivity pattern of many molecules. An ambident nucleophile such as the cyanide ion,  $\text{CN}^-$ , possesses a soft side that reacts with soft electrophile (e.g., alkylhalogenids) and a hard side that reacts with hard electrophiles (e.g., carbenium ions). Hard and soft side of  $\text{CN}^-$  can be nicely visualized from perspective and contourline diagrams of the Laplace concentration shown in Fig. 49. The concentration lumps at the lone pair side of the N atom is considerably higher than that at the lone pair side of the C atom (Fig. 49a). However, the latter is diffuser and reaches much



**Fig. 48.** Relationship between the  $\text{pK}_a$  value and the Laplace concentration  $-\nabla^2\rho(\mathbf{r})$  in  $\text{e \AA}^{-5}$  at the site of the lone pair electrons of nitrogen. 1: pyridine; 2: quinoline; 3: isoquinoline; 4: 2,7-methanoaza[10]annulene; 5: 3,8-methanoaza[10]annulene. (HF/4-31G calculations [45])

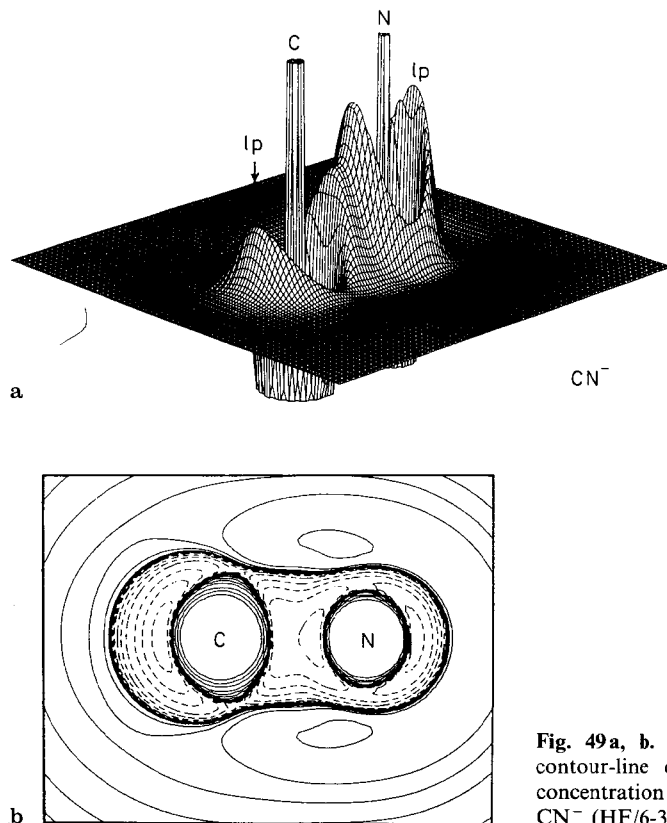


Fig. 49 a, b. Perspective drawing a and contour-line diagram b of the Laplace concentration  $-\nabla^2 \rho(\mathbf{r})$  of the cyanide ion,  $\text{CN}^-$  (HF/6-31G(d) calculations)

more into space and, therefore, is earlier “seen” by an approaching electrophile than the more tightly bound lone pair concentration at nitrogen. This example demonstrates that soft and hard sides of ambident nucleophiles can easily be identified by the Laplace concentration.

Holes in the valence sphere concentration correspond to (3, +1) critical points of  $-\nabla^2 \rho(\mathbf{r})$ . The Laplace concentration at a valence shell critical point is always a maximum in the radial direction, i.e. the eigenvalue  $\lambda$  associated with this direction is always negative. If in addition  $-\nabla^2 \rho(\mathbf{r})$  is a maximum in the tangential plane (perpendicular to the radial direction), all three  $\lambda < 0$  and a (3, -3) critical point will be encountered, corresponding to a concentration maximum in the bond or in the lone pair region. A minimum of  $-\nabla^2 \rho(\mathbf{r})$  in the tangential plane is indicative of a valence shell concentration hole and a (3, +1) critical point of the Laplacian concentration.

Valence shell holes and (3, +1) critical points are found, e.g., where the  $\pi^*$  MOs of alkenes, imino, keto, and other compounds with unsaturated functional groups adopt their largest amplitude. This is shown for ethylene in Fig. 50. The size and depth of the hole provides not only an idea where a nucleophile N might attack but also where an electrophile E might attack. Certainly, E will approach first the “ $\pi$ -concentration” in the bond region yielding a  $\pi$ -complex (Fig. 50). Then, to



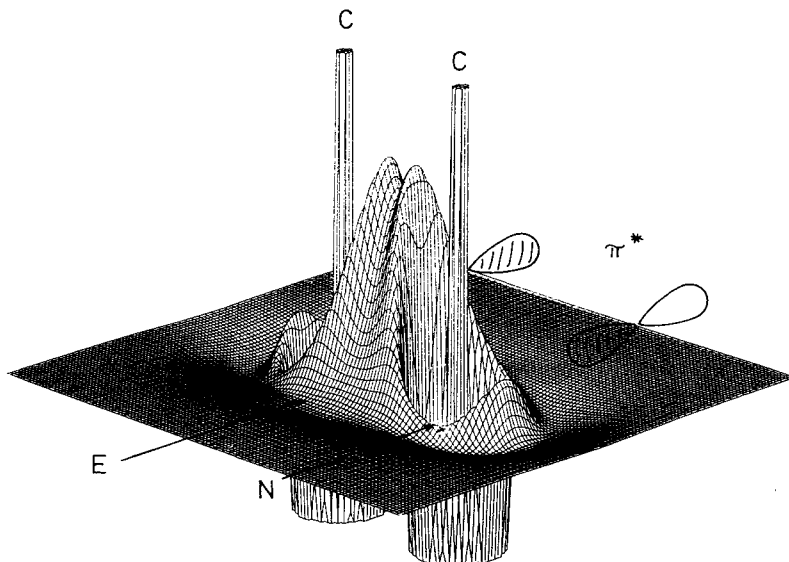


Fig. 50. Perspective drawing of the Laplace concentration  $-\nabla^2\rho(r)$  of ethylene shown with regard to the plane perpendicular to the molecular plane and containing the C nuclei ("π-direction"). Concentration holes in the valence shell can be associated with the  $\pi^*$  MO. The positions of electrophilic (E) and nucleophilic attack (N) are indicated. Laplace values above and below a threshold are cut off. (HF/6-31G(d) calculations)

establish a bond to one of the atoms of the double bond, it will turn to the atom with the largest  $\pi$ -electron density and the smallest  $\pi^*$  concentration hole. In this way, the size of the valence shell concentration hole determines both the site of the nucleophilic and the electrophilic attack.

As an example, the Laplace concentrations at the (3, +1) critical points of the  $\pi^*$  holes of benzene, fluorobenzene, and nitrobenzene are listed in Table 8. They possess

Table 8. Description of the concentration holes in the valence shell below and above the molecular plane<sup>a</sup>

Molecule	Critical point	Position <sup>b</sup>	$-\nabla^2\rho(r)$ [e Å <sup>-5</sup> ]	p [Å]
C <sub>6</sub> H <sub>6</sub>	C1 (3, +1)		4.32	0.528
C <sub>6</sub> H <sub>5</sub> F	C1 (3, -1)		8.54	0.511
	C2 (3, +1)	Ortho	5.02	0.524
	C3 (3, +1)	Meta	3.97	0.529
	C4 (3, +1)	Para	4.64	0.526
C <sub>6</sub> H <sub>5</sub> NO <sub>2</sub>	C1 (3, -1)		9.35	0.510
	C2 (3, +1)	Ortho	3.20	0.531
	C3 (3, +1)	Meta	4.54	0.527
	C4 (3, +1)	Para	3.23	0.532

<sup>a</sup> HF/4-31G calculations. Ref. [133];

<sup>b</sup> with regard to substituent.

different sizes as reflected by the values of  $-\nabla^2 \rho(\mathbf{r})$  and the position parameter  $p$  of the hole. The smaller the Laplace concentration and the larger  $p$  is, the deeper is the hole. From the values in Table 8, it becomes immediately clear that a F substituent directs an electrophile (nucleophile) into *para* and *ortho* (*meta*) position, because the holes are less (very) deep in these positions. A  $\text{NO}_2$  substituent, however, directs an electrophile (nucleophile) into *meta* (*ortho* and *para*) position. This is completely in line with experimental observations [132]. Obviously, knowledge of the Laplace concentration is sufficient to predict the preferred position of substitution in aromatic compounds [133].

## 9 Concluding Remark and Outlook

In the previous Sections, the usefulness and feasibility of the analysis of the total electron density distribution have been outlined and demonstrated for a number of examples. The analysis is best carried out in three steps which comprise first the determination of the paths of maximum electron density (MED paths) in a molecule, second the calculation of the properties of electron density  $\rho(\mathbf{r})$  and energy density  $H(\mathbf{r})$  at the path critical points  $\mathbf{r}_b$  and, finally, the investigation of the Laplace concentration. All Steps of this analysis are easily implemented and require only marginally more computer time than, for example, a Mulliken population analysis, i.e. they require only seconds of computer time [134, 135].

The three-step analysis of the total electron density distribution leads to

1. an identification of chemical bonds and molecular structure;
2. the distinction between covalent bonds and closed shell interactions (ionic bonds, hydrogen bonds, van der Waals interactions);
3. an assessment of the  $\pi$ -character of a bond;
4. a measure for the degree of  $\pi$ -delocalization and bond equalization in unsaturated systems;
5. knowledge of the distortion of the valence sphere of an atom upon bond formation;
6. the location of concentration lumps arising from inner shell, bond, and lone electron pairs;
7. detection of those sites in the molecule that are prone to nucleophilic or electrophilic attack.

Furthermore, the investigation of the properties of the electron density distribution facilitates the description of through-space and through-bond interactions, in particular  $\pi$ -conjugation, homoconjugation, and  $\sigma$ -conjugation, thereby laying the basis for a clear definition of aromaticity, antiaromaticity, homoaromaticity,  $\sigma$ -aromaticity, etc.

With somewhat more computational effort bond path lengths and interpath angles are calculated. Their knowledge is important in the case of strained molecules, for which the analysis of  $\rho(\mathbf{r})$  leads to a description of bent bonds and their chemical or physical consequences. For example, calculation of the interpath angles helps to quantify the energetic consequences of bond angle or Baeyer strain.

Even more information is obtained by investigating  $\rho(\mathbf{r})$  in the zero-flux surface  $S(A, B)$  that separates the atomic subspaces of atoms A and B. Integration of  $\rho(\mathbf{r})$  or  $H(\mathbf{r})$  over  $S(A, B)$  leads to quantities that are measures for the number of electrons forming bond AB or for the bond energy  $E(AB)$  [41]. Integration of  $\rho(\mathbf{r})$  and  $H(\mathbf{r})$  over the basins of A and B gives similar quantities for the atoms. Also, atomic multipole moments, which provide a detailed insight into the electronic structure of a molecule, can be obtained by applying the appropriate one-electron operator and integrating over the atomic subspaces.

However, all calculations which involve integration over a surface or a subspace are costly because they have to be done numerically. The distributions  $\rho(\mathbf{r})$  and  $H(\mathbf{r})$  like energy, geometry, and other molecular properties depend on the method and the basis set used and, therefore, it is reasonable to carry out integrations only if the molecular wave function has been obtained with a DZ or DZ + P basis set.

The three-step analysis of  $\rho(\mathbf{r})$  has been successfully applied in many cases as was discussed above. Furthermore, it has opened some fascinating avenues that have led to the discovery of novel compounds [48–52]. To illustrate this we briefly discuss here an example taken from our investigations on helium chemistry [50–52].

Helium possesses the highest ionization potential of all elements and, therefore, shows a very moderate tendency of establishing an electron pair bond by donating its electrons to an electron acceptor. A suitable acceptor, however, can be found by bearing in mind 1) that the acceptor ability of an atom or molecule requires a hole in its valence shell concentration and 2) that helium does not possess  $\pi$ -electrons, i.e. it can donate only  $\sigma$ -electrons into a  $\sigma$ -hole of the acceptor. In other words, the bonding

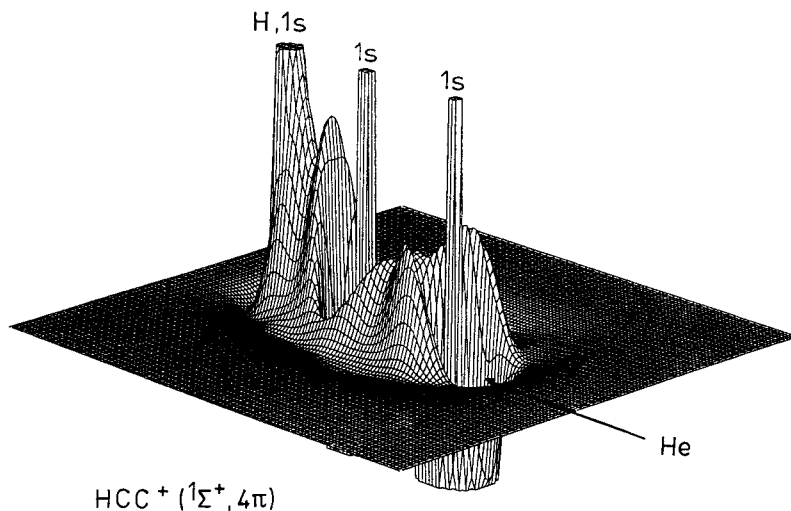


**Fig. 51.** Perspective drawing of the Laplace concentration  $-\nabla^2\rho(\mathbf{r})$  of the ethynyl cation,  $\text{HCC}^+$ , in its  $^1\Sigma^+(4\pi)$  state. The reference plane contains the three nuclei. The site of the  $\sigma$ -hole to which He binds is indicated by an arrow. Laplace values above and below a threshold are cut off. (HF/6-31G(d, p) calculations)

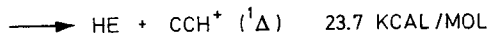
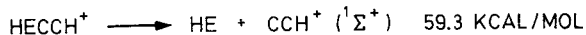
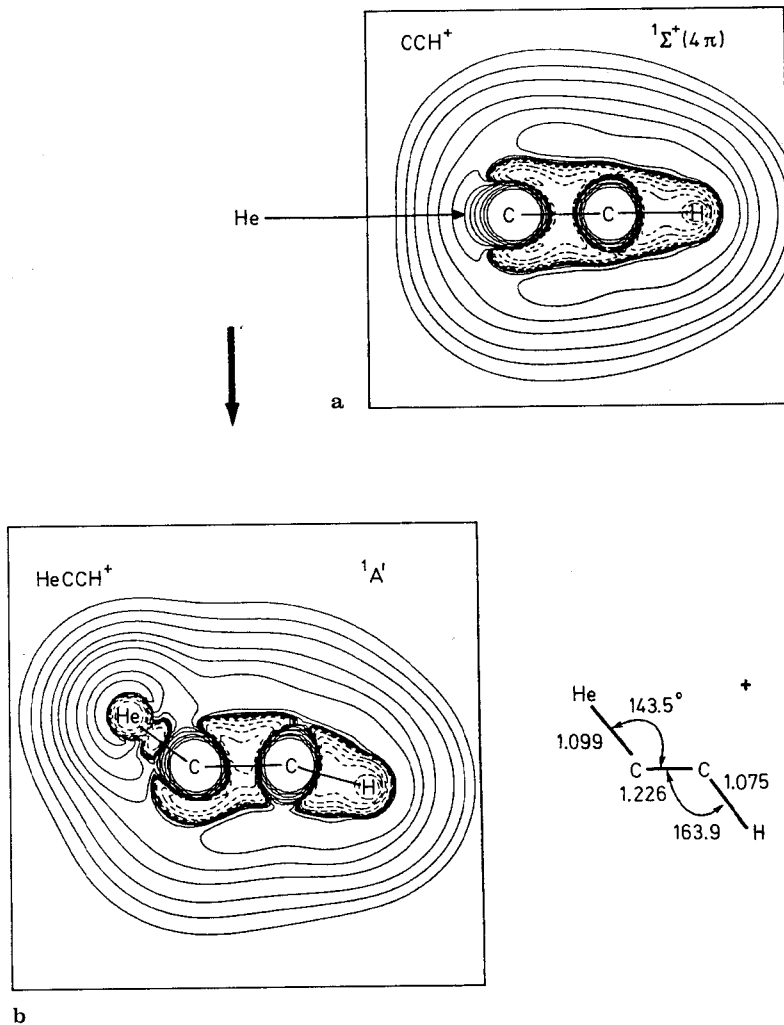


**Fig. 52 a, b.** Contour-line diagrams of the Laplace concentration  $-\nabla^2\rho(\mathbf{r})$  of **a**  $\text{CCH}^+ ({}^1\Sigma^+, 4\pi)$  and **b**  $\text{HeCCH}^+ ({}^1A')$ . The nuclei are in the reference plane. Inner-shell concentrations for C are not shown. For  $\text{HeCCH}^+$  the calculated MP2/6-31G(*d, p*) geometry and the MP4(SDTQ)/6-311G(2*df, 2dp*) dissociation energies are also given [51]

partner for helium must possess low-lying unoccupied  $\sigma$ -MOs that accept the He electrons.

By checking the Laplace concentration of various carbon cations, it has been found [51] that, among other, the ethynyl cation,  $\text{CCH}^+$ , should bind helium.

Figure 51 gives the calculated Laplace concentration of  $CCH^+$  in an excited  ${}^1\Sigma^+(4\pi)$  state. The concentration peaks of the  $1s$  electrons of H and the two C atoms are indicated. There are holes in the valence sphere of the central C atom that are typical of a  $\pi^*$  LUMO. However, there is an even deeper hole at the terminal C atom in the nonbonding region that is indicative of an unoccupied  $\sigma$  MO. This hole imparts pronounced electron acceptor ability to  $CCH^+$ . The electrons of an approaching He atom can be drawn in this hole as indicated in Fig. 51.

Figure 52a gives the contourline diagram of the Laplace concentration of  $CCH^+$  ( ${}^1\Sigma^+, 4\pi$ ), which also shows the large  $\sigma$ -hole at the terminal C atom. Upon collision of He and  $CCH^+$ , the monoheliumacetylene monocation,  $HeCCH^+$ , is formed (Fig. 52b).  $HeCCH^+$  is nonlinear and stable with regard to decomposition to He and  $CCH^+$  by at least 24 kcal/mol. The contourline diagram of the Laplace concentration reveals that the spherical concentration of He is distorted toward the C atom. It forms a droplet-like appendix in the CHe bonding region that is typical of a *semipolar covalent bond*. This is confirmed by the analysis of  $H(\mathbf{r})$ , which is negative at the bond critical point. Hence, *HeCCH<sup>+</sup> is a stable covalently bonded compound* that should be synthesizable. By substituting the H atom by alkyl or aryl groups, a whole class of stable helium organic compounds should be obtained, the monoheliumalkyne cations.

This example demonstrates how the analysis of  $\rho(\mathbf{r})$ ,  $H(\mathbf{r})$ , and  $\nabla^2\rho(\mathbf{r})$  can be used to discover novel compounds or a whole new area in chemistry. Future developments will definitely lead to further examples in this respect. Investigation of atom, atom interactions in nonclassical compounds, in transition metal compounds, in molecules with fluctuating valences, in atom clusters, etc. will probably unravel new interesting features of the bonding mechanism. Also, an analysis of the changes in  $\rho(\mathbf{r})$  and  $H(\mathbf{r})$  along a reaction path and a comparison with the corresponding changes in the molecular energy present a challenging and probably highly rewarding enterprise.

*Acknowledgements:* We thank Prof. W. H. E. Schwarz and Prof. T. P. Radhakrishnan for valuable comments on the manuscript. This work was supported by the Deutsche Forschungsgemeinschaft and the Fonds der Chemischen Industrie. Calculations for this article have been carried out on the CRAY XMP 48 of the National Supercomputer Center (NSC), University of Linköping, Sweden. We thank the NCS for a generous allotment of computer time.

## 10 References

1. (a) Pople JA, Beveridge DL (1970) Approximate molecular orbital theory. McGraw-Hill, New York  
(b) Dewar MJS (1969) The molecular orbital theory of organic chemistry. McGraw-Hill, New York  
(c) Parr RG (1964) Quantum theory of molecular electronic structure. WA Benjamin, New York
2. Roothan CCJ (1951) Rev. Mod. Phys. 23:69
3. (a) Hoffman R (1963) J. Chem. Phys. 39: 1397  
(b) For a review see (1977) Semiempirical methods of electronic structure calculations. In: Segal GA (ed) Modern theoretical chemistry, New York (vols 7 and 8)

4. (a) Salem L (1966) *The molecular orbital theory of conjugated systems*. WA Benjamin, New York
- (b) Heilbronner E, Bock H (1968) *Das HMO-Modell und seine Anwendung — Grundlagen und Handhabung*, Verlag Chemie, Weinheim
5. (a) Pauling L (1960) *The nature of the chemical bond*, 3rd edn, Cornell University Press, Ithaca, New York
- For a recent review on hybrid orbitals, see (b) Bingel WA, Lüttke W (1981) *Angew. Chem.* 93: 944; *Angew. Chem. Int. Ed. Engl.* 20: 899
6. (a) Boys SF (1960) *Rev. Mod. Phys.* 32: 296
- (b) Edminton C, Ruedenberg K (1963) *Rev. Mod. Phys.* 35: 457
7. See, e.g. Gimarc BM (1979) *Molecular structure and bonding — the qualitative molecular orbital approach*. Academic, New York
8. Mulliken RS (1955) *J. Chem. Phys.* 23: 1833; 23: 1841; (1962) 36: 3428
9. Dewar MJS, Dougherty R (1975) *The PMO theory of organic chemistry*. Plenum, New York
10. (a) Woodward RB, Hoffmann R (1970) *Die Erhaltung der Orbitalsymmetrie*, Verlag Chemie, Weinheim
- (b) Woodward RB, Hoffman R (1969) *Angew. Chem.* 81: 797
- (c) Anh NT (1972) *Die Woodward-Hoffmann-Regeln und ihre Anwendungen*, Verlag Chemie, Weinheim
11. (a) Fukui K (1982) *Angew. Chem.* 94: 852
- (b) Fleming I (1979) *Grenzorbitale und Reaktionen organischer Verbindungen*, Verlag Chemie, Weinheim
12. Fukui K, Yonezawa T, Nagata C, Shingu H (1954) *J. Chem. Phys.* 22: 1433
13. For reviews see: (a) Warner PM (1976) In: Nozoe T, Breslow R, Hafner K, Ito S, Murata I (eds) *Topics in nonbenzenoid aromatic chemistry*. Hirokawa, Tokyo, vol 2
- (b) Paquette LA (1978) *Angew. Chem. Int. Ed. Engl.* 17: 106
14. Becker P (1980) *Electron density and magnetization densities in molecules: Nato advanced study institutes, series B: Phys.* Plenum, New York, vol. 48
15. Coppens P, Hall MB (1981) *Electron density distributions and the chemical bond*, Plenum, New York
16. Breitenstein M, Dannöhl H, Meyer H, Schweig A, Seeger R, Seeger U, Zittlan W (1983) *Int. Rev. Phys. Chem.* 3: 335
17. Hohenberg P, Kohn W (1964) *Phys. Rev.* 136B: 864
18. Bader RFW, Nguyen-Dang TT, Tal Y (1981) *Rep. Prog. Phys.* 44: 893
19. Bader RFW, Nguyen-Dang TT (1981) *Adv. Quantum Chem.* 14: 63
20. Bader RFW (1981) in: Deb BM (ed) *The force concept in chemistry*. Van Nostrand Reinhold, New York, p 39
21. Bader RFW, Slee TS, Cremer D, Kraka E (1983) *J. Am. Chem. Soc.* 105: 5061
22. Cremer D, Kraka E (1984) *Croat. Chem. Acta* 57: 1259
23. Cremer D (1988) In: Maksic ZB (ed) *Modelling of structure and properties of molecules*. Ellis Horwood, Chichester, England, p 125
24. Bader RFW, Essen H (1984) *J. Chem. Phys.* 80: 1943
25. (a) Bader RFW, MacDougall PJ, Lau CDH (1984) *J. Am. Chem. Soc.* 106: 1594
- (b) Bader RFW, MacDougall PJ (1985) *J. Am. Chem. Soc.* 107: 6788
26. Cremer D, Kraka E (1984) *Angew. Chem. Int. Ed. Engl.* 23: 62
27. (a) Kraka E, Cremer D (1985) *Z. Kristallogr.* 170: 106
- (b) Cremer D, Kraka E (1985) *Z. Kristallogr.* 170: 32
28. Kraka E (1984) Thesis, University of Cologne, Cologne, West Germany
29. Cremer D, Schmidt T (1985) *J. Org. Chem.* 50: 2684
30. Cremer D, Bock CW, to be published
31. Cremer D (1983) In: Patai S (ed) *The chemistry of functional groups, peroxides*, John Wiley, New York, p 1
32. LaBarge MS, Hillig II KW, Kuczkowski RL, Cremer D (1986) *J. Phys. Chem.* 90: 3092
33. LaBarge MS, Keul H, Kuczkowski RL, Wallasch M, Cremer D (1988) *J. Am. Chem. Soc.* 110: 2081
34. Cremer D, Kraka E, Slee TS, Bader RFW, Lau CDH (1983) *J. Am. Chem. Soc.* 105: 5069
35. Cremer D, Dick B, Christen D (1984) *J. Mol. Struct.* 110: 227
36. Cremer D, Dick B (1982) *Angew. Chem. Int. Ed. Engl.* 21: 865

37. Cremer D, Gauss J, Schleyer PvR, Budzelaar PHM (1984) *Angew. Chem. Int. Edt. Engl.* 23: 370
38. Cremer D, Kraka E (1985) *J. Am. Chem. Soc.* 107: 3800
39. Cremer D, Kraka E (1985) *J. Am. Chem. Soc.* 107: 3811
40. Cremer D, Kraka E (1988) In: Liebman JF, Greenberg A (eds) *Molecular structure and energetics*, VCH Publishers, Deerfield Beach, vol 7, p 65
41. Cremer D, Gauss J (1986) *J. Am. Chem. Soc.* 108: 7467
42. Cremer D (1988) *Tetrahedron* 44: 7427
43. Budzelaar PHM, Cremer D, Wallasch M, Würthwein M E-U, Schleyer PvR (1987) *J. Am. Chem. Soc.* 109: 6290
44. Cremer D, Gauss J, Kraka E (1988) *J. Mol. Struct. (THEOCHEM)* 169: 531
45. Tückmantel W, Andree G, Seidel A, Schmickler H, Lex J, Kraka E, Haug M, Cremer D, Vogel E (1985) *Angew. Chem.* 97: 592; *Angew. Chem. Int. Edt. Engl.* 24: 592
46. Cremer D, Bock CW (1986) *J. Am. Chem. Soc.* 108: 3375
47. Cremer D (1985) *Jahrbuch der Akademie der Wissenschaften, Göttingen*, p 1
48. Koch W, Frenking G, Gauss J, Cremer D, Sawaryn A, Schleyer PvR (1986) *J. Am. Chem. Soc.* 108: 5732
49. Koch W, Frenking G, Gauss J, Cremer D (1986) *J. Am. Chem. Soc.* 108: 5808
50. Koch W, Franking G, Gauss J, Cremer D, Collins JR (1987) *J. Am. Chem. Soc.* 109: 5917
51. Frenking G, Koch W, Gauss J, Cremer D (1988) *J. Am. Chem. Soc.* 110: 8007
52. Frenking G, Cremer D (1989) *Structure and bonding* in press
53. The maximum in  $\rho(\mathbf{r})$  at the nuclear positions is not a true critical point since  $\nabla\rho(\mathbf{r})$  is discontinuous there as a consequence of the cusp condition on  $\Psi$ . However, there always exists a function homeomorphic to  $\rho$  that coincides with  $\rho$  almost everywhere and for which the nuclei are (3, -3) critical points.
54. Collard K, Hall GG (1977) *Int. J. Quant. Chem.* 12: 623
55. This is an observation that has been made in all cases investigated so far. However, at the moment there is no proof that each subspace of a molecule possesses just one and only one atomic nucleus.
56. Hellmann H (1933) *Z. Phys.* 35: 180
57. Bader RWF, Preston HJT (1969) *Int. J. Quant. Chem.* 3: 327
58. Feinberg MJ, Ruedenberg K (1971) *J. Chem. Phys.* 54: 1495
59. Kutzelnigg W (1973) *Angew. Chem.* 13: 551
60. Nordholm S (1988) *J. Chem. Educat. (in press)*
61. The kinetic energy  $T$  is always  $>0$  and the potential energy  $V$  always  $<0$ . Since  $E = T + V$ , a drop in  $T$  leads to a decrease in  $E$  and, hence, a stabilization of the molecule
62. We note that the simplified statement "bonding leads to a decrease in the kinetic energy  $T$ " often found in text books is not correct. Only the component of  $T$  parallel to the bond decreases; the two components perpendicular to the bond increase
63. Preston HJT (1969) Thesis, McMaster University, Hamilton, Canada
64. (a) Ruedenberg K (1975) in Chelvet O, Daudel R, Diner S, Malrieu JP (eds) *Localization and delocalization in quantum chemistry*. D Reidel, Dordrecht vol 1, p 223  
(b) Ruedenberg K (1962) *Rev. Mod. Phys.* 34: 326
65. (a) Edmiston C, Ruedenberg K (1963) *J. Phys. Chem.* 68: 1628  
(b) Layton Jr. EM, Ruedenberg K (1963) *J. Phys. Chem.* 68: 1654  
(c) Rue RR, Ruedenberg K (1963) *J. Phys. Chem.* 68: 1676
66. (a) Wilson CW, Goddard III WA (1972) *Theor. Chim. Acta* 26: 195  
(b) Goddard III WA, Wilson CW, (1972) *Theor. Chim. Acta* 26: 211
67. Driessler F, Kutzelnigg W (1976) *Theoret. Chim. Acta* 43: 1
68. Cohen L (1979) *J. Chem. Phys.* 70: 788
69. Davidson ER (1976) *Reduced density matrices in quantum chemistry*. Academic, New York
70. Bader RFW (1980) *J. Chem. Phys.* 73: 2871
71. We note that Bader (see Refs. 18 through 20) uses these terms differently by calling all MED paths bond paths, not differentiating between covalent bonds and closed shell interactions. This, however, is contrary to general chemical understanding.
72. See, e.g. Ref. 20, p 108
73. Pan DK, Gao JN, Lin HL, Huang MB, Schwarz WHE (1986) *Int. J. Quantum Chem.* 29: 1154
74. Of course, the analysis of  $\rho(\mathbf{r})$  at a single point  $\mathbf{r}_b$  rather than in the whole bonding region is a

- simplification. Also, the bond order defined in such a way depends on the theoretical method used. For a detailed discussion see Ref. 22 and 23
75. If bonds between atoms of different rows of the periodic table are considered, the different number of inner shells will have to be taken into account
  76. (a) Bader RFW, Tal Y, Anderson SG, Nguyen-Dang TT (1980) *Israel J. Chem.* 19: 8  
(b) Bader RFW, Nguyen-Dang TT, Tal Y (1979) *J. Chem. Phys.* 70: 4316
  77. Note that structural stability of the molecular graph is a mathematical term that is not necessarily related to thermodynamical stability of the molecule
  78. (a) Thom R (1975) *Structural stability and morphogenesis*. Benjamin/Cummings, Reading, MA  
(b) Poston T, Stewart I (1981) *Catastrophe theory and its applications*. Pitman, Boston
  79. Investigation of isomerization reactions suggest that  $R_c$  and the location of the transition state are very close. Cremer D (unpublished results)
  80. Morse PM, Feshbach H (1953) *Methods of theoretical physics*. McGraw-Hill, New York, vol 1, p 6
  81. Generally, concentration of charge is discussed with the aid of difference density maps, which strongly depend on the proper choice of a reference state. For a discussion see, e.g., Ref. 26
  82. See, e.g., Drago RS (1977) *Physical methods in chemistry*. Saunders, WB Company, London, p 323
  83. See, e.g., Arfken G (1985) *Mathematical methods for physicists*. Academic, New York, p 57
  84. See, e.g., Pauli W (1980) *General principles of quantum mechanics*. Springer Verlag, Berlin Heidelberg New York
  85. Bader RFW (1985) *Acc. Chem. Res.* 18: 9; see also Ref. 18 and references cited therein
  86. HF/6-31G(*d, p*) calculations, Ref. 28
  87. Of course,  $\nabla^2 q(\mathbf{r})$  depends on the method and the basis set of the ab initio calculation. If  $q(\mathbf{r})$  is not adequately described, an analysis of  $\nabla^2 q(\mathbf{r})$  will be difficult. But the same considerations apply to an analysis of the energy or other molecular properties obtained by ab initio calculations
  88. See Ref. 30. Note that values of Table 3 have been calculated at the HF/6-31G(*d*) level of theory while those of Fig. 15 have been obtained at HF/4-31G. Small differences in  $\eta$  reflect basis set dependency
  89. See, e.g. Bock CW, George P, Trachtman M (1984) *J. Mol. Struct. (THEOCHEM)* 109: 1
  90. See, e.g., (a) Garrat PJ (1971) *Aromaticity*. McGraw-Hill, London  
(b) Stevenson GR (1986) in Liebman JF, Grrenberg A (eds) *Molecular structure and energetics*. VCH Publishers, Deerfield Beach, vol 3, p 57
  91. (a) Dewar MJS, Schmeising HN (1959) *Tetrahedron* 5: 166; (1960) *Tetrahedron* 11: 96  
(b) de LLano C, Dewar MJS (1969) *J. Am. Chem. Soc.* 91: 789  
(c) see also Ref. 1b
  92. (a) Bergmann ED, Pullman B (1971) *Aromaticity, pseudo-aromaticity, anti-aromaticity*. Proc. Int. Symp, Jerusalem  
(b) Lloyd D (1984) *Non-benzoid conjugated carbocyclic compounds*. Elsevier, Amsterdam
  93. Oda M, Oikawa H (1980) *Tetrahedron Lett.* 21: 107
  94. Kawka D, Mues P, Vogel E (1983) *Angew. Chem. Int. Ed. Engl.* 22: 1003
  95. (a) Ferguson LN (1973) *Highlights of alicyclic chemistry*. Franklin Palisades, NJ (part 1, chap 3)  
(b) Charton M (1970) In: Zabicky J (ed) *The chemistry of alkenes*. Wiley-Interscience, New York, vol 2  
(c) Wendisch D (1971) In: *Methoden der Organischen Chemie*. Houben-Weyl-Müller, Thieme Verlag, Stuttgart vol IV, p 3
  96. In Refs. 38 and 39 the symbol  $\eta$  is used. Since in this work  $\eta$  denotes  $\pi$ -character,  $\eta$  has been replaced by  $\xi$
  97. (a) Winstein S (1959) *J. Am. Chem. Soc.* 81: 6524  
(b) Winstein S. (1969) *Q. Rev. Chem. Soc.* 23: 141
  98. See, e.g.,  
(a) Hehre WJ, Hilbert PC (1974) *J. Am. Chem. Soc.* 96: 302  
(b) Hehre WJ, Hilbert PC (1972) *J. Am. Chem. Soc.* 94: 5917  
(c) Levi DA, Blurock ES, Hehre WJ (1979) *J. Am. Chem. Soc.* 101: 5537  
(d) Hanack M, Schneider H-J (1967) *Topics Curr. Chem.* 554



99. Haddon RC (1987) *J. Am. Chem. Soc.* 109: 1676. Haddon has defined an orbital overlap criterion for homoconjugation. Although this is very useful to investigate through-space interactions, it cannot provide an answer to the question whether a homoaromatic bond is formed or not. See also Ref, 13b
100. For a review on the homotropylium, see Childs RF (1984) *Acc. Chem. Res.* 17: 347
101. Childs RF, Varadarajan A, Lock CJL, Faggiani R, Fyfe CA, Wasylishen RE (1982) *J. Am. Chem. Soc.* 104: 2452
102. (a) Haddon RC (1979) *J. Org. Chem.* 44: 3608  
(b) Haddon RC, Raghavachari KJ (1983) *J. Am. Chem. Soc.* 105: 118
103. Turner RB, Meader WR, Doering WvE, Knox LH, Mayer JR, Wiley DW (1957) *J. Am. Chem. Soc.* 79: 4127
104. Roth WR, Böhm M, Lennartz H-W, Vogel E (1983) *Angew. Chem.* 95: 1011; *Int. Ed. Engl.* 22:1007
105. See, e.g.  
(a) Canrow K (1961) *J. Am. Chem. Soc.* 83: 2958  
(b) Dewar MJS (1974) *Pure Appl. Chem.* 767
106. (a) Christoph GG, Muthard JL, Paquette LA, Böhm MC, Gleiter R (1978) *J. Am. Chem. Soc.* 100: 7782  
(b) McMurry JE, Haley GJ, Matz JR, Clardy JC, Dyne GV, Gleiter R, Schäfer W (1984) *J. Am. Chem. Soc.* 106: 5018  
(c) For a differing view see Liebman JF, Paquette LA, Petersen JR, Rogers DW (1986) *J. Am. Chem. Soc.*, 108: 8267
107. Houk KN, Gandour RW, Strozier RW, Rondan NG, Paquette LA (1979) *J. Am. Chem. Soc.* 101: 6797
108. The authors do not rule out neutral homoaromaticity but constrain this to the case in which two interacting  $\pi$  moieties are substituted by strong donors (the first) and strong acceptors (the second), thus benefiting from stabilizing HOMO LUMO interactions
109. (a) Cremer D, Pople JA (1975) *J. Am. Chem. Soc.* 97: 1358  
(b) Essen H, Cremer D (1984) *Acta Cryst.* B40: 418  
(c) Cremer D (1984) *Acta Cryst.* B40: 498
110. (a) Cox JD, Pilcher G (1970) *Thermochemistry of organic and organometallic compounds.* Academic, New York  
(b) Benson SW, Cruickshank FR, Golden DM, Hangen GR, O'Neal HE, Rodgers AS, Shaw R, Wash R (1969) *Chem. Rev.* 69: 279  
(c) Benson SW (1976) *Thermochemical Kinetics*, Wiley, London
111. Homoaromaticity of norcaradiene has also been suggested on the basis of MO considerations:  
(a) Jorgensen WL (1975) *J. Am. Chem. Soc.* 97: 3082  
(b) Jorgensen WL (1976) *J. Am. Chem. Soc.* 98: 6784
112. Vogel E, Scholl T, Lex J, Hohlneicher G (1982) *Angew. Chem.* 94: 878; (1982) *Angew. Chem. Suppl.* 1882
113. For example, homoantiaromaticity has been suggested by Jorgensen for bicyclo[3.1.0]hexenylation and bicyclo[2.1.0]pent-2-ene. See Ref. 111
114. (a) Childs RF, Sakai M, Parrington BD, Winstein S (1974) *J. Am. Chem. Soc.* 96: 6403  
(b) Childs RF, Winstein S (1974) *J. Am. Chem. Soc.* 96: 6409  
(c) Childs RF, Zeya M (1974) *J. Am. Chem. Soc.* 96: 6418
115. This seems to be the case for 3*H*-cyclo-nona[def]biphenylene that has been investigated by Wilcox CF, Blain DA, Clardy J, Duyne vG, Gleiter R, Eckert-Maksić M (1986) *J. Am. Chem. Soc.* 108: 7693
116. See, e.g. Haddon RC, Raghavachari K (1983) *J. Am. Chem. Soc.* 105: 118 and references cited therein
117. For reviews on strain, see (a) Ref. 40  
(b) Greenberg A, Liebman JF (1978) *Strained molecules.* Academic, New York  
(c) Liebman JF, Greenberg A (1976) *Chem. Rev.* 76: 311  
(d) Wiberg K (1986) *Angew. Chem. Int. Ed. Engl.* 25: 312
118. (a) Dewar MJS (1945) *Nature* 156: 748  
(b) Dewar MJS (1946) *J. Chem. Soc.* 406: 777  
(c) Dewar MJS (1951) *Bull. Soc. Chim. Fr.* C71

- (d) Dewar MJS, Marchand AP (1965) *Annu. Rev. Phys. Chem.* 16: 321  
(e) Walsh AD (1947) *Nature* 159: 165; *Nature* 159: 712
119. Dewar MJS, Ford GP (1979) *J. Am. Chem. Soc.* 101: 183  
120. Dunitz JD, Schomaker V (1952) *J. Chem. Phys.* 20: 1703  
121. Bauld NL, Cesak J, Holloway RL (1977) *J. Am. Chem. Soc.* 99: 8140  
122. (a) Dewar MJS (1979) *Bull. Soc. Chim. Belg.* 88: 957  
(b) Dewar MJS, McKee ML (1980) *Pure Appl. Chem.* 52: 1431  
(c) Dewar MJS (1984) *J. Am. Chem. Soc.* 106: 669  
123. (a) Dewar MJS, Petit R (1954) *J. Chem. Soc.* 1617  
(b) Sandorfy C (1955) *Canad. J. Chem.* 33: 1337  
(c) Pople JA, Santry DP (1964) *Mol. Phys.* 7: 269; 7: 301  
124. Cremer D, Reichel F (1989) *J. Am. Chem. Soc.* (to be published)  
125. Coulson CA, Moffit WE (1949) *Philos. Mag.* 40: 1  
126. Ahlrichs R, Ehrhardt C (1985) *Chem. Z.* 19: 120 and personal communication  
127. Emsley JW, Feeney J, Sutcliffe LH (1966) *High resolution nuclear magnetic resonance spectroscopy*. Pergamon, Oxford, p 690  
128. Zilm KW, Beeler AJ, Grant DM, Michl J, Clou T, Allred EL (1981) *J. Am. Chem. Soc.* 103: 2119  
129. (a) Buchanan JG, Sable HZ (1972) in: Thagarajan BS (ed) *Selective organic transformations*. Wiley, New York, vol 2, p 1  
(b) Smith JG (1984) *Synthesis* 629  
130. A family of functions describing a given type of catastrophe is called unfolding [78]  
131. (a) Pearson RG (1963) *J. Am. Chem. Soc.* 85: 3533  
(b) Pearson RG, Songstad J (1967) *J. Am. Chem. Soc.* 89: 1827  
(c) Ho T-L (1975) *Chem. Rev.* 75: 1  
132. See, e.g. Ref. 11 b, chap 3  
133. Cremer D, Bock CW (to be published)  
134. For example, the analysis of  $\varrho(\mathbf{r})$ ,  $\mathbf{H}(\mathbf{r})$ , and  $\nabla^2\varrho(\mathbf{r})$  for a three-heavy atom system with 70 basis functions carried out with the ab initio package COLOGNE 87 [135] requires 6 s while the Mulliken population analysis requires 5 s of computer time  
135. Gauss J, Kraka E, Reichel F, Cremer D, (1988) Universität Köln, COLOGNE 88